Online ISSN: 2249-460X
Print ISSN: 0975-587X
DOI: 10.17406/GJHSS

Global Journal

of Human Social Sciences: B

Geography, Geo-Sciences & Environmental Science & Disaster Management

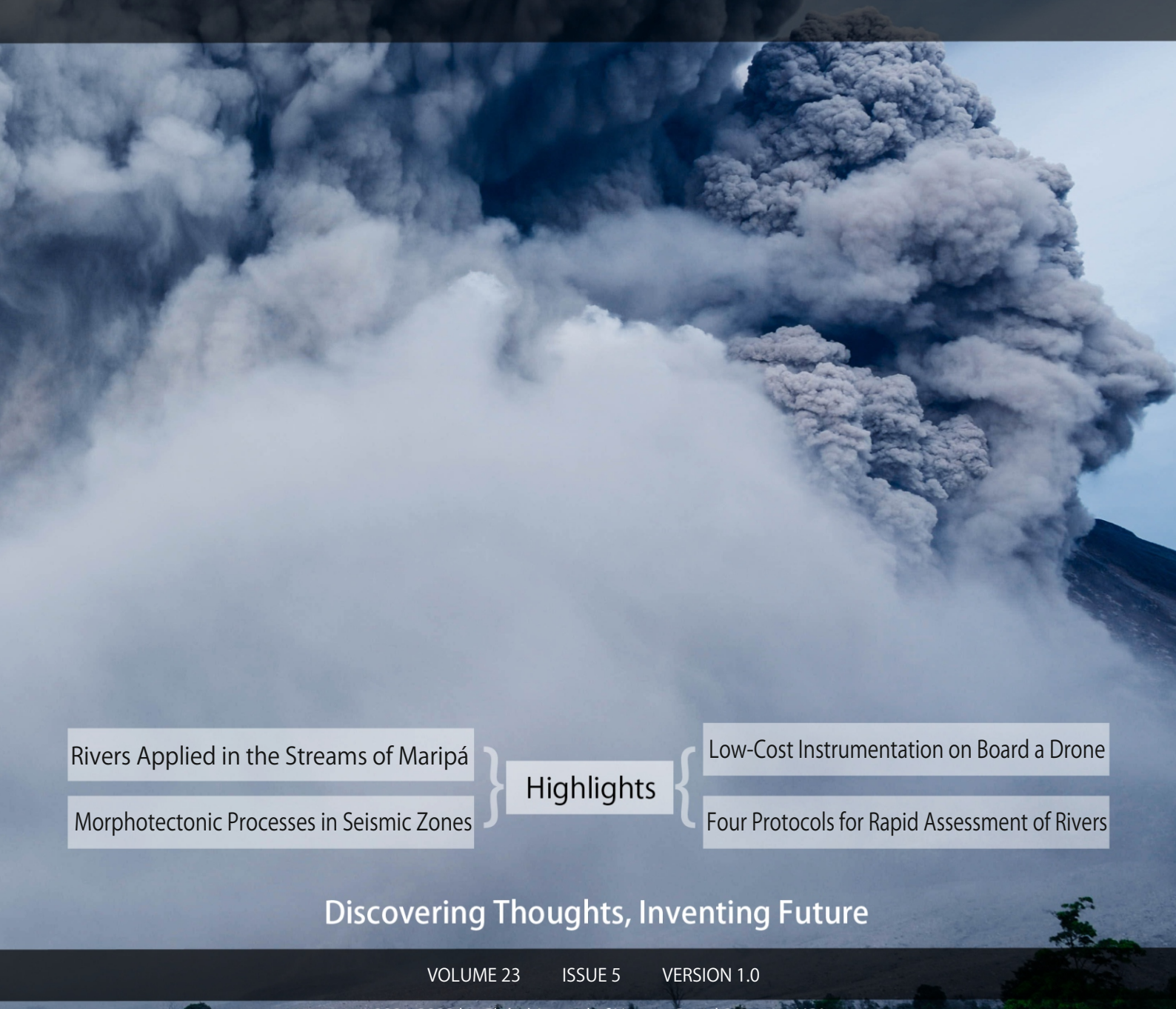

Highlights

- Rivers Applied in the Streams of Maripá
- Morphotectonic Processes in Seismic Zones
- Low-Cost Instrumentation on Board a Drone
- Four Protocols for Rapid Assessment of Rivers

Discovering Thoughts, Inventing Future

VOLUME 23 ISSUE 5 VERSION 1.0

Global Journal of Human-Social Science: B
Geography, Geo-Sciences, Environmental Science & Disaster Management

Global Journal of Human-Social Science: B
Geography, Geo-Sciences, Environmental Science & Disaster Management

Volume 23 Issue 5 (Ver. 1.0)

Open Association of Research Society

Incorporation No.: 0423089
License No.: 42125/022010/1186
Registration No.: 430374
Import-Export Code: 1109007027
Employer Identification Number (EIN):
USA Tax ID: 98-0673427

Global Journals Inc.

*(A Delaware USA Incorporation with "Good Standing"; **Reg. Number: 0423089**)*
Sponsors: Open Association of Research Society
Open Scientific Standards

Publisher's Headquarters office

Global Journals® Headquarters
945th Concord Streets,
Framingham Massachusetts Pin: 01701,
United States of America
USA Toll Free: +001-888-839-7392
USA Toll Free Fax: +001-888-839-7392

Offset Typesetting

Global Journals Incorporated
2nd, Lansdowne, Lansdowne Rd., Croydon-Surrey,
Pin: CR9 2ER, United Kingdom

Packaging & Continental Dispatching

Global Journals Pvt Ltd
E-3130 Sudama Nagar, Near Gopur Square,
Indore, M.P., Pin:452009, India

Find a correspondence nodal officer near you

To find nodal officer of your country, please email us at *local@globaljournals.org*

eContacts

Press Inquiries: *press@globaljournals.org*
Investor Inquiries: *investors@globaljournals.org*
Technical Support: *technology@globaljournals.org*
Media & Releases: *media@globaljournals.org*

Pricing (Excluding Air Parcel Charges):

Yearly Subscription (Personal & Institutional)
250 USD (B/W) & 350 USD (Color)

Editorial Board

Global Journal of Human-Social Science

Contents of the Issue

Global Journal of human-social science: b
Geography, Geo-Sciences, Environmental Science & Disaster Management
Volume 23 Issue 5 Version 1.0 Year 2023
Type: Double Blind Peer Reviewed International Research Journal
Publisher: Global Journals
Online ISSN: 2249-460x & Print ISSN: 0975-587X

Aerosol Typology and Trajectories in the Metropolitan Region of Rio De Janeiro, Brazil

By Filipe Pungirum, José Ricardo de A. França & Edson Pereira Marques Filho
Federal University of Rio de Janeiro

Abstract- Aerosols are liquid or solid particles suspended in the atmosphere. Correct determination of the distribution of aerosol types in the atmosphere is of paramount importance for long-term climate predictions. The latest report of the International Panel on Climate Change (IPCC) addresses aerosols as representing the most significant uncertainties in the context of forcing climate sources. These particles can interfere with the climate directly, indirectly, or semi-directly. Directly, we can highlight the interaction of these particles with solar radiation through their scattering or absorption. Indirectly, the role of these aerosols as nuclei for the condensation of liquid and ice in clouds is significant. Depending on their quantity, these aerosols can form larger or smaller droplets, leading to changes in the cloud's albedo. As for semi-direct effects, we can emphasize the role of aerosols as radiation absorbers within clouds, consequently leading to changes in the stability of the air parcel. As a semi-direct effect, we can highlight changes in the life cycle and the ability to make convective clouds colder and more profound.

Keywords: *aerosol, optical depth, CALIPSO, hysplit.*

GJHSS-B Classification: *LCC Code: QC869*

Strictly as per the compliance and regulations of:

Aerosol Typology and Trajectories in the Metropolitan Region of Rio De Janeiro, Brazil

Filipe Pungirum [α], José Ricardo de A. França [σ] & Edson Pereira Marques Filho [ρ]

Abstract- Aerosols are liquid or solid particles suspended in the atmosphere. Correct determination of the distribution of aerosol types in the atmosphere is of paramount importance for long-term climate predictions. The latest report of the International Panel on Climate Change (IPCC) addresses aerosols as representing the most significant uncertainties in the context of forcing climate sources. These particles can interfere with the climate directly, indirectly, or semi-directly. Directly, we can highlight the interaction of these particles with solar radiation through their scattering or absorption. Indirectly, the role of these aerosols as nuclei for the condensation of liquid and ice in clouds is significant. Depending on their quantity, these aerosols can form larger or smaller droplets, leading to changes in the cloud's albedo. As for semi-direct effects, we can emphasize the role of aerosols as radiation absorbers within clouds, consequently leading to changes in the stability of the air parcel. As a semi-direct effect, we can highlight changes in the life cycle and the ability to make convective clouds colder and more profound. Therefore, this work aimed to characterize the types of aerosol and study their optics and trajectories on the properties of the Rio de Janeiro Metropolitan Region, considered one of the largest urban centers in the world, with a population of approximately 12 million people. The study area comprises different vegetation types, is close to the coast, and is highly urbanized. This study uses data from the product TOTSCATAU, which refers to the optical thickness of aerosols providing total column integration, from the MERRA-2 reanalysis. From the CALIPSO satellite, the Feature Classification Flags were utilized to first classify the pixel into (a) Feature Type (clouds, tropospheric aerosols, stratospheric aerosols), (b) Feature Subtype, (c) Water Phase (ice or water, available only for clouds), and (d) the required sampling quantity for layer detection. From the HYSPLIT model, the investigation was conducted by simulating back trajectories every 6 hours over the entire 13-year study period. Subsequently, all trajectories were grouped into clusters, using variance as a parameter for grouping. Finally, to understand the aerosols originating from biomass burning, the MCD64* product from the Moderate Resolution Imaging Spectroradiometer (MODIS) sensor on the Terra and Aqua satellites was used to provide information on the burned area at a 500m grid scale. The results showed that marine aerosols are the most prevalent in the study area; however, they do not significantly impact the total absolute scattering. Their seasonality is linked to the influx of maritime winds in the study area. Dust aerosols exhibited well-defined seasonality. In addition to local sources, they are also transported by continental trajectories and are more prevalent in the winter when there are lower precipitation rates. On the other hand, carbonaceous aerosols were found to be significant contributors to the seasonal variation in total scattering, with their peak values coinciding with the peaks in the total optical depth variation for aerosols in the atmosphere. The highest black carbon, smoke, and optical depth values are observed between August and October. This contribution primarily stems from emissions from biomass burning, indicating that this type of particulate matter has the most significant impact on the optical characteristics in the study area throughout the year. The study of back trajectories made it possible to identify that the peaks in optical thickness occurring in the winter are linked to local sources of aerosols. As the results indicated that carbonaceous aerosols exhibit the most significant seasonal variations, it was possible to conclude, through the analysis of burned areas data (MODIS-MCD64), that the origin of these aerosols is associated with emissions from biomass burning and fossil fuel combustion throughout the year, both within the study area and in other biomes. Finally, it was identified that the movement of the South Atlantic Subtropical High influences the average aerosol pattern in the study area.

Keywords: aerosol, optical depth, CALIPSO, hysplit.

Author α: Institute of Geosciences, Federal University of Rio de Janeiro, Rio de Janeiro, 21941-916, RJ, Brazil.
e-mail: filipepungirum@hotmail.com
Corresponding Author σ: Institute of Geosciences, Federal University of Rio de Janeiro, Rio de Janeiro, 21941-916, RJ, Brazil.
e-mail: jricardo@igeo.ufrj.br
Author ρ: Interdisciplinary Center for Energy and Environment, Federal University of Bahia, Bahia, 40170-115, BA, Brazil.
e-mail: edson.marques@ufba.br

I. Introduction

Atmospheric aerosol is the combination of all condensed-phase materials present in the atmosphere. Aerosol particles play two distinct roles. As a condensed phase material, they have physical functions as absorbers, emitters, and scatters of atmospheric radiation [1]. They also provide favorable surfaces for depositing molecules and/or ions from the fluid in which they are embedded. These atmospheric particles also participate in many processes with climate impact. In addition, they exert a direct and indirect effect on the radiative balance of the atmosphere, acting as condensation nuclei in the hydrological cycle on regional and global scales [2, 3].

According to the latest Intergovernmental Panel on Climate Change reports, atmospheric aerosols are still responsible for one of the greatest uncertainties in understanding their role in climate change [4]. Aerosols, such as sea salt, mineral particles, carbonaceous aerosols, and particles from fauna and flora, can be of natural origin. In addition to natural sources, it is also necessary to consider anthropogenic emissions, which are responsible for a substantial portion of this particulate matter in the atmosphere [5]. They also play

a significant role in the hydrological cycle, acting as condensation nuclei [6]. Therefore, its quantification and characterization are essential for understanding the behavior of processes operating in the Earth's atmosphere [7]. Many studies indicate that depending on their type, they can change the rainfall pattern of seasonal systems such as monsoons [8, 9], climate oscillation patterns such as Southern Ring Mode (SAM) [10], and transient systems [7]. Although the number of studies on atmospheric aerosols has increased in recent years, mainly due to the greater availability of data obtained by remote sensing, some areas still need further investigation. For example, as is the case of the study area of this work, which comprises the Metropolitan Region of Rio de Janeiro (MARJ). This region is such a city, situated at a tropical latitude (~22.8°S, 43.1°W) over a complex terrain partially covered with rainforest and includes multiple watershed basins feeding the Guanabara Bay. It is the second largest conurbation in Brazil and the second region with the most significant economic importance for the country. Because of its fast development in the past years, it is becoming a region with more than 12 million people. During the last decade, MARJ has undergone several changes in structure and urbanization. A suitable air quality monitoring network for the entire region did not accompany these changes.

The main goal of this work is to trace a temporal analysis of aerosols for a region of Rio de Janeiro centered on the MARJ, analyzing its origin and characteristics. In the absence of a conventional observation network, the use of remote sensing and reanalysis data becomes of crucial importance. For this, a set of remote sensing data and reanalysis were used: the Cloud-Aerosol Lidar with Orthogonal Polarization (CALIOP) sensor aboard the Cloud-Aerosol Lidar and Infrared Pathfinder Satellite Observation (CALIPSO) satellite, one of the leading remote observation instruments for the study of aerosols; the reanalysis of the Modern Era Retrospective Analysis Version 2 (MERRA 2), which takes into account various physical processes in which aerosols are involved; simulations made with the Hybrid Single Particle Lagrangian Integrated Trajectory (HYSPLIT), for tracking air masses and understanding from where these air masses that bring these particles; and finally, the Moderate Resolution Imaging Spectroradiometer (MODIS) sensor, with high-resolution products for the study of fires.

II. Methods

The CALIOP sensor, on board the CALIPSO, is a lidar that generates vertical profiles of the distribution of aerosols and clouds with their respective optical properties [11]. It is the only orbital platform that enables these observations. CALIPSO maintains a near sun-synchronous orbit with an altitude of 705 km, an inclination of 98.2°, and a period of 98.3 minutes, providing a worldwide high-resolution aerosol vertical profiles with a temporal resolution of 16 days. It takes measurements at two different wavelengths, 532 nm in the visible spectrum and 1064 nm in the near-infrared spectrum. The sensor's accuracy allows measurements at the same point on the earth's surface with a variation of only 10 km. Therefore, the number of passes in the study area is approximately two per month, one in the ascending and one in the descending orbit. In this study, thirteen years of data from the CALIPSO satellite were used between 2006, the year of the beginning of operations, and 2019, the year chosen before the suspension of activities due to the COVID-19 pandemic, totaling 530 satellite passes. Two products from CALIPSO were used, the Feature Classification Flags, with processing level 1, and the "Aerosol," with processing level 3, following the methodology proposed by [11, 12]. The Feature Classification Flags classify different atmospheric elements in vertical profiles, while the "Aerosol" has variables related to the physical properties of aerosols in vertical layers.

The Vertical Feature Mask (VFM) variable was used from the Feature Classification Flags. The VFM decision tree first separates each pixel of the vertical profile as cloud, aerosol, or undetermined. After this initial process, other branches in the decision tree emerge, classifying each cloud type and aerosols. In the next step, only the pixels classified as aerosols were filtered, and finally, the different types of aerosols were separated throughout the database. Classifying aerosol pixels into clean marine, dust, polluted continental, clean continental, polluted dust, and smoke is possible. Smoke and polluted continental are attributed to anthropogenic emissions, while dust, clean continental, and clean marine are from natural emissions. The polluted continental type is a hybrid, a mixture of smoke and dust [12]. As for the Aerosol Optical Depth, the average across the entire atmospheric column was used as the data are arranged in vertical layers. These data have a horizontal and vertical resolution that varies with altitude, as shown in Table 1. Vertically and horizontally, respectively, the resolution up to 8.2km is 30 and 333m; between 8.2 and 20km, the resolution is 60 and 1000m; between 20 and 30km, the resolution is 180 and 1667m. The present study used version 4.10 of level 2 aerosol products, which substantially improved the aerosol type, lidar algorithms, and rigid quality control [13].

In order to compare and complement the data obtained by the CALIOP sensor, MERRA 2 data were used, a reanalysis with a horizontal resolution of 0.5^{o} x 0.625^{o} and 72 ETA-hybrid vertical levels. This reanalysis uses version 5.12.4 of the GEOS system for assimilating observed data from the atmosphere and takes into account some essential factors for the study of aerosols, such as the assimilation of observed radiance data and the deposition of aerosols in its simulations [14].

Table 1: Spatial resolutions of the CALIOP sensor for two wavelength- CALIPSO Satellite.

Altitude (km)	Horizontal Resolution (km)	Vertical Resolution (m) (532nm)	Vertical Resolution (m) (1064nm)
30.1 to 40.0	5.0	300	-
20.2 to 30.1	1.67	180	180
8.2 to 20.2	1.0	60	60
-0.5 to 8.2	0.33	30	60
-2.0 to -0.5	0.33	300	300

From the data of the MERRA-2 reanalysis, the grid points with all or most of their area within the polygon corresponding to the study area were chosen. Data on optical depth, density in the atmospheric column, and the zonal and meridional fluxes of different types of aerosols were used: organic carbon, resulting from chemical processes involving carbon; black carbon, which accompanies organic carbon and is a consequence of anthropogenic emissions, arising from pollution in large cities and natural from fires; sea salt, which concentrates marine emissions, basically from marine spray; dust, which represents most of the mineral emissions, similar to CALIPSO.

To identify the origin of the air masses over the MARJ, the Hybrid Single-Particle Lagrangian Integrated Trajectory Model (HYSPLIT) model that simulates the trajectories and retro trajectories of particles suspended in the atmosphere was used. HYSPLIT is a model used to investigate particle dispersion [15]. It can be used in several applications, such as in the study of radionuclide dispersion [16], pyrogenic particle dispersion [17], pollen transport [18], the transport of volcanic ash [19], the transport of pollution [5] and the transport of dust between continents [20]. This work used a global grid with 1° horizontal resolution, with meteorological data from the National Center for Environmental Prediction (NCEP) Global Data Assimilation System.

HYSPLIT model simulations were performed for all Reanalysis 2 meteorological data [21]. Four daily simulations of the retro trajectories were performed for 72 hours each, at 00, 06, 12, and 18Z. As the top of the trajectories, an altitude of 10 km was chosen. Once all the trajectories were calculated, they were divided by month and then grouped into average clusters. Then, the elbow method was applied, which consists of evaluating the change in the percentage of variance of the trajectories. The method shows these groups an optimal number of clusters to represent reality satisfactorily. Ultimately, the method arrives at a result where adding one more cluster would not bring significant gains to the analysis. For this study, the number of clusters was between 3 and 5 in each average trajectory.

The MCD64 product of the MODIS sensor that operates on board the Terra and Aqua satellites was used, which provides monthly averages of burned area with a spatial resolution of 500 meters and global coverage [22]. The MODIS MCD64 data counted the monthly totals of burned areas within the study area. For this, a filter was made where only the pixels that were more than half in the polygon corresponding to the study area were counted. After this step, the average monthly and annual data were stored.

Finally, data from the Meteorological Aerodrome Report (METAR) and the Instituto Nacional de Meteorologia (INMET) were used for the surface meteorological stations. The METAR messages from Tom Jobim International Airport were used to study the incidence of large-scale winds over the study region. With these data, a hodography of the monthly average of the daily averages was elaborated. The method was chosen to exclude small-scale effects, such as breezes, and keep only large-scale effects. With INMET data, the seasonal behavior of cloud cover and rainfall was raised through simple averages. As seen in Figure 1, the study area is a box containing the Metropolitan Region of Rio de Janeiro and its surroundings. In addition to being a coastal area, it also has areas of dense vegetation and urbanized areas.

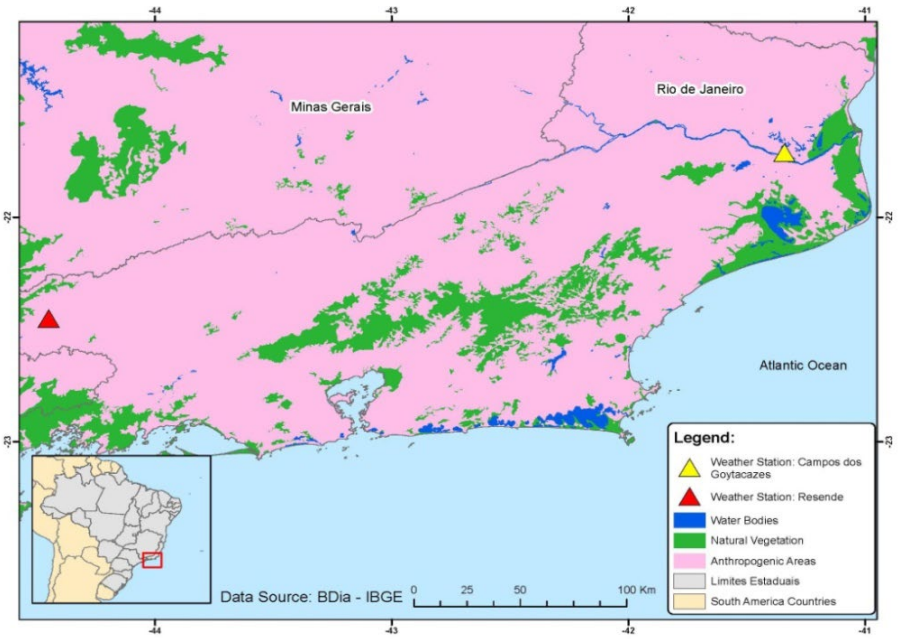

Figure 1: Study area comprising an expanded space in the Metropolitan Region of Rio de Janeiro. Water bodies in blue, natural vegetation in green, and areas with human action in pink. The stars signal the location of the INMET weather stations used in this study.

III. Results

Based on the CALIOP sensor data series, the values of the monthly mean totals of the AOD at 532 nm for the RMRJ represented in Figure 2 were first calculated. It can be observed that the AOD has a well-defined seasonal behavior. The highest values were observed between August and November. The meteorological stations used as a source of rainfall data are in the central portion and on the periphery of the study area to represent the rainfall behavior throughout the region. These stations (indicated in Figure 1) were chosen for having the most comprehensive data series and for representing extreme regions within the study area. Considering the synoptic-scale movements, due to the size of the study area, the pluviometric data points have similar behavior. During this period, there is a transition between the driest months of winter and the beginning of the wettest period of spring [23]. In addition, a secondary peak is also observed in the elevation of optical thickness in May. This month presents a considerable drop in the rate of precipitation and cloudiness, which enables the highest accumulation of particles in the atmosphere.

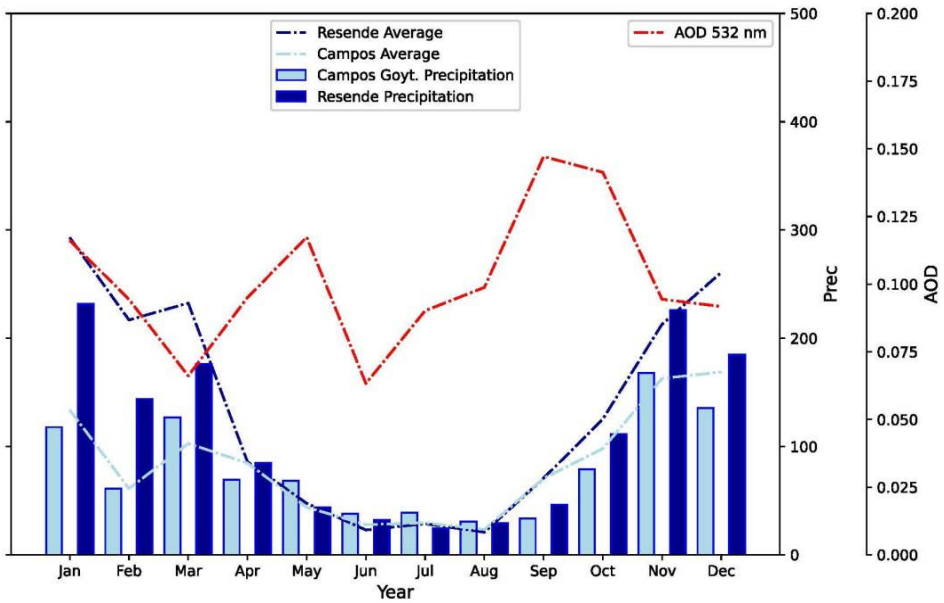

Figure 2: Average monthly totals of Aerosol Optical Depth from the CALIPSO satellite, with a study period from 2006 to 2019, are represented in red. Light (dark) blue bars indicate precipitation values from INMET's normals for the cities of Campos dos Goytacazes (Resende). The blue lines represent the average precipitation over the period between 2006 and 2019.

To examine the year-round distribution of various atmospheric aerosol types, we conducted a classification using CALIPSO VFM. The results are shown in Table 2. Based on these results, Figure 3 was constructed, which shows the proportion of pixels classified as smoke, dust, and marine to the total number of verified pixels. The other types of aerosols (polluted continental, clean continental, and polluted dust) did not show significant levels and, therefore, were omitted in this figure. This figure was constructed to remove the seasonal effect of sea salt to analyze the proportions of smoke and dust in the total composition of atmospheric aerosols in the region. This is because marine aerosol, which is always present, exhibits a seasonal variation that strongly depends on the positioning of the South Atlantic Subtropical Anticyclone. In other words, the graphically represented values correspond to the total percentage that each type of aerosol (excluding marine aerosol) presents in the study area. The absolute values obtained and the standard error are shown in Table 2. These values indicate the total percentage of observation for each type of aerosol.

The standard error was calculated as it represents a critical measure for understanding the variability and precision of statistical estimates. As can be observed in Table 2, the values obtained for the standard error are minimal, which indicates the more reliable the estimate.

It is also verified that the pixels classified as dust are the most common after the marine, reaching values above the marine during Jan (39.7%), Feb (48.2%), Jul (44.4%), and Dec (54.1%). They represent all types of mineral particles originating from the erosion processes of rocks and soil, which are suspended in the atmosphere. Pixels classified as marine aerosols represent a large part of the classifications, exceeding 40 percent in 7 of the 12 months of the year. The reason may be due to the circulation of the South Atlantic Subtropical High (ASAS) [24] and the sea breeze [25] that causes the advection of this type of aerosol to the study area. As for the pixels classified as smoke type, the highlight goes to January (wet season) and August (dry season), where the proportion of this type reaches values of 34,7% (being the most important).

Table 2: The percentage contribution of each type of aerosol and the sample's standard error value.

Month	Marine (%) – (Standard error)	Dust (%) – (Standard error)	Smoke(%) – (Standard error)
Jan	29.5 - (0.014)	39.7 – (0.048)	30.8 – (0.047)
Feb	29.7 - (0.019)	48.2 – (0.039)	22.1 – (0.047)
Mar	63.8 - (0.016)	30.7 – 0.054)	5.5 – (0.018)
Apr	47.6 - (0.020)	39.0 – (0.046)	13.4 – (0.041)
May	59.9 - (0.037)	31.0 – (0.055)	9.1 – (0.027)
Jun	64.6 - (0.041)	30.7 – (0.049)	4.7 – (0.022)
Jul	41.5 - (0.026)	44.4 – (0.058)	14.1 – (0.041)
Aug	30.7 - (0.029)	34.6 – (0.033)	34.7 – (0.064)
Sep	53.9 - (0.036)	36.6 – (0.047)	9.5 – (0.042)
Oct	47.1 - (0.027)	41.0 – (0.051)	11.9 – (0.025)
Nov	49.2 - (0.034)	42.4 – (0.049)	8.4 – (0.018)
Dec	29.3 - (0.017)	54.1 – (0.062)	16.6 – (0.030)

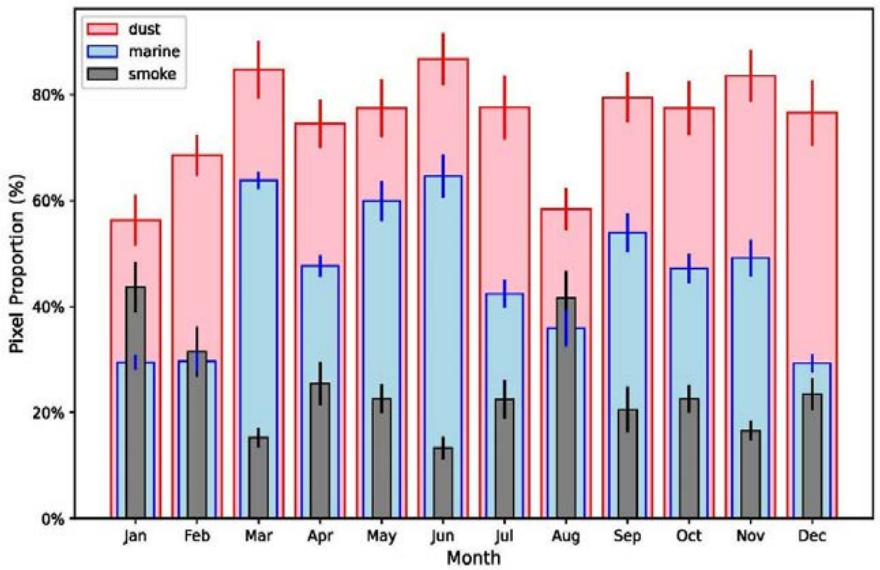

Figure 3: Total pixels classified as smoke (gray), marine (blue) and dust (red). The total is in percentage, in relation to the total value of pixels. The data refer to the CALIPSO satellite's Vertical Feature Mask product. Period 2006 to 2019.

From the CALIOP sensor data, the trend in the proportion of these aerosols during the study period was also estimated. Figure 4 shows that the proportion of dust aerosols has been increasing significantly over this period compared to the presence of marine aerosols and smoke. These results align with the findings in [26], which demonstrated that this region has been experiencing increased aridity throughout nearly all months of the year, leading to a concurrent rise in diffuse solar radiation, particularly during the dry season.

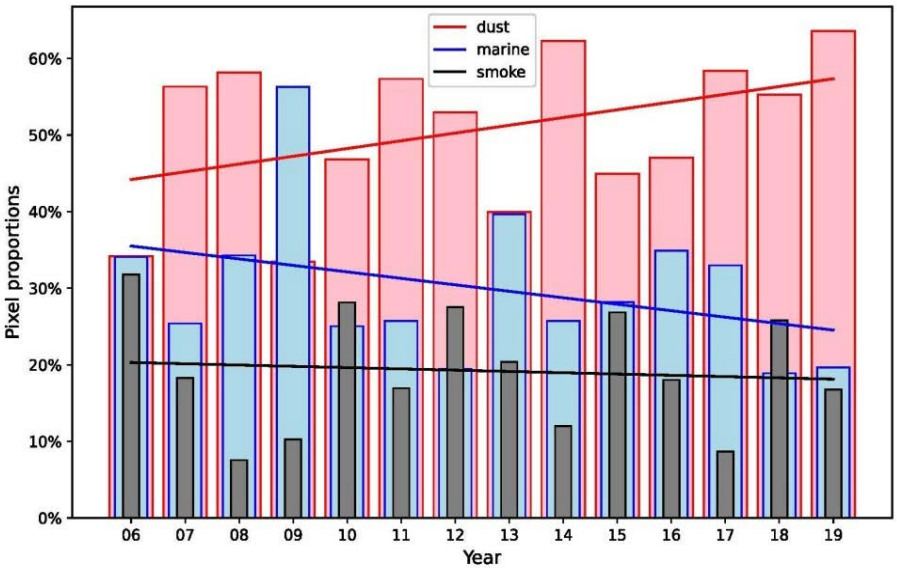

Figure 4: Trend of total pixels classified as smoke (gray), marine (blue) and dust (red). The total is in percentage, in relation to the total value of pixels. The data refer to the CALIPSO satellite's Vertical Feature Mask product. Period 2006 to 2019.

It can be observed that the AOD has a well-defined seasonal behavior. The highest values were observed between August and November. The meteorological stations used as a source of rainfall data are in the central portion and on the periphery of the study area to represent the rainfall behavior throughout the region. Considering the large-scale movements, due to the size of the study area, the pluviometric data points have similar behavior. During this period, there is a transition between the driest months of winter and the beginning of the wettest period of spring [23]. In addition, a secondary peak is also observed in the elevation of optical thickness in May. This month presents a considerable drop in the rate of precipitation and cloudiness. To supplement the analysis conducted using CALIOP sensor data, an additional analysis was performed utilizing the data from the MERRA-2 reanalysis.

In Figure 5, the totals of optical scattering and aerosol volume in the atmosphere can be observed. Notably, the volumes of black and organic carbon exhibit pronounced seasonality, with a substantial difference between the total observed during the dry season (May-September) and the total observed during the wet season (October-March). On the other hand, aerosols of mineral origin do not show significant variation throughout the year. Likewise, sea salt does not display a pronounced seasonal signal, showing peaks in the wet and dry months (summer and spring) and the dry months (autumn and winter). Despite not showing a pronounced seasonal signal, it is present throughout the year in a significant manner, as mapped in the literature.

When examining scattering patterns, it's evident that carbonaceous aerosols exhibit distinct seasonality. In the case of mineral aerosols, their atmospheric volume magnitude doesn't result in significant changes in their optical characteristics. Moreover, the elevated values of pixels classified as black carbon in January can be attributed to their hydrophobic properties [4], as other aerosol types are typically employed as condensation nuclei.

As shown in Figure 5, marine aerosols are the most prevalent in the study area, however, they do not have the most significant impact on the total absolute scattering. On the other hand, carbonaceous aerosols substantially contribute to the seasonal variation in total scattering, with their peak values coinciding with the peaks in the total optical depth variation for atmospheric aerosols. Their substantial variation is due to being more easily removed from the atmosphere by precipitation. Aerosols of mineral origin, in contrast, showed no significant seasonal variation. Another notable characteristic of atmospheric aerosols is that the volume of particulate matter in the atmosphere is not necessarily proportional to their effects on optical depth, as can be observed in Table 3. The table presents the coefficients of variation for the different quantities related to aerosols measured by MERRA-2.

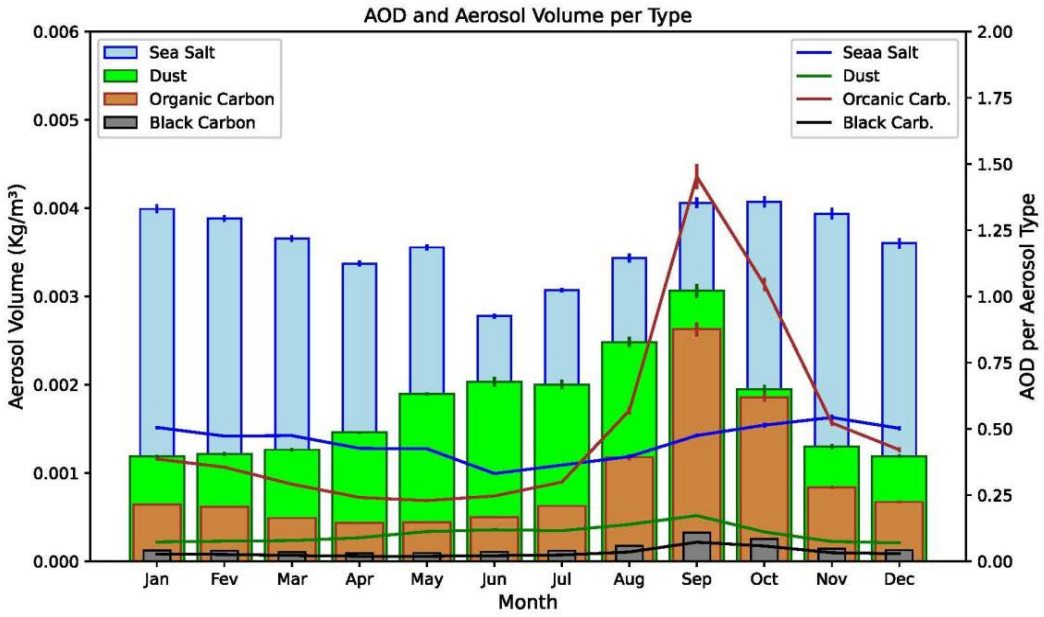

Figure 5: Total volume (bars) and optical thickness (line) for aerosol types. In orange, data refers to organic carbon; in blue, those refer to sea salt; in green, those refer to dust; and in light black, those refer to black carbon. Data are from the MERRA2 reanalysis, with a study period from 2006 to 2019.

Table 3: Annual Variation Coefficient of aerosols optical depths and volume. The data refer to the MERRA-2 aerosols products. Period 2006 to 2019.

Annual Variation Coefficient	
Organic Carbon Optical Depth	3
Black Carbon Optical Depth	0.1
Sea Salt Optical Depth	0.1
Dust Optical Depth	0.1
Organic Carbon	$4.5x10^{-4}$
Black Carbon	$3.1x10^{-5}$
Sea Salt	$4.2x10^{-5}$
Dust	$1.8x10^{-4}$

The seasonality of marine aerosols in the atmosphere is linked to the incursion of sea winds in the study area, as can be seen in Figure 6, which represents the hodography generated from METAR message data from Tom Jobim International Airport in the city of Rio de Janeiro.

In the synoptic context, the position and intensity of the South Atlantic Subtropical Anticyclone (ASAS) system most interfere with the advection of maritime air. In winter, this system is positioned more to the southwest, making the atmosphere of the Southeast Region of Brazil more stable and the winds less intense. In summer, ASAS helps transport particles from the sea to the region [24, 27]. Thus, while the other types of aerosols decrease their concentrations in the atmosphere in the summer due to precipitation, the concentration of sea salt is maintained due to the advection of air coming from the ocean. On a smaller scale, there is a configuration of sea breezes throughout the year, contributing to the incursion of aerosols in the study area.

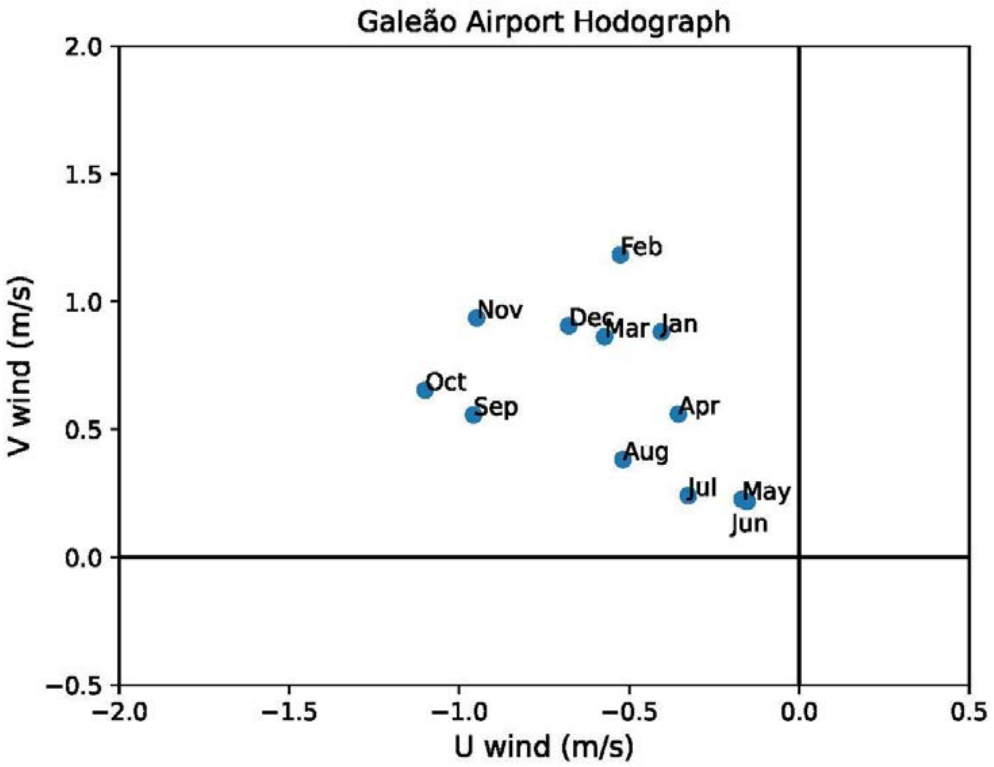

Figure 6: Hodograph of monthly average winds, from 1 to 12, obtained with observed data from METAR, located at Tom Jobim International Airport in Rio de Janeiro, for the sampling period from 2006 to 2019.

To better understand the origin of the different types of aerosols, the HYSPLIT model was used, which made it possible to study the retro trajectories of air masses in the study area.

Figure 7 represents the retrotrajectories of the air masses that ended in the study area. Each of the twelve images refers to the total number of simulations performed each month during the sixteen years of the study period. The retrojectives are grouped into clusters that were divided using the elbow method. There is no apparent connection between the direction and direction of the trajectories with the time of year. What can be seen in the simulations is that there is a trend of increasing advection of sea air in the summer months (DJF). This result was expected since, in the summer months, as previously mentioned, there is a more significant influence of the winds coming from the ASAS. As a result, the atmospheric circulation related to the anticyclone is northeast, mainly wind in the study area, which results in greater advection and, consequently, a greater concentration of sea salt (marine aerosols) during these months.

Similarly, practically half of the simulations had continental coordinates as their starting point in June and July. This result is consistent, considering that the frequency of cold fronts increases in winter. Additionally, the westward shift of the ASAS center extends further into the continent during the summer months [24]. With this configuration of the ASAS, the incursion of the northeast winds in the study area decreases, as indicated in Figures 6 and 7. Consequently diminishing the trajectories that characterize air masses originating from the sea. Thus, there is evidence that the optical thickness peaks that occur in winter are linked to local sources of aerosols.

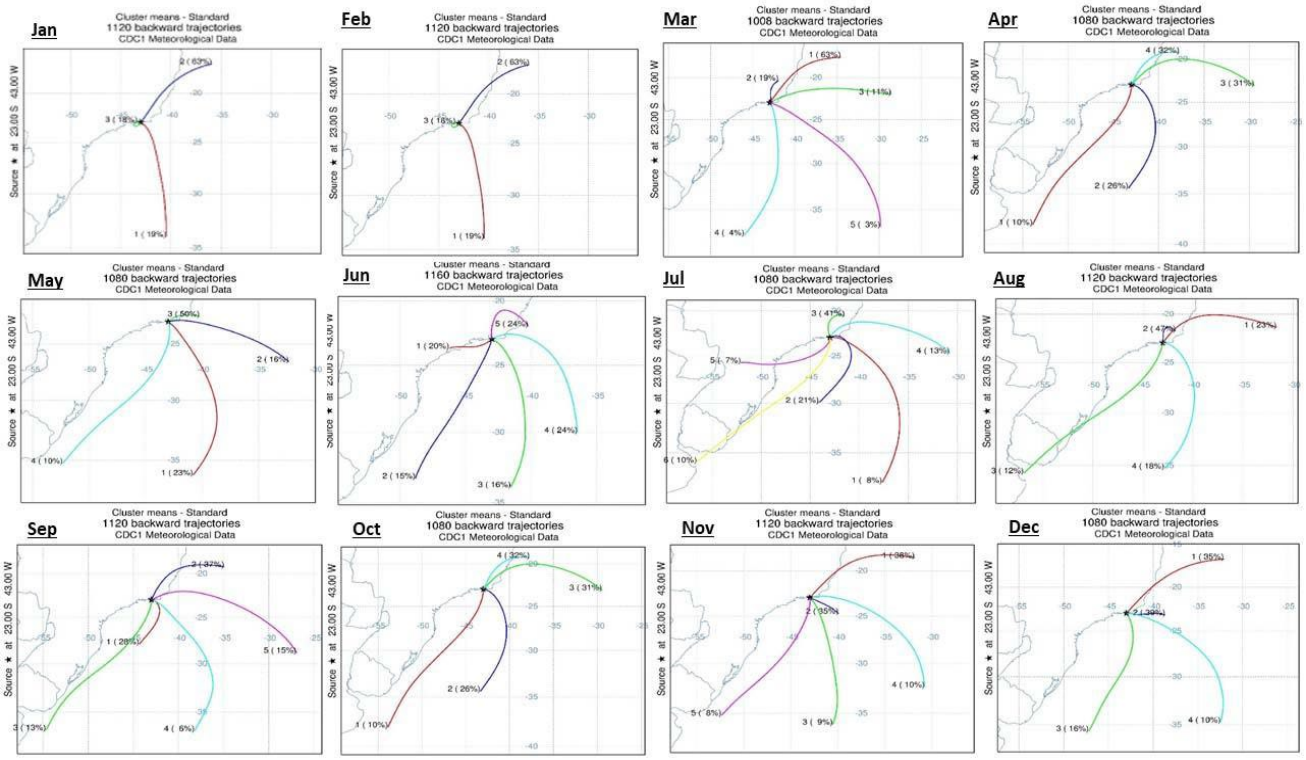

Figure 7: Retrotrajectories clusters of air masses, separated by month (compiled from 2006 to 2019).

As the results showed that the greatest seasonal variations are related to carbonaceous aerosols, commonly produced by burning biomass and fossil combustion, an analysis was performed with data from the MCD64 product from MODIS [22] on the presence of fires near the study area. The standardized anomalies were calculated to generate a more complete analysis of the aerosols, which are shown in Figure 8. The graphs represent the temporal evolution of the standardized anomalies of the density of particulate matter in the atmosphere, separated monthly. Figure 8a shows the curves corresponding to the total thickness of the MERRA-2 reanalysis: Black Carbon, Sea Salt, AOD, and Dust. Figure 7b shows the totals of Black Carbon, AOD of CALIPSO, POLLC (Polluted Continental) of CALIPSO, and Burnt Area of the product MCD64 of MODIS. Finally, in Figure 7c, the pixels classified by the Vertical Feature Mask are represented as POLLC, DUST, and MARINE. This last graph also represents CALIPSO's AOD 532 and AOD 1064. To compare the behavior between the historical series of the data used, a correlation table was built in Table 4. In other words, the matrix supports the evaluation of how the reanalysis represents the atmospheric aerosols with reference to the data observed by the satellite.

The Table 4 shows that the MERRA black carbon has a 94% correlation with the MCD64 fire product and 93% with the aerosols classified as smoke by the CALIPSO satellite. Furthermore, the correlation between CALIPSO smoke and MCD64 is 97%. Therefore, the representation of this type of aerosol seems to be in accordance with the reanalysis. When analyzing the sea salt, there is a negative correlation. In other words, there is no good representation of sea salt by the MERRA-2 reanalysis, considering the CALIPSO VFM data as a validator. The AOD 532 and 1064 correlation with the MERRA-2 AOT 550nm is 77 and 78%, respectively. The correlation value of this quantity is not so high because they are measurements at different wavelengths. The correlation between CALIPSO and MERRA-2 dust products is 78%. Therefore, there is evidence that fire products' representation is better than dust aerosols. It is also necessary to consider that the two products have different methods for classifying each aerosol type.

Table 4: Correlation matrix of CALIPSO, Merra-2, and MODIS MCD64 products. Period 2006 to 2019.

	(1)	(2)	(3)	(4)	(5)	(6)	(7)	(8)	(9)	(10)
MERRA-2										
(1): Black Carbon	1.00	0.53	0.96	0.70	0.93	0.09	0.86	0.77	0.78	0.94
(2): Sea Salt	0.53	1.00	0.70	-0.110	0.45	-0.29	0.38	0.68	0.55	0.48
(3): AOT	0.96	0.70	1.00	0.50	0.86	-0.03	0.76	0.78	0.75	0.87
(4): Dust	0.70	-0.11	0.50	1.00	0.69	0.59	0.78	0.46	0.61	0.66
CALIPSO										
(5): Smoke	0.93	0.45	0.86	0.69	1.00	0.08	0.89	0.76	0.73	0.97
(6): Marine	0.09	-0.29	-0.03	0.59	0.08	1.00	0.39	0.13	0.41	-0.01
(7): Dust	0.86	0.38	0.76	0.78	0.89	0.39	1.00	0.76	0.86	0.82
(8): AOD 532	0.77	0.68	0.78	0.46	0.76	0.13	0.76	1.00	0.84	0.77
(9): AOD 1064	0.78	0.55	0.75	0.61	0.73	0.41	0.86	0.84	1.00	0.71
MCD64										
(10): B. Area	0.94	0.48	0.87	0.66	0.97	-0.01	0.82	0.77	0.71	1.00

In Figure 8, a typical behavior can be observed in all graphs, which is most with higher anomalies between August and October. The highest values of black carbon, smoke, burned area, dust, and optical thickness are found in these months. The only curve that does not behave similarly to the others is that of sea salt, as shown by the two data sources. This type of aerosol has peaks in the dry season, and, in addition, it also has peaks when the center of the ASAS is further away from the continent. Considering the data from the MERRA-2 reanalysis, the dust and sea salt aerosols bear little resemblance to the variation patterns in aerosols' general scattering. While in CALIPSO, despite the correlation with marine aerosols remaining low, dust aerosols have a 76 percent correlation with optical thickness. The two data sources highly correlated with thickness and optical scattering for carbonaceous aerosols. In addition, the number of scars in the burned area also shows a high correlation with the carbonaceous aerosol samples and, consequently, with the mentioned optical properties. This indicates that, in fact, in the study region, the type of aerosol responsible for the main variations in the optical properties of the atmosphere is carbonaceous aerosols. This contribution occurs mainly through emissions from the fires located in the study region itself.

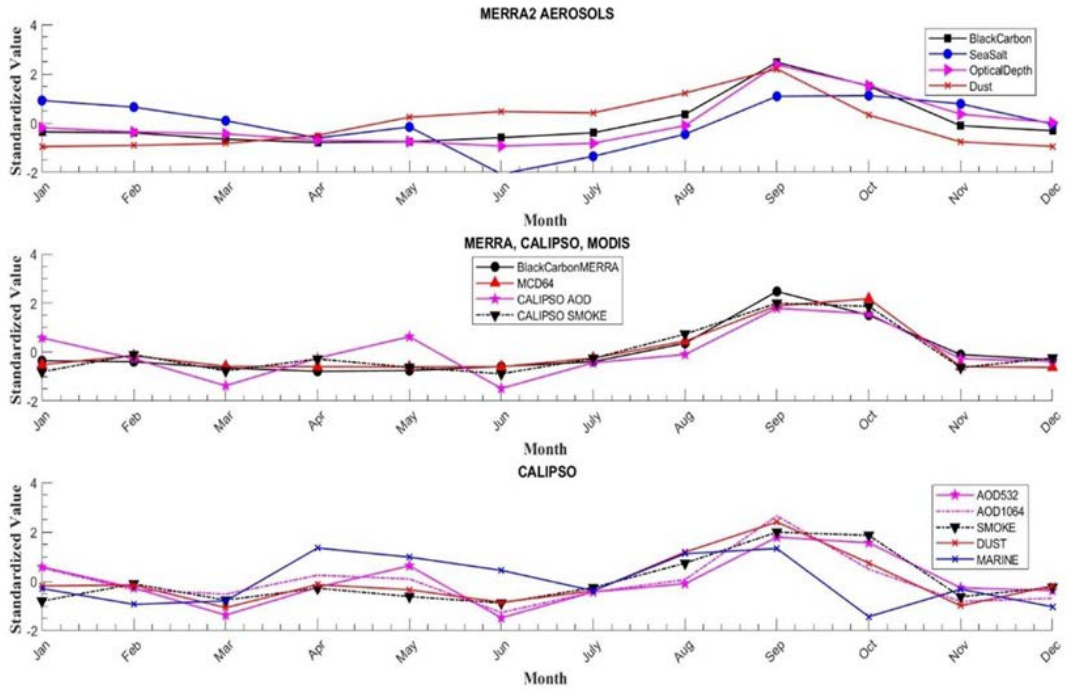

Figure 8: Monthly average standardized anomalies for the period 2006 to 2019, using MERRA-2 data (8a), the comparison between CALIPSO, MERRA, and MODIS data (8b) and CALIPSO data (8c). In Figures 8a and 8c, the colors of the lines represent purple, the aerosol optical thickness data; blue, marine aerosol data; red, dust data; and black, the smoke and/or black carbon data. In Figure 8b, the color black represents the black carbon data from MERRA-2 and the smoke data from the VFM from CALIPSO, the red color represents the burned area data from MCD64, and, in purple, the optical thickness data from the CALIPSO aerosols.

IV. Conclusion

This study aimed to conduct a temporal analysis of the primary aerosol characterization in a region centered on the Metropolitan Region of Rio de Janeiro, Brazil, examining their origin based on air mass back trajectories. The chosen study area is Brazil's second-largest conurbation and the country's second-most economically important region. Moreover, it is a region near the Atlantic coast with considerable ecological diversity. It has utilized remote sensing data from the CALIOP (Cloud-Aerosol Lidar with Orthogonal Polarization) sensor aboard the CALIPSO satellite. CALIOP stands out as one of the primary remote observation instruments for aerosol studies. In addition to this, it has incorporated data from the Modern-Era Retrospective Analysis Version 2 (MERRA-2) reanalysis to complement our analysis. MERRA-2 considers various physical processes involving aerosols. Simulations were conducted using the Hybrid Single Particle Lagrangian Integrated Trajectory (HYSPLIT) model for tracking air masses and gaining insight into their origins, which transport these particles.

Furthermore, data from the Moderate Resolution Imaging Spectroradiometer (MODIS) sensor, with high-resolution products for fire studies, were integrated into the analysis. The study period, spanning from 2006 to 2019, was chosen primarily due to the availability of CALIOP sensor data, which commenced its operations in 2006 and extends until 2019, the year preceding the suspension of activities due to the COVID-19 pandemic.

From a meteorological perspective, this period was marked by a drier spell compared to the climatology of the area located further northeast of the region (Campos dos Goytacazes station). In the western region (Resende station), the average precipitation closely adhered to the climatological precipitation pattern.

It was observed that AOD has a well-defined seasonal behavior. The highest values were observed between August and November, with a peak of 0.15 in September, the transition period between the driest months of winter and the beginning of the wettest period of spring. A secondary peak was also observed, with a value of 0.10 in the optical thickness values in May, a month that presents a considerable drop in the average precipitation rate.

The results show that the pixels classified as dust are the most common after the marine aerosols, reaching total values above the marine during Jan (39.7%), Feb (48.2%), Jul (44.4%), and Dec (54.1%) months. They represent all types of mineral particles originating from the erosion processes of rocks and soil, which are suspended in the atmosphere. Pixels classified as marine aerosols represent a large part of the classifications, exceeding 40 percent in 7 of the 12 months of the year, and smoke is more important during Aug (34.7%).

The standard error for all data was calculated as it represents a critical measure for understanding the variability and precision of statistical estimates. The values obtained for the standard error are minimal, which indicates the more reliable the estimate.

From the CALIOP sensor data, the trend in the proportion of these aerosols during the study period shows that the proportion of dust has increased significantly over this period compared to the presence of marine aerosols and smoke. These results align with other studies, which demonstrated that this region has been experiencing increased aridity throughout nearly all months of the year, leading to a concurrent rise in diffuse solar radiation, particularly during the dry season. What was also observed in this study were the highest AOD values during the dry season.

It has shown that each type of aerosol contributes differently to the optical thickness of the atmosphere. Marine aerosols are the most present in the study area. However, they are not the ones that most impact the total amount and absolute seasonality of the total scattering. The variation throughout the year in the amount of marine aerosols is linked to the incursion of sea winds in the study area, particularly the position and intensity of the South Atlantic Subtropical High (ASAS). In addition, sea salt aerosols need a better atmospheric representation by the MERRA2 reanalysis compared to the data observed by the CALIPSO satellite.

On the other hand, carbonaceous aerosols have the highest coefficients of variation among the optical thicknesses listed, even with lower absolute volumes. What it indicates that it is the type of particulate that most contributes to changes in optical characteristics in the study area during the year. Dust aerosols also show well-evidenced seasonality. In addition to the local source, they are brought by continental trajectories and are more present in winter, with the lowest precipitation rates. In this period, the Subtropical High of the South Atlantic is more evident. With a more significant continental portion, therefore, the winter values of this type of aerosol are higher. Contrasting this idea, the trajectories analyzed in the study period (2006-2019) indicate a more significant predominance in the northeast direction in the summer months. The study of retro trajectories made it possible to identify that the optical thickness peaks that occur in winter are linked to local sources of aerosols. As the results showed the carbonaceous aerosols presenting the most significant seasonal variations, it was possible to conclude through the analysis of data from burned areas (MD64 from MODIS), that the origin of these aerosols is linked to biomass burning and fossil combustion in the study region, as observed through the correlations between the black carbon series, MCD64, and optical thickness. Therefore, the type of

aerosol that most impacts the seasonality of the optical properties of the atmosphere over the Rio de Janeiro Region is carbonaceous aerosols. Everything indicates that emissions are governed by the distribution of fires throughout the year in the study area and other biomes. In addition, sea salt aerosols are the most common in the region during most of the year.

The use of CALIPSO satellite data provides a detailed analysis of aerosol presence in the atmosphere. Its classification is based on algorithms considering Particle Depolarization Ratio, Layer-Integrated Attenuated Backscatter, and Layer Top and Base Altitudes. This study used only aerosol types with the highest classification levels, including marine, dust, and smoke. Other aerosol types, such as polluted continental, clean continental, and polluted dust, did not exhibit significant levels and were therefore omitted.

Remote sensing data allows for better spatial coverage. However, some local events may be missed due to its temporal coverage of one pass every 16 days. The results indicate that in the study area, despite being a coastal region with relatively dense vegetation, dust particles have been increasing over the past few years. This is likely due to reduced precipitation rates, which allow particles to linger in the atmosphere for extended periods, and wind erosion that injects soil particles from the surface into the atmosphere due to disorganized urban infrastructure.

These totals and proportions are crucial for modeling the physical processes of the atmosphere and aerosol-cloud interaction. They play a significant role in understanding energy and the hydrological cycle in the Rio de Janeiro region, allowing for more realistic data in weather and climate modeling.

Future work should include vertical profiles of aerosols and the use of data from new satellites such as the Sentinel series.

Funding

The authors declare that no funds, grants, or other support were received during the preparation of this manuscript.

Author Contributions

Filipe Pungirum and José Ricardo de Almeida França wrote and structured the entire article, generated the manuscript figures, and analyzed the results. Edson Pereira Marques Filho collaborated with exploring climate data and revised the paper.

Data Availability

The datasets generated during and/or analyzed during the current study are available from the organization that maintains the data on reasonable request.

Conflicts of Interest

The authors declare that they have no known competing financial interests or personal relationships that could have appeared to influence the work reported in this paper.

References Références Referencias

1. Pathak, B., Kalita, G., Bhuyan, K., Bhuyan, P.K., Moorthy, K.K.: Aerosol temporal characteristics and its impact on shortwave radiative forcing at a location in the Northeast of India. Journal of Geophysical Research Atmospheres 115 (19), 1–14 (2010). https://doi.org/10.1029/ 2009JD013462
2. Lamb, D., Verlinde, J.: Physics and Chemistry of Clouds, (2011). https://doi.org/10.1017/CBO97805 11976377
3. Ramanathan, V., Crutzen, P.J., Kiehl, J.T., Rosenfeld, D.: Aerosols, Climate, and the Hydrological Cycle 294 (5549), 2119–2124 (2016).
4. McMeeking, G.R., Good, N., Petters, M.D., McFiggans, G., Coe, H.: Influences on the fraction of hydrophobic and hydrophilic black carbon in the atmosphere. Atmospheric Chemistry and Physics 11 (10), 5099–5112 (2011). https://doi.org/10.5194/ acp-11-5099-2011
5. Zhao, Z., Cao, J., Shen, Z., Xu, B., Zhu, C., Chen, L.W.A., Su, X., Liu, S., Han, Y., Wang, G., Ho, K.: Aerosol particles at a high-altitude site on the Southeast Tibetan Plateau, China: Implications for pollution transport from South Asia. Journal of Geophysical Research Atmospheres 118 (19), 11360–11375 (2013). https://doi.org/10.1002/jgrd. 50599
6. Hoose, C., Mohler, O.: Heterogeneous Ice Nucleation on Atmospheric Aerosols: A Review of Results from Laboratory Experiments vol. 12, pp. 9817–9854 (2012). https://doi.org/10.5194/acp-12-9817-2012
7. Khain, A., Lynn, B., Dudhia, J.: Aerosol Effects on Intensity of Land- falling Hurricanes as Seen from Simulations with the WRF Model with Spectral Bin Microphysics. Journal of the Atmospheric Sciences 67 (2), 365–384 (2010). https://doi.org/10.1175/20 09JAS3210.1
8. Das, S., Dey, S., Dash, S.K., Giuliani, G., Solmon, F.: Dust aerosol feedback on the Indian summer monsoon: Sensitivity to absorption property. Journal of Geophysical Research: Atmospheres 120 (18), 9642–9652 (2015). https://doi.org/10.1002/2015JD 023589
9. N'Datchoh, E.T., Diallo, I., Konaré, A., Silué, S., Ogunjobi, K.O., Diedhiou, A., Doumbia, M.: Dust induced changes on the West African summer monsoon features. International Journal of Climatology 38 (1), 452–466 (2018). https://doi.org/ 10.1002/joc.5187
10. Korhonen, H., Carslaw, K.S., Forster, P.M., Mikkonen, S., Gordon, N.D., Kokkola, H.: Aerosol climate feedback due to decadal increases in

southern hemisphere wind speeds. Geophysical Research Letters 37 (2), 0–5 (2010). https://doi.org/10.1029/2009GL041320
11. Winker, D.M., Vaughan, M.A., Omar, A., Hu, Y., Powell, K.A., Liu, Z., Hunt, W.H., Young, S.A.: Overview of the CALIPSO Mission and CALIOP Data Processing Algorithms. Journal of Atmospheric and Oceanic Technology 26 (11), 2310–2323 (2009). https://doi.org/10.1175/ 2009JTECHA1281.1
12. Tian, P., Cao, X., Zhang, L., Sun, N., Sun, L., Logan, T., Shi, J., Wang, Y., Ji, Y., Lin, Y., Huang, Z., Zhou, T., Shi, Y., Zhang, R.: Aerosol vertical distribution and optical properties over China from long-term satellite and ground-based remote sensing. Atmospheric Chemistry and Physics 17 (4), 2509–2523 (2017). https://doi.org/10.5194/acp-17-2509-2017
13. Kim, M-H., Omar, A.H., Tackett, J.L., Vaughan, M.A., Winker, D.M., Trepte, C.R., Hu, Y., Liu, Z., Poole, L.R., Pitts, M.C., Kar, J., Magill, B.E.: The CALIPSO Version 4 Automated Aerosol Classification and Lidar Ratio Selection Algorithm. Atmos. Meas. Tech. Discuss, June 2018 (2018). https://doi.org/10.5194/amt-2018-166.
14. Rienecker, M.M., Suarez, M.J., Gelaro, R., Todling, R., Bacmeister, J., Liu, E., Bosilovich, M.G., Schubert, S.D., Takacs, L., Kim, G.K., Bloom, S., Chen, J., Collins, D., Conaty, A., Da Silva, A., Gu, W., Joiner, J., Koster, R.D., Lucchesi, R., Molod, A., Owens, T., Pawson, S., Pegion, P., Redder, C.R., Reichle, R., Robertson, F.R., Ruddick, A.G., Sienkiewicz, M., Woollen, J.: MERRA: NASA's modern-era retrospective analysis for research and applications. Journal of Climate 24(14), 3624–3648 (2011). https://doi.org/10.1175/JCLI-D-11-00015.1
15. Stein, A.F., Draxler, R.R., Rolph, G.D., Stunder, B.J.B., Cohen, M.D., Ngan, F.: Noaa's hysplit atmospheric transport and dispersion modeling system. Bulletin of the American Meteorological Society 96 (12), 2059– 2077 (2015). https://doi.org/10.1175/BAMS-D-14-00110.1
16. Kinoshita, N., Sueki, K., Sasa, K., Kitagawa, J., Ikarashi, S., Nishimura, T., Wong, Y.-S., Satou, Y., Handa, K., Takahashi, T., Sato, M., Yamagata, T.: Assessment of individual radionuclide distributions from the Fukushima nuclear accident covering central-east Japan. Proceedings of the National Academy of Sciences 108 (49), 19526–19529 (2011). https://doi.org/10.1073/pnas.1111724108
17. Rolph, G.D., Draxler, R.R., Stein, A.F., Taylor, A., Ruminski, M.G., Kondragunta, S., Zeng, J., Huang, H.-C., Manikin, G., McQueen, J.T., Davidson, P.M.: Description and Verification of the NOAA Smoke Fore- casting System: The 2007 Fire Season. Weather and Forecasting 24 (2), 361–378 (2009). https://doi.org/10.1175/2008WAF2222165.1
18. Efstathiou, C., Isukapalli, S., Georgopoulos, P.: A mechanistic modeling system for estimating large-scale emissions and transport of pollen and co-allergens. Atmospheric Environment 45 (13), 2260–2276 (2011). https://doi.org/10.1016/j.atmosenv.2010.12.008
19. Stunder, B.J.B., Heffter, J.L., Draxler, R. R.: Airborne Volcanic Ash Fore- cast Area Reliability. Weather and Forecasting 22 (5), 1132–1139 (2007). https://doi.org/10.1175/WAF1042.1
20. Yu, H., Chin, M., Yuan, T., Bian, H., Remer, L.A., Prospero, J.M., Omar, A., Winker, D., Yang, Y., Zhang, Y., Zhang, Z., Zhao, C.: The fertilizing role of African dust in the Amazon rainforest: A first multiyear assessment based on data from Cloud-Aerosol Lidar and Infrared Pathfinder Satellite Observations. Geophysical Research Letters 42 (6), 1984–1991 (2015). https://doi.org/10.1002/2015GL063040
21. Kanamitsu, M., Ebisuzaki, W., Woollen, J., Yang, S.-K., Hnilo, J.J., Fiorino, M., Potter, G.L.: NCEP-DOE AMIP-II Reanalysis (R-2). Bul- letin of the American Meteorological Society 83 (11), 1631–1643 (2002). https://doi.org/10.1175/BAMS-83-11
22. Giglio, L., Werf, G.R.V.D., Randerson, J.T., Collatz, G.J., Kasibhatla, P.: and Physics Global estimation of burned area using MODIS active fire observations (1), 957–974 (2006)
23. Pristo, M.V.J., Dereczynski, C.P., de Souza, P.R., Menezes, W.F.: Climatologia de Chuvas Intensas no Município do Rio de Janeiro. Revista Brasileira de Meteorologia 33 (4), 615–630 (2018). https://doi.org/10.1590/0102-7786334005
24. Bastos, C.C., Ferreira, N.J.: Análise Climatológica da Alta Subtropical do Atlântico Sul. Anais do Congresso Brasileiro de Meteorologia, 612–619 (2008).
25. Pimentel, L.C.G., Marton, E., da Silva, M.S., Jourdan, P.: Caracterização do regime de vento em superfície na região Metropolitana do Rio de Janeiro. Engenharia Sanitária e Ambiental 19 (2), 121–132 (2014). https://doi.org/10.1590/S1413-41522014000200003
26. Marques Filho, E.P., Oliveira, A.P., Vita, W.A., Mesquita, F.L.L., Codato, G., Escobedo, J.F., Cassol, M., França, J.R.A.: Global, diffuse and direct solar radiation at the surface in the city of Rio de Janeiro: Observational characterization and empirical modeling. Renewable Energy, 91, 64-74 (2016). https://doi.org/10.1016/j.renene.2016.01.040
27. Dereczynski, C.P., Oliveira, J.S., Machado, C.O.: Climatologia da precipitação no município do Rio de Janeiro. Revista Brasileira de Meteorologia 24 (1), 24–38 (2009). https://doi.org/10.1590/ S0102-77862009000100003

This page is intentionally left blank

Global Journal of human-social science: b
Geography, Geo-Sciences, Environmental Science & Disaster Management
Volume 23 Issue 5 Version 1.0 Year 2023
Type: Double Blind Peer Reviewed International Research Journal
Publisher: Global Journals
Online ISSN: 2249-460x & Print ISSN: 0975-587X

Morphotectonic Processes in Seismic Zones of ModerateIntensity, Argentina

By Adolfo Antonio Gutiérrez
Universidad Nacional de Tucumán

Abstract- This study deals with the neotectonic deformation in seismic zones of moderate intensity in some areas of the Sierras Pampeanas, Santa Bárbara System and Chaqueña Plain of Argentina. In the study region, the location of earthquakes of ≥ three, ≥ four, and ≥ six Richter magnitudes agree with the traces of regional faults, evidencing their neotectonic activity. Seismic energy is generally transmitted over inherited faults, such as in the Metan basin. Minor new faults occur in Quaternary terraced deposits, and others move, taking advantage of the Neogene sedimentary strata. The folds are generally buried, but the younger sequences are gently undulating. The seismic energy dissipated through fewer cohesion materials that form the valleys' fill, developing discrete fault scarps and strongly folded conglomerate strata. The foothills deposits and basins absorbed most of the seismic energy released during the reactivation of the faults. Tectonic activity is deforming 630 BP deposits in the Cumbres Calchaquíes piedmont.

Keywords: *neotectonics. earthquakes. andean foreland. natural hazards.*

GJHSS-B Classification: *LCC: QE521-545*

Strictly as per the compliance and regulations of:

Morphotectonic Processes in Seismic Zones of Moderate Intensity, Argentina

Adolfo Antonio Gutiérrez

Abstract- This study deals with the neotectonic deformation in seismic zones of moderate intensity in some areas of the Sierras Pampeanas, Santa Bárbara System and Chaqueña Plain of Argentina. In the study region, the location of earthquakes of≥ three, ≥ four, and ≥ six Richter magnitudes agree with the traces of regional faults, evidencing their neotectonic activity. Seismic energy is generally transmitted over inherited faults, such as in the Metan basin. Minor new faults occur in Quaternary terraced deposits, and others move, taking advantage of the Neogene sedimentary strata. The folds are generally buried, but the younger sequences are gently undulating. The seismic energy dissipated through fewer cohesion materials that form the valleys' fill, developing discrete fault scarps and strongly folded conglomerate strata. The foothills deposits and basins absorbed most of the seismic energy released during the reactivation of the faults. Tectonic activity is deforming 630 BP deposits in the Cumbres Calchaquíes piedmont. Considering deformation values, neotectonic deformation in the outcrops and seismic profiles evidence, it is possible to interpret that the seismic activity in the study area from the Pleistocene to the present remained between the current records. This seismic activity, sustained over time, is sufficient to produce deformation in the foothills, reactivate pre-existing faults with small displacements and generate minor new faults in recent conglomeratic deposits. Many faults are blind. However, the deformation of the landscape and the modification of the drainage network are direct indicators of the activity of these structures.

Keywords: neotectonics. earthquakes. andean foreland. natural hazards.

I. Introduction

The deformation of the Andean foreland by neotectonics processes has been treated extensively in the literature. This evidence the interest of the scientific community in understanding tectonic rotations, the direction of tectonic shortening, depths of the detachment of the main structures, the position of the front deformation, vergence of the structures, seismic activity associated with the movements of the faults and deformations of the mountain fronts.

In the plate tectonics context, subjected to compressive stress with NE strike during the Cenozoic, the study area coincides with the latitude where the Nazca plates change the angle dip, high angle north of 27° S and the low angle at south (Schwanghart and Scherler, 2014; Somoza and Ghidella, 2005) (Figure 1). Strecker et al. (1989) and Mon (1993) agree that the faults that raise the edges of the mountain ranges could be reactivated Palaeozoic structures. Marrett et al. (1994) document for northwestern Argentina two kinematic regimes that characterise the late Cenozoic deformation, a WNW shortening and a strike-slip phase with ENE shortening. The tectonic deformation that was active since the Middle Eocene (Del Papa et al., 2005) was migrating from the Puna towards the east (Carrapa et al., 2005; Deeken et al., 2006; Carrapa and De Celles, 2015), modifying, in the Miocene, the drainage network of the western edge of the Eastern Cordillera (Jordan and Alonso, 1987; Starck and Vergani, 1996; Carrera and Muñoz, 2008; Carrapa et al., 2011; Pearson et al., 2013).

An approximation of the evolution of neotectonic deformation in the Eastern Cordillera is obtained by recording GPS (Global Positioning System) speeds that decrease from 10 to 4 mm/yr (McFarland and Bennett, 2017). Other authors also estimated the rates of shortening in the region. Echavarria et al. (2003) obtained shortening rates for the Quaternary of the Sub-Andean System of Argentina between 8 and 11 mm/yr. Pearson et al. (2013) calculated the shortening rates at latitude 25-26° S and obtained averages of 6.5 mm/y from 12 to 4 Ma and 3.6 mm/y from 4 Ma to the Holocene. Uplift rates for the Late Pleistocene–Holocene were determined by (García et al., 2013; García et al., 2019) obtaining values of 0.3 to 0.7 mm/yr in the Lerma Valley. In the Lomas de Olmedo, shortening rates of 2.34 mm/yr for most of the Holocene was calculated (Ramos et al., 2006). According to the seismic classification for Argentina, based on studies carried out until 1983, except for the areas surrounding the cities of Salta and San Salvador de Jujuy, the north and a large part of the Sierras Pampeanas are in Zone 2 of moderate danger and Chaqueña Plain in Zone 1 reduced risk (INPRES, 2018).

Author: Facultad de Ciencias Naturales e IML, Universidad Nacional de Tucumán, Miguel Lillo 205,4000 San Miguel de Tucumán, Argentina.
e-mail: gutierrez.aa@hotmail.com

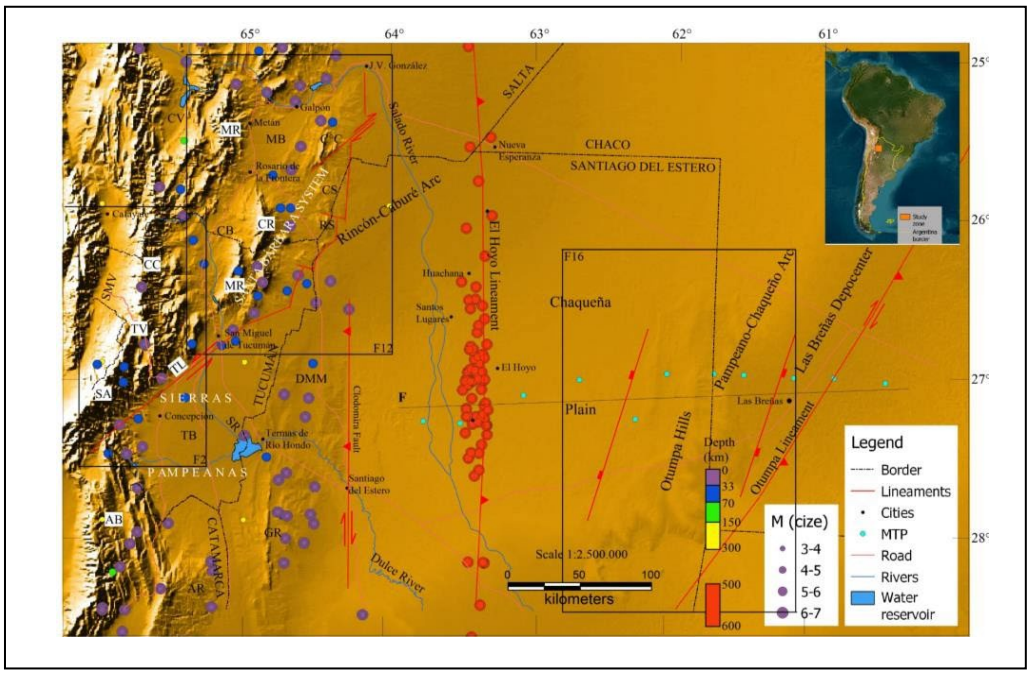

Figure 1: Regional location of the study area. The morphotectonic map shows the significant orographic units and the regional structures that mark the contact between the Andean front and the Chacopampeana Plain. MTP: Magnetotelluric profile. With coloured circles, the epicentres ofthe earthquakes are located. The depth of the earthquakes is indicated with a colour scale, and their magnitudes with grey circles. A box with black lines indicates the location of the figures (F12). CV: Calchaquí Valley. MR: Metán Range. MB: Metán Basin. C°C: Cerro Colorado. CC: Cumbres Calchaquíes. CB: Choromoro Basin. CR: La Candelaria Range. MR: Medina Range. SMV: Santa María Valley. TV: Tafi Valley. SA: Sierra de Aconquija. TL: Tucumán Lineament. SR: SalíRiver. DMM: Dorsal Mujer Muerta. TB: Tucumán Basin. AB: Ambato Block. AR: Ancasti Range. F: Profile, Figure 19.

In the seismogenic region of the continental crust (15–18 km), earthquakes produce an episodic rigid frictional deformation (Sibson, 1982; Scholz, 2002) whose rupture by propagation during deformation is controlled by the anisotropic fabric at the cortical scale (Allen and Shaw, 2011). When an earthquake is generated, oscillations occur in existing faults or, less frequently, in new faults (Scholz, 2002; Brace and Byerlee, 1966), the elastic stress accumulating in the rocks surrounding the fault zone until the resulting stress in the plane exceeds its frictional resistance and failure occurs (Fagereng and Toy, 2011).

The conditions of the shear stress (rf) at which the failure is going to slip are indicated bythe equation (Eq. (1)):

$$rf = C^{\circ} + \mu_S(\sigma n - Pf), \quad (1)$$

Where C° is the cohesion force, μ_S is the coefficient of static friction, σn is normal effort, and Pf is the fluid pressure (Fagereng and Toy, 2011), high fluid pressures would favour the reactivation of faults, reducing the cohesion force (Nortje et al., 2011). However, for new faults to form in a region where faults already exist, it is required that those old faults develop sufficient cohesion and have insufficient fluid pressure in the pores in such a way as to prevent them from reactivating, even with favourable orientations (Nortje et al., 2011). It was also suggested that themigration of the fault activity towards the foothills is due to the cessation of movement of the faults of the mountain fronts, with these new structures inheriting the style of the primary faults (Costa, 2019). Most earthquakes result from increased shear displacement in the fault (Ambraseys and Tchalenko, 1969), generating rupture and slip that are roughly related to the magnitude of the earthquake (Wells and Coppersmith, 1994; Hanks and Kanamori, 1979) (Table 1).

Zeckra (2020) installed a temporary seismic network in the Santa Bárbara System and discovered high seismic activity confined along the Andean thrust front. The catalogue of locations of primary hypocenters, with a magnitude of completion MC 1.45, allowed him to interpret the distribution of events along steep and deep thrust faults generated through the inversion of Cretaceous normal faults.

Table 1: Approximate source parameters for different magnitude earthquakes (partial magnitudes), with average stress drop (3 MPa) over a circular rupture [Length (L) = Width (W)] (Fagereng and Toy, 2011; Wells and Coppersmith, 1994).

Magnitude of Mw	Average slip (cm)	L=W
5	10	3 km
4	3	1 km
3	1	30 m

Our work shows the differential deformation in the mountain front due to the propagation of seismic energy through basins, foothills deposits, and fault reactivations. The cohesion of the geological material is considered relevant for the propagation of the seismic energy produced by the activity of the faults. The moderate seismic energy transmitted by the faults, but sustained over time, is sufficient to make morphostructural changes in the landscape. This moderate energy is transferred and generates changes in less cohesive materials. This moderate energy was maintained with magnitudes similar to those in the study region, probably since the Pleistocene. We take as examples the neotectonic activity in the north of Sierras Pampeanas (Tafí and Amaicha valleys and the structural relationship between the Cumbres Calchaquíes and Sierra de Aconquija), Santa Bárbara System (Cerro Colorado, Metán basin, La Candelaria Range, and Choromoro basin), and the Chaqueña Plain (Otumpa Hills) (Figure 1).

Different effects of seismic wave propagation are observed in the study area. We shownew structures with vertical and horizontal components and fold morphologies generated in allthese areas. They occur in basins and the foothills, close to regional structures on the mountain front. Other recent and recurrent evidence of tectonic activity in the region is river captures (Gutiérrez et al., 2003), landslides, and retrograde erosion. We observe that earthquakes are aligned with regional structures.

II. Methodology

The research was carried out based on the collection of bibliographic antecedents, interpretation of satellite images, and field data surveys. To develop thematic cartography, the visual and digital interpretation of satellite images LANDSAT 8, SENTINEL 1, and RADARSAT was carried out. The digital treatment for the visual interpretation of the LANDSAT and SENTINEL images consisted of combining different bands. All satellite and radar images were interpreted using the QGis software; then, thematic maps were drawn. To prepare the topographic profiles, we used high-resolution digital elevation models (12.5 m) provided by the ALOS PALSAR mission. During fieldwork, the surfaces deformed by neotectonic processes were identified (fault steps, landslide zones, deformed foothills, whale-back morphologies in alluvial fans, erosion of conglomerate terraces, and transport of rolling by surface drainage, development of drainage networks as indicators of deformation) and data on the structures that generated these morphologies were collected. We collect information on the seismicity around the study area, recording only earthquakes with magnitudes between 2 and 7 (IRIS, 2020) (Figure 1). Four earthquakes of magnitude ≥ six were recorded at 0 to 33 km depths. And eight at 500 to 600 km (Table 2) (Figure 1). Between 300 and 500 km deep, a zone of seismic silence is observed (Table 2).

Table 2: Seismic frequency of occurrence.

Depth (km)	Total	Magnitude of Mw
0-33	68	3.3 - 6.12
33-70	33	4.0 - 5.9
70-150	2	4.3
150-300	4	2.2 - 3.0
300-500	Silence	---
500-600	76	3.8 - 6.9

III. Regional Tectonic Mophology

In the north of the Sierras Pampeanas, the Sierra de Aconquija and Cumbres Calchaquíesseem to have formed a single mountain block with an NNE strike and slightly curved, concave towards the west. It has been raised by high-angle, double-vergent, reverse faults on both edges (Lavenu, 2006; Cristallini et al., 2004), Cumbres Calchaquíes and Aconquija faults on the western border and Periquillo fault on the eastern boundary (Figure 2).

Probably in the Pleistocene, the drainage system developed on the eastern edge of the Cumbres Calchaquíes, Sierra de Aconquija, and Ambato block had an approximate general direction towards the east and ended in the Chaco plain, covering a large area of surface runoff, maintaining the contribution of coarse sediments by the continuous uplift of the mountain systemand appropriate climatic conditions (Gutiérrez et al., 2003). The records of these hydrogeological processes are the thick conglomerate deposits arranged in the upper parts of the Los Sosa River terraces, eroded by the current surface runoff. Later, with the progress of tectonic activity, this drainage system completely eroded, configuring the current network (Gutiérrez et al., 2003).

In the Santa Bárbara System, the mountainous belt shows two sections: the northern one with thick Cretaceous sequences and the southern one with no Cretaceous layers, and the Tertiary lies directly on Paleozoic rocks (Figure 1). The evolution of this part of the Santa Bárbara System began in the middle Eocene, coinciding with a tectonic pillar that was already elevated at this time. The Andean shortening in the last 5 Ma caused a NE strike fault generating dextral displacements that, in turn, originated complex structures. To the west, the Metán Basin and the Choromoro Valley separate it from the Eastern Cordillera and Sierras Pampeanas. To the east, the Chaco Plain extends (Mon and Gutiérrez, 2007).

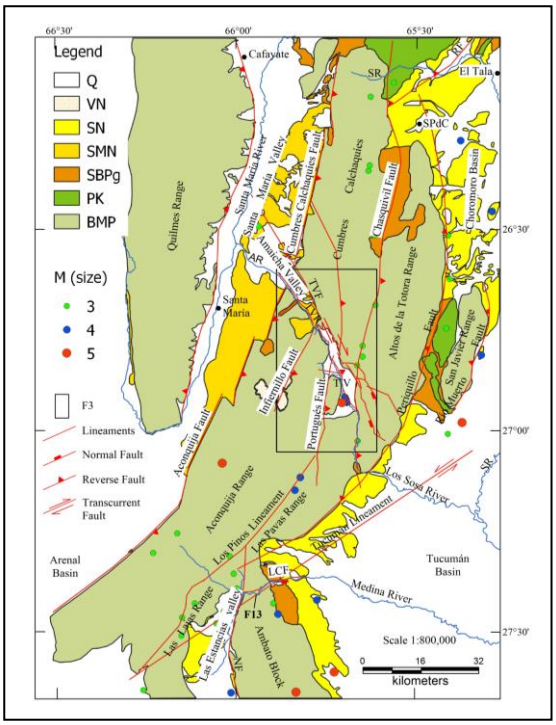

Figure 2: Morphotectonic map of the Sierra de Aconquija and Cumbres Calchaquíes. It shows the depressions of Tafí and Amaicha and the regional structures that gave rise to them. In addition, they do indicate the larger geological units that condition the fracturing that gave rise to the valleys. The location of seismic epicentres and their magnitudes are shown. Q: Fluvio-eolian deposits, Quaternary. VN: volcanic rocks, Neogene. SN: Sedimentary, Neogene. SMN: Santa María Group, Neogene. SBP: Santa Bárbara Subgroup, Paleogene. PK: Pirgua Subgroup, Cretaceous. BMP: Metamorphic Basement, Proterozoic. 3, 4, and 5M: Seismic magnitude. SR: Salí River. SPdC: San Pedro de Colalao. RF: Rearte Fault. AR: Amaicha River. TVF: Tafí del Valle Fault. TVR: Tafí del Valle River. TV: Tafí Valley. LCF: Las Cañas Fault. F3: Figure 3 location. F13: Figure 13 location.

The Chaqueña Plain's sedimentary basin constitutes the Andean front's foothills. The topographic relief rises just 200 m a.s.l. in the Otumpa Hills (Figure 1). Towards the southeast, the Pampean-Chaqueño Arc stands out, which rises above the Las Breñas Basin with the Otumpa Lineament (Figure 1) (Pezzi and Mozetic, 1989; Chebli et al., 1999). With the magnetotelluric data obtained, Pomposiello et al. (2010) interpret that the marked lateral discontinuity observed in the resistivity model could represent the boundary between the Río de la Plata craton and the Pampean terrane or another Precambrian cratonic fragment (Figure 1). In the central western zone of the Chaqueña Plain, there is an N-S strip of seismic epicentres of more than 500 km in length, originating between 500 and 600 km in depth (Figure 1). It is the highest seismic frequency in the study area and where the most intense earthquakes occur (Table 2). Peri (2012) hypothesises that these earthquakes are linked to the presence of the Pacific slab at depth (Figure 1). Based on the marked N-S linearity of these seismic epicentres and the coincidence with one of the high resistivity zones of the 2D magnetotelluric model (Pomposiello et al., 2010), the existence of a blind structure El Hoyo Lineament was interpreted (Figure 1).

IV. Quaternary Deformations

Numerous works document the recent tectonic activity in the Geological Provinces of Argentina that occur in the foothills, in the intra and intermontane basins, or also refer to the geological processes triggered on the mountain fronts by active seismic activity, such as landslides in the slopes of the mountains, formation of dikes by obstruction of rivers, etc. The earthquake rupture zone is not located in the central fault zone of the mountain front but on theflank of the mountain range (Kamb et al., 1971), in a new fault zone called FAF (frontal active fault/flexure) that is generated due to the marked difference in stiffness between the piedmont and basement deposits (Costa, 2019; Ikeda, 1983).

On the southeastern edge of the Precordillera, the Neogene strata ride on quaternary deposits of the foothills of the mountain front and, in the Sierra Chica de Córdoba, Sierras Pampeanas, the most recent deformations linked to the Sierra Chica fault system is not located in the topographic break of the mountain slope, but usually appear associated with a secondary structure (Costa, 2000; Costa et al., 2014; Costa, 2019;). The topographic growth in the sedimentary basins on the eastern edge of the Sierras Pampeanas shows the progressive deformation towards the east, obstructing and diverting surface drainage. The Alto de Mansilla isa topographic elevation just 130 m high. It was generated by convergent heading faults and overlapped with step-over restraining bend geometry, dividing a large lake into the Salinas Grandes and Salinas de Ambargasta (Gutiérrez et al., 2017). In the south end of the Sierra de Aconquija, thick conglomeratic piedmont deposits were deposited during the Pliocene-Pleistocene and were deformed and detached from their contribution areas by neotectonics (Gutiérrez et al., 2023).

In the Tafí and Amaicha valleys (Figures 2 and 3), in the foothills of the south end of the Cumbres Calchaquíes, the surface relief is disturbed by structures that were generated during neotectonic activity that give the landscape a morphology that breaks the monotony of the forms caused by alluvial fans and the fluvio-aeolian erosion (Gutiérrez et al., 2021). In the alluvial fans of the foothills of the La Candelaria range (Santa Bárbara System), topographic highlights attributed to neotectonic activity and related to seismic events were observed (Gutiérrez et al., 1997).

The sedimentary cover in the Cretaceous Rift basins is very thick (3554 m in the Metán basin, 3000 m

in the Choromoro basin, and 7000 m in the Tucumán basin) (Iaffa et al., 2011; Iaffa et al., 2011; Abascal, 2005), so the Neogene and Quaternary deformation folded these sedimentary piles, laying them on the Proterozoic-Paleozoic basement that is exposed in small outcrops, in the upper parts of the mountains. This tectonic morphology is mainly due to the inverse reactivation of normal faults inherited from the Cretaceous Rift, sometimes blind (Iaffa et al., 2011; Abascal, 2005; Grier et al., 1991). In the Metán basin, recent deformation was documented in folded surfaces, associated with blind and inherited structures. A case study with deep seismic and shallow geophysical prospecting methods evidenced the deformation produced by the El Galpón fault, folding neogenic and quaternary units, which would have experienced a seismic movement of M 5.7 in 2015 (Zeckra, 2020).

In the Cafayate valley, the Quaternary deformation produced folds in the lake deposits from the Upper Pleistocene to the Middle Holocene, evidencing the reactivation of the main high-angle faults, verging to the west, of the eastern edge of the valley, generating secondary faults that affect the quaternary coverage (Figueroa-Villegas et al., 2017).

Sierras Pampeanas (Cumbres Calchaquíes – Sierra de Aconquija)

a) Regional Geology

The Cumbres Calchaquíes, Sierra de Aconquija, and Ambato Block ranges are made up of an igneous-metamorphic basement (Upper Proterozoic-Lower Paleozoic) (Mon and Drozdzewski, 1999; Turner, 1960) (Figure 2). Sediments from the Cretaceous Rift could not have covered these mountain ranges because they were elevated (Gutiérrez et al., 2019; Mon et al., 2012), the outcrops of the Pirgua Subgroup of the Salta Group reached the northern end of the Cumbres Calchaquíes and the western edge of the Sierra de San Javier (Figure 2).

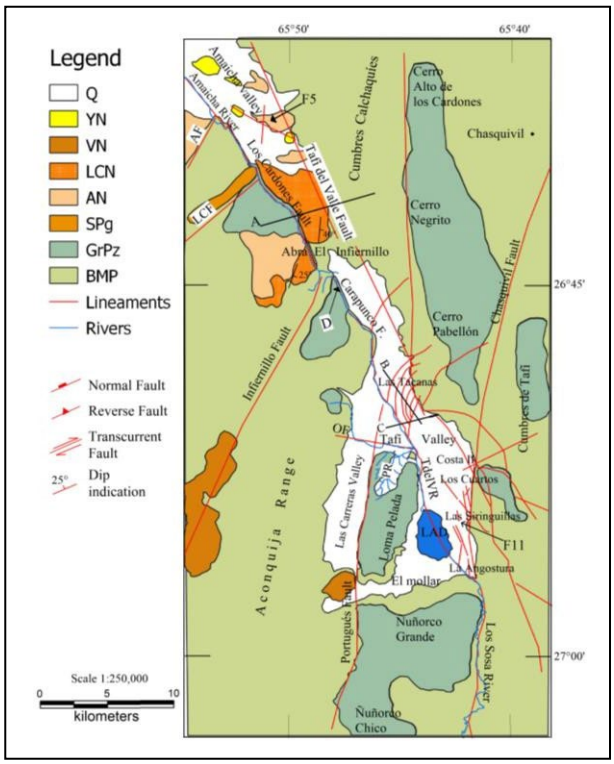

Figure 3: Morphotectonic map of the Tafí and Amaicha valleys. It shows the depressions of Tafíand Amaicha and the regional structures that gave rise to them. In addition, they do indicate the larger geological units that condition the fracturing that gave rise to the valleys. In this scheme, the recently generated structures deforming the foothills were drawn with red lines. Q: Fluvio- eolian deposits, Quaternary. YN: Yasyamayo Formation, Neogene. VN: Volcanic rocks, Neogene. LCN: Los Corrales Formation, Neogene. AN: Andalhuala Formation, Neogene. SPg: Saladillo Formation, Paleogene. GrPz: Paleozoic granites. BMP: Proterozoic early – Paleozoic Basement. AF: Aconquija Fault. LCF: Los Corpitos Fault. LAD: La Angostura Dam. OF: Ovejería Fault. PR: Pelado River. A: Profile Figure 4. B: Profile Figure 6. C: Profile Figure 8. D: Profile Figure F10. F5: Profile Figure 5 location. F11: Figure 11 location.

Neogene sediments occupied the Choromoro and Las Estancias basins in Tucumán and the Santa María basin in Catamarca (Gutiérrez et al., 2019). In the Santa María valley, the sedimentary sequence overlaps the metamorphic basement towards the Amaicha valley, reachingthe Infiernillo pass (Mon et al., 2012; Aceñolaza and Toselli, 1981; Porto et al., 1982), while in the northern end from the Sierra de Aconquija, the volcanism that gave rise to the extrusive rocks of Cerro Las Ánimas occurred ca. 13 Ma (Gutiérrez et al., 2019; González, 1990). The sedimentary column of the Santa María Valley was ordered in Sequences by Bossi et al. (2001) (Table 3).

The Tafí and Amaicha Valleys are intramontane tectonic basins at the Sierras Pampeanas' northern end (Figures 1, 2). The Tafí Valley is independent of the Amaicha Valley; the water sub-basins of both valleys

have springs in the Infiernillo pass (Figure 2). The waters of the Amaicha Valley are part of the Plata basin through the Santa María, Las Conchas, and Salado rivers, and the waters of the Tafí Valley ending in the Salí - Dulce River, forming part of the endorheic basin of the Mar Chiquita lagoon (Gutiérrez et al., 2017; Bossi et al., 2001).

b) Regional structures

Currently, the Sierra de Aconquija-Cumbres Calchaquíes mountain range is separated at the western edge, where it opens towards the Santa María Valley through the Amaicha Valley (Figure 2). On the eastern border, it remains together, but both mountains are unlinked by the Tafí del Valle fault (Figure 2). The north end of the Ambato Block joins the southeastern edge of the Sierra de Aconquija through the Tucuman Lineament (Figure 2).

Two faults limit the Sierra de Aconquija and Cumbres Calchaquíes mountains; the Tafídel Valle fault marks the southern edge of the Cumbres Calchaquíes, and the Los Cardones (Amaicha valley) and Carapunco (Tafí valley) faults the north edge of the Sierra de Aconquija(Gutiérrez et al., 2021) (Figure 3).

The Tafí del Valle fault zone has evidence of variations along strike, proved by the interpretation of satellite images, surface geometry, and the rock outcrops in the Tafí and Amaicha valleys. A single plane separates the Sierra de Aconquija from the Cumbres Calchaquíes in the southeastern end. It was possible to measure the fault plane in a stream at theentrance to the Tafí valley, registering the following values (225°/88°, 228°/85°) (Figures 2, 3) (Gutiérrez et al., 2021).

In the north end of the Tafí valley, at the foot of the fault, a vast deposit of piedmont develops, reaching 23 km in length and extending between 2 and 4 km in width. These depositsare assumed to be arranged on a metamorphic basement hiding the fault plane (Figure 3). In theAmaicha Valley, the fault zone is about 6 km wide, hosts the upper sequence of the Santa María Group, and opens towards the Santa María Valley, where the dextral transcurrent geometry of the fault was verified (Mon et al., 2012) (Figure 3).

Table 3: Stratigraphic sequence of the Santa María Group according to Bossi et al. (Bossi et al., 2001). Datings made by Powell and González (1997), Spagnuolo et al. (2015), Georgieff and Díaz (2014), Butler et al. (1984), Marshall and Patterson (1981), Strecker et al. (1984). Identifying quaternary morpho-sedimentary units by Peña-Monné and Sampietro-Vattuone (2018) and Sampietro-Vattuone et al. (2019). Q: Quaternary.

ERA	Period/Epoch		Ma	Stratigraphy		
CENOZOIC	Q	Holocene	0.00006 0.0004 0.0013	H2 H1		
		Pleistocene	1.15	Tafí del Valle Formation Lomitas Pegadas Formation		
	NEOGENE	Pliocene	2.5 3.4	SANTA MARÍA GROUP	Sequence IV	Yasyamayo
			4.0		Sequence III	Los Corrales Upper Andalhuala
		Miocene	6.02 6.7 6.88 9.1		Sequence II	Lower Andalhuala Chiquimil Las Arcas San José
						Paranense
	PALEOGENE	Oligocene				
		Eocene			Sequence I	Saladillo Formation
		Paleocene	16	SANTA BÁRBARA GROUP		
Paleozoic - Proterozoic early				Basement		

Internally, the mountainous ensemble is also cut by regional NNE structures (Infiernillo, Portugués, Chasquivil faults, and Los Pinos lineament), which do not manage to separate them, but give the ensemble a morphology that allows identifying minor mountain ranges such as Las Lajas, Las Pavas and Altos de la Totora, which, had the initial deformation continued, would have formed independent units, as is the case with the San Javier range (Figure 2). In some cases, these structures gave rise to important rivers such as the Amaicha, Tafí del Valle-Los Sosa and Las Cañas rivers and, other times, they separate mountain blocks, such as the Los Pinos lineament that separates the Las Lajas and Santa Ana mountains from the Sierra de Aconquija (Figure 2).

The central zone of the Cumbres Calchaquíes and the northern end of the Sierra de Aconquija, crossed by the NNE structures, the Portuguese fault (to the west), and the Chasquivil fault (to the east), are intruded by granite bodies that constitute a strip with the same orientation as structures that limit them, where the Alto de los Cóndores, Negro, Pabellón, Loma Pelada, Ñuñorco Grande, and Ñuñorco Chico hills stand out (Figure 3).

A cortical extension was postulated in the early Miocene to explain the origin of Cenozoic basins in the northwestern Sierras Pampeanas that were inverted at approximately 5 Ma (Bossi et al., 2001; Ruiz-Huidobro, 1972; Gutiérrez and Mon, 2004). However, it is likely that these regional structures were partially active during the Cretaceous Rift but did not evolve sufficiently to form

depocenters. For example, the Sierra de Aconquija and Cumbres Calchaquíes remained elevated during the Cretaceous because no outcrops of this age were found in the inner valleys (Mon et al., 2012). But, in all these regional NNE structures, spaces were generated during the Cretaceous Rift where small outcrops of red sandstones and conglomerate siltstones are preserved, attributed to the Santa Bárbara Subgroup of the Salta Group (Paleogene) (Figure 2). We can see them along the Aconquija and Cumbres Calchaquíes faults, in the Los Corpitos fault, on the eastern edge of the Los Pinos lineament and the east slope of the Santa Ana mountain range, on the northeastern border and southern end of the Chasquivil fault, in the Los Sosa riverbed and on the eastern edge of the Periquillo fault (Figures 2, 3). These reduced outcrops of red strata are attributed to the Santa Bárbara Subgroup and arranged on a metamorphic basement document. The other lower sequences of the Salta Group are not found in these regional structures. Possibly, in the Cretaceous Rift stage, the Aconquija, Cumbres Calchaquíes, Los Corpitos, Infiernillo, and Portugués faults constituted incipient steps that dipped towards the west, just as the Chasquivil fault represented a step dipping to the east, and the mountainous group remained elevated (Figures 2, 3). The granite bodies represented by the Alto de los Cardones, Negrito, Pabellón, Loma Pelada, Ñuñorco Grande, and Ñuñorco Chico hills constituted a longitudinal block towards which the steps of the normal faults converged, those that inclined to the east and those that sloped to the west (Figure 3). In the lower Tertiary, these small steps began to fill up with the sediments of the Santa Bárbara Subgroup. They were protected in the elevated parts of the slopes of the mountains, such as on the western edge of theSierra de Aconquija and Cumbres Calchaquíes, in the Los Corpitos fault. (Mon et al., 2012; Gutiérrez et al., 2019), in the Chasquivil fault and many other places (Figures 2, 3). Against the Infiernillo fault, the Santa María Group's upper sequence ends and fills the Amaicha Valley without reaching the Tafí Valley (Mon et al., 2012).

These areas of regional weakness, Cretaceous or Paleozoic, were reactivated with the Andean tectonics. Sometimes the normal faults of the Cretaceous Rift were reactivated in the same direction as the initial fault plane. Still, in the opposite sense (Iaffa et al., 2011; Abascal, 2005; Grier et al., 1991), and later on, these faults were cut by others with opposite sense and direction, such as the Aconquija, Cumbres Calchaquíes, and Infiernillo faults (Mon et al., 2012; Gutiérrez et al., 2019; Gutiérrez and Mon, 2004; Gutiérrez and Mon, 2008). However, the Chasquivil fault would have had a reverse reactivation because it arranged the preserved red strata in the Los Sosa River dipping 40° to the SE (Figure 3). Pilger (1984) interpreted that the uplift of the marginal mountain ranges to the Calchaquí Valley would have started at 13 Ma. The tectonic activity would have accelerated around 4 Ma, affecting the Yasyamayo Formation (ca. 1.5 Ma), therefore, would have occurred at approximately 1.2 Ma, extending to at least 0.6 Ma (Strecker et al., 1987) and the eastern edge of the Sierra de Aconquija began to rise at 9 Ma (Löbens et al., 2013) (Figure 3).

c) Amaicha valley

The Amaicha Valley, with an NW strike, extends to the northwest of the Tafí Valley, from the Infiernillo pass to the Santa María Valley, limited to the north by the Cumbres Calchaquíes and tothe south by the Sierra de Aconquija (Figures 2, 3).

The Amaicha valley is narrow, with an average width of about 4 km (Figure 3). The developed piedmonts belong to the southern foothills of the Cumbres Calchaquíes; it is covered by Sequences III and IV of the Santa María Group and the Quaternary alluvial fan deposits (Figure 3; Table 3).

The Tafí del Valle fault had a normal component separating the Sierra de Aconquija from the Cumbres Calchaquíes and forming the Tafí and Amaicha valleys. This fault allowed the deposition of the Tertiary sequence in the Amaicha Valley, resulting from an underdeveloped heritage from the Cretaceous Rift (Mon et al., 2012) (Figures 3, 4). The Tafí del Valle fault probably could have had an incipient development during the Cretaceous Rift stage, which did not prosper.

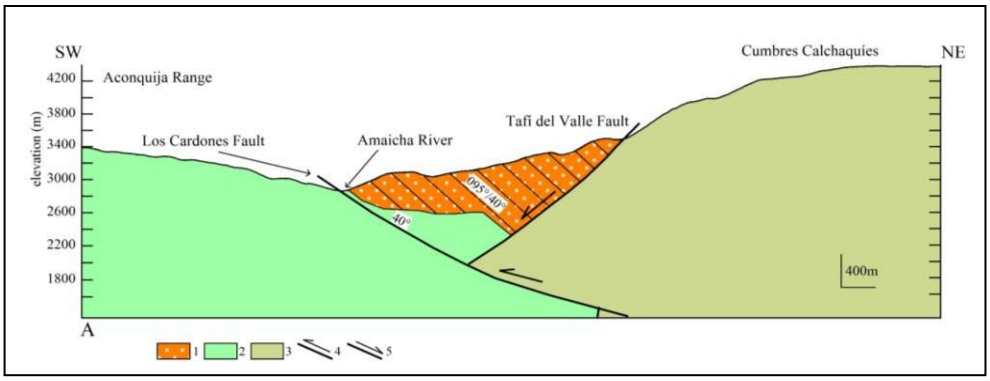

Figure 4: Geological profile A, transverse to the Amaicha Valley. 1: Los Corrales Formation, Santa María Group, Neogene. 2: Paleozoic granite. 3: Proterozoic early - Paleozoic Basement. 4:Reverse fault. 5: Normal fault. The Los Cardones fault zone has a general dip direction to the NE, dipping 40° (Figure 3).

Sediments of Cretaceous or Tertiary age were not yet found in the Tafí valley, possibly because the area remained elevated, until in the lower Tertiary, it began to partially fill up on the Amaicha valley side, reaching the Neogene deposits at the foot of the Infiernillo fault. For example, remnants of the lower Tertiary red sediments (Santa Bárbara Subgroup) occur at the foot of the Los Corpitos and Chasquivil faults (Gutiérrez et al., 2021).

Neogene sedimentary sequences of the Santa Maria Group spread eastward into the Sierra de Aconquija against the dipping ramp to the west, which was later cut by the reverse Infiernillo fault, vergent to the NW (Mon et al., 2012). The Infiernillo fault separated the Amaicha Valley from Tafí Valley. It would have also facilitated the magmatic ascent that originated the vulcanites in the northern zone of the Sierra de Aconquija (Figure 2). The horizontal displacement of the Tafí del Valle fault is affecting the sedimentary sequence of theSanta María Group in the Santa María Valley (Mon et al., 2012).

In the Amaicha River, the plane of the Los Cardones fault was measured (Gutiérrez et al., 2021). It is a reverse fault that dips to the NE. Because the fault plane in the granite outcrops is broken, it was possible to measure a plane dipping 40° to the NE (Figure 4). The Los Cardones fault cuts the Tafí del Valle fault and places the layers of the Los Corrales Formation with a 40° dip to the east (Table 3; Figures 3, 4). Southwest of the Los Cardones fault, the layers of the Los Corrales Formation slope 20° to the SE (Figure 3).

In the Amaicha Valley, tectonic activity is affecting the Quaternary conglomerate sequence. It is possible to see how the layers of the Andalhuala Formation are riding on the Yasyamayo Formation, and the faults also affect the quaternary gravels (Table 3; Figures 3, 5). These faults occur in the central zone of the valley, far from the main faults that limit the mountains.

d) Tafí valley

The Tafí Valley is located at the northeast end of the Sierra de Aconquija, bordered to the north by the Cumbres Calchaquíes. In the valley's centre, the independent relief of Loma Pelada stands out, dividing the valley into two related areas, Las Carreras Valley to the west and Tafí Valley to the east (Figures 2, 3). The bottom of the Tafí Valley is between 1800 and 2300 ma.s.l.,crossed from north to south by the Tafí del Valle River.

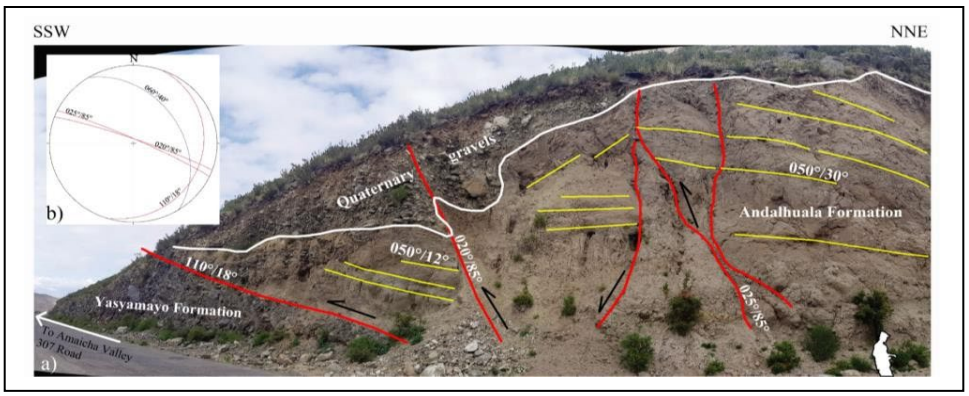

Figure 5: A: Photographic illustration in the Amaicha Valley. A reverse fault places the Andalhuala Formation on the Yasyamayo Formation. Other faults also affect quaternary gravels. The white lines mark the contacts of the sedimentary units. Yellow lines indicate bedding. Red lines identify structures. On the lower right edge, in white, a person's half-length silhouette indicates scale. B: Diagram of resulting fractures represented in Schmidt's equiareal network, lower hemisphere. Los Cardones fault in blue line. In red lines faults in this figure.

In the Tafí valley, on the igneous-metamorphic basement (López et al., 2017) rest thick greyish-brown conglomerates, called Lomitas Pegadas Formation (González, 1999), covered by loess from Tafí del Valle Formation (Collantes et al., 1993), dated at 1.15 Ma (Middle Pleistocene) by Schellenberger et al. (2002) (Table 3).

Organic matter contained in lake sediments in the area of El Rincón, Tafí del Valle, was dated with 14C, registering ages between 10,350 ± 80 and 4120 ± 60 a BP (Garralla et al., 2001). Ortíz and Jayat (2007) carried out radiocarbon dating on bone remains found in the Tafí del Valle Formation and located at the Pleistocene-Holocene limit (10.25–9.65 ka cal. BP). Recent studies carried out an evolutionary geomorphological model of the Lateglacial and Holocene accumulations in the valleys, determining four degradation stages dated between 13,000 and 630a BP with 14C, thermo Luminescence, and tephra layers underlying charcoal samples (Peña-Monné and Sampietro-Vattuone, 2018; Sampietro-Vattuone et al., 2019; Sampietro-Vattuone and Peña-Monné, 2016) (Table 3).

Alluvial fans are fed from Cumbres Calchaquíes and Sierra de Aconquija. The deposits corresponding to the Cumbres Calchaquíes are better developed, covering the entire southern edge mountain front and reaching up to 4 km wide. On the other hand, the deposits in the foothills of the Sierra de Aconquija occupy only half of the northern front of the mountain range.

They are 2 or 3 km wide (Figure 3). The thickness of the Quaternary deposits at the Mesada Lamedero is estimated to be about 200 m.

Peña-Monné and Sampietro-Vattuone (2018) defined in Tafí Valley morpho-sedimentary units constituting aggradation phases. Unit H1 represents the oldest hill-side accumulations, riverterraces, and alluvial cones, consisting of well-stratified coarse sands and gravels. Unit H2 occupies a large area constituting alluvial fan deposits made up of sediments similar to H1 (Table 3).

The differential tectonic behaviour of both mountain blocks (Sierra de Aconquija and Cumbres Calchaquíes) generated the segmentation of the NW structures that limit both mountain ranges, the Tafí del Valle fault on the southern edge of the Cumbres Calchaquíes and Los Cardones-Carapunco faults on the edge north of the Sierra de Aconquija (Figures 2, 3). This differential behaviour can be observed in the Los Cardones and Carapunco faults (Figure 3). The Los Cardones fault only has a dip-slip. On the other hand, the Carapunco fault has vertical and horizontal displacement. The Tafí valley reflects a differential tectonic behaviour in neotectonic processes; several zones are distinguished in the foothills of the Cumbres Calchaquíes (Las Tacanas, La Costa II, Los Cuartos, Las Siringuillas, and La Angostura), limited to the west by the Portuguese fault and to the east by the Chasquivil fault (Figure 3).

e) Las Tacanas – El Infiernillo

The Carapunco fault marks the northern limit of the Sierra de Aconquija; the river Tafí del Valle runs through it. The fault begins in the El Infiernillo pass and ends in the La Angostura area (Figure 3). Towards the Tafí del Valle River, the alluvial fans of the Cumbres Calchaquíes and the Sierra de Aconquija converge.

In the Las Tacanas area, it is observed in the satellite images and the geomorphology of the landscape that the alluvial fans of the Cumbres Calchaquíes were reworked and modelled by other processes, different from the accumulation and erosion that characterise these geoforms.

These surfaces are furrowed by deep, parallel, and curved ravines that descend from the Cumbres Calchaquíes and end in the Tafí del Valle River, forming positive reliefs and hills between them (Figures 3, 6). This drainage network with a curved and parallel pattern is represented by deep ravines generated by reverse faults that formed a series of ascending steps tothe NW in the foothills (Figure 6a). In this area, retrograde erosion and landslides on the southern slopes of the streams due to reverse faults that changes the local base level allow evidence of recent tectonic activity.

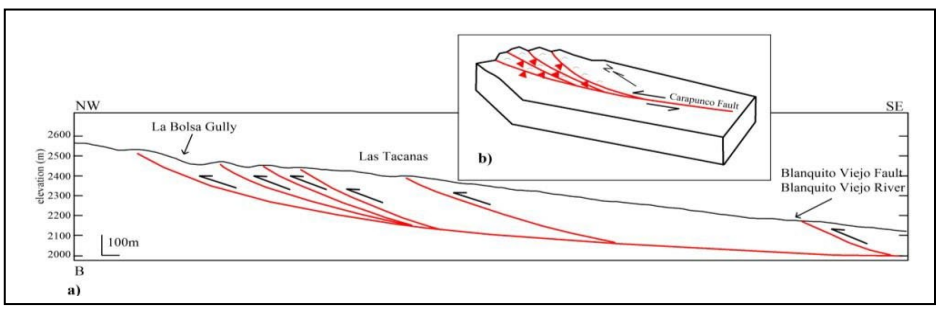

Figure 6: A: Topographic profile B showing the positive relief and the hills formed in the foothills of the Cumbres Calchaquíes, generated by reverse faults, configuring a rough surface limited by deep ravines. B: The plant diagram shows an interpretation of the geometry of interposed contractional fans drawn based on the distribution of the drainage network in Figure 3 and the attitudes of the fault planes.

In the upper parts of the foothills, the strata of a sequence of sandy silts, of a light brown colour, with intercalations of conglomerate lenses, with large clasts, maintain an inclination of 18° to the south (Figure 7). Together, these streams and the Tafí del Valle River form an interlaced contractional fan geometry (Figure 6b), like the examples from the literature (Woodcock and Fisher, 1986; Cunningham and Mann, 2007).

This geometry allows us to determine that the Carapunco fault has a sinistral transcurrent component (Figures 3, 6b).

The Cumbres Calchaquíes are exerting pressure on the Sierra de Aconquija, generating the deformation of the foothills of the valley in such a way that the foothills of the Cumbres Calchaquíes are higher than the foothills of the Sierra de Aconquija (Figure 8a). This tectonic process that generates a characteristic morphology and a typical structural geometry is evidenced in the Mesada Lamedero (Figure 8). There, a positive relief structure is formed by the Carapunco and Blanquito Viejo reverse faults, arranging the conglomerate layers of the alluvial fans of the Cumbres Calchaquíes with strong east and west dips (Figures 3, 8b, 9).

Figure 8 shows the ravine raised on the left bank of the Tafí del Valle River. On the right bank of the Blanquito Viejo river, the river terrace comprises light brown sandy silts, with intercalations of conglomerate lenses at the base, passing into a fanglomerate in the upper half of the profile. The conglomeratic lenses dip 30° to the west (265°/30°), a product of the activity of the Blanquito Viejo fault (Figures 8, 9).

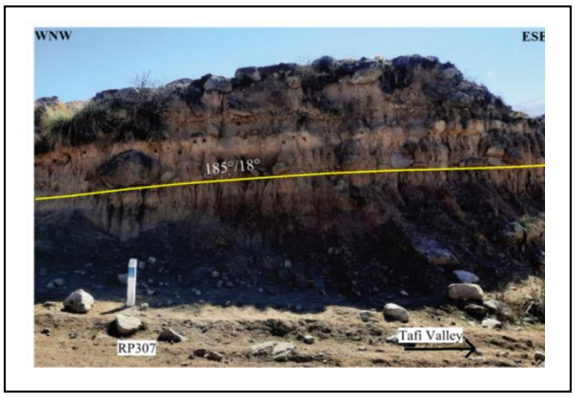

Figure 7: Stratigraphic sequence of the foothills on the right bank of the La Bolsa ravine. The conglomerate strata slope south (185°/18°).

In the Infiernillo, where the Tafí del Valle River is born, the Carapunco Fault can be seen (Figure 10). In some sectors, the fault lays out the metamorphic basement on granitic rocks and sometimes cuts through the granitic rocks (Figure 10a). The Carapunco Fault, with a 40° dip in a NE direction, arranges the Cumbres Calchaquíes on the Sierra de Aconquija (Figure 10b).

f) La Costa II, Los Cuartos

These zones are in the southeast end of the Tafí Valley, where the Tafí del Valle and Chasquivil faults converge (Figure 3). In this area, the Loma Pelada constitutes a positive element that divides the Tafí Valley (Figure 3). The foothill deposits of the Sierra de Aconquija are better developed in the Las Carreras Valley but not on the eastern edge of the Loma Pelada, which is where the piedmonts deposits of the Cumbres Calchaquíes will end up, against the Tafí del Valle River (Figure 3).

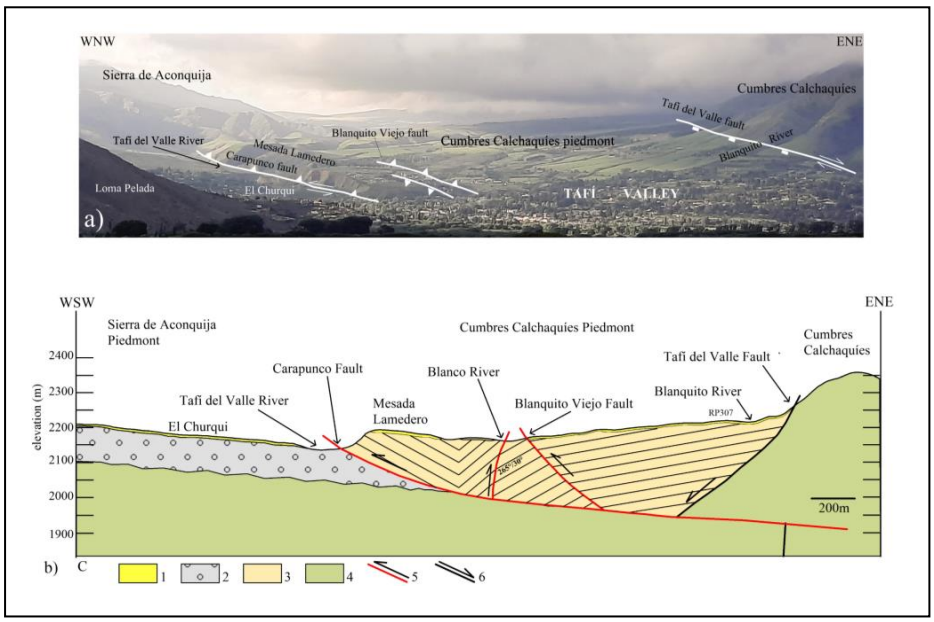

Figure 8: A: Panoramic view of the Tafí Valley tectonics morphology displayed in Figure b. Wecan see the topographic relief of the alluvial fans disturbed by the reverse faults generating the counter slope. It is also observed how the piedmonts of the Cumbres Calchaquíes rise above the Sierra de Aconquija piedmonts through the Carapunco fault. B: C topographic profile showing the

Mesada Lamedero positive relief structure formed by the Carapunco and Blanquito Viejo faults. It is observed that the foothills of the Cumbres Calchaquíes are raised and folded over thefoothills of the Sierra de Aconquija. 1: Loess deposits (Q). 2: Alluvial fan deposits (Q). 3: Alluvial fan deposits (Q). 4: Proterozoic basement. 5: Recent reverse faults. 6: Normal fault.

Quaternary structures were generated in the foothills and the mountain front of the Cumbres Calchaquíes (Figure 3). The deformation of the alluvial fans adequately reflects neotectonic activity (Figure 11).

In the La Costa II área, the tectonic deformation of the Quaternary sediments occurs on the mountain front. Here we can see the cuspid zone of the deformed dejection cones, ridden by a metamorphic basement, through a reverse fault dipping to the ENE (080°/80°) (Figure 3).

This fault corresponds to a reactivation of the Tafí del Valle and Chasquivil faults, and the quaternary sediments would be represented by the H1 accumulations (Peña-Monné and Sampietro-Vattuone, 2018) (Figure 3). Other reverse faults (130°/88°, 280°/50°, 115°/80°), measured in the metamorphic basement, also affect the quaternary sedimentary sequence. One ofthese faults (045°/90°) coincides with the Tafí del Valle fault (Figure 3). Here, the quaternary faults affect the accumulations identified as H1, dated by Peña-Monné and Sampietro-Vattuone (2018) between ca. 13000 and 4200 a BP(Figure 3; Table 3).

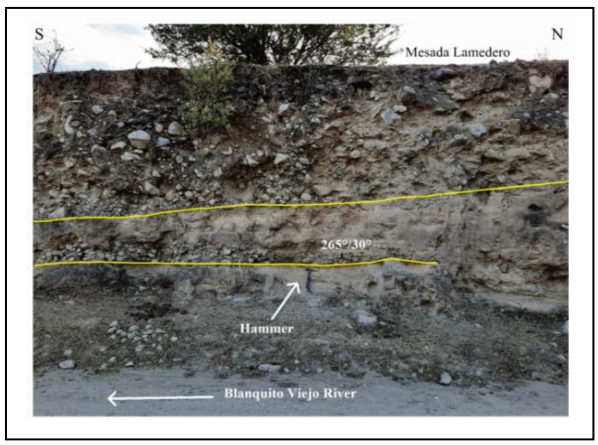

Figure 9: Quaternary terrace on the right bankof the Blanquito Viejo River. The Blanquito Viejo fault affected the sequence, disposing of the conglomerate strata with a west dip (265°/30°).

In this area, rock falls by the terraces' destruction on the ravines' margins are also observed, which allows evidence of recent tectonic activity. The discrete deformation associated with the recent seismic activity recorded in the area generates these neotectonic indicators.

Between the Los Cuartos and Las Siringuillas area, the piedmont landscape is crossed by structures with NW and NE strikes and disturbed by hills of about 400 to 800 m in length and 140 m in width, with NNW strike (Figures 3, 11). These hills comprise Pleistocene sediments, deforming the H1 and H2 accumulations (Figure 11, Table 3). Two anticline fold structures are observed, with NW and NE strikes, which dispose of the Pleistocene conglomerate strata dipping to the NE, SW, and SE, NW, respectively (Figures 11, 12; Table 3).

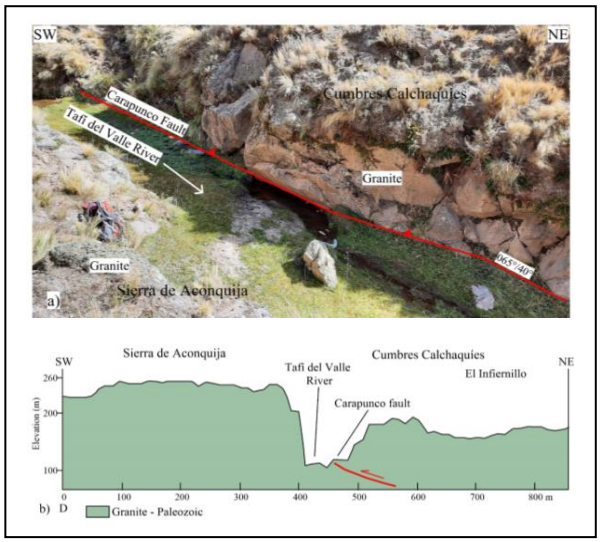

Figure 10: The Carapunco Fault cuts granitic rocks with a 40° dip in a NE direction. It disposes of the Calchaquíes Summits on the Sierra de Aconquija.

The faults have reverse displacement, dipping to the NW and NE (300°/45°, 080°/80°, 125°/70°, 115°/85°, 060°/84°). One of them (060°/84°) also evidenced dextral transcurrent movement, dividing one of the hills and generating a typical whale-back structure and a fault gap. Other structures affect the folds and H1 and H2 accumulations (Figure 12; Table 3) (Gutiérrez et al., 2021).

The faults generated between Los Cuartos are found in the cuspid part of the alluvial fans near the mountain front and generate anticline folds in the Pleistocene deposits (Figures. 11, 12; Table 3). These structures and associated morphologies appear closely related to the Chasquivil fault. The layers of the H2 accumulations, dated by Peña-Monné and Sampietro-Vattuone (2018)between ca. 4200–630 to BP, are also affected by tectonic activity (Figure 12a). The drainage network also shows tectonic activity. The anticline structures interrupt and divert the channels, showing recent incisions in the H2 accumulations (Figures 11, 12).

g) Ambato Block

The morphology of the tectonic depression Las Estancias - Campo del Pucará represents an inverted alluvial fan, and the morphotectonics of the north end of the Ambato Block evidence tectonic processes of counterclockwise rotation (Figure 2) (Gutiérrez, 2000; Gutiérrez and Mon, 2008). The northern end of the Ambato Block evidences a break, marked by the Tucumán Lineament and the Las Cañas River, representing structures oblique to the Andean strike.

The deformation processes are active (Gutiérrez et al., 2019).

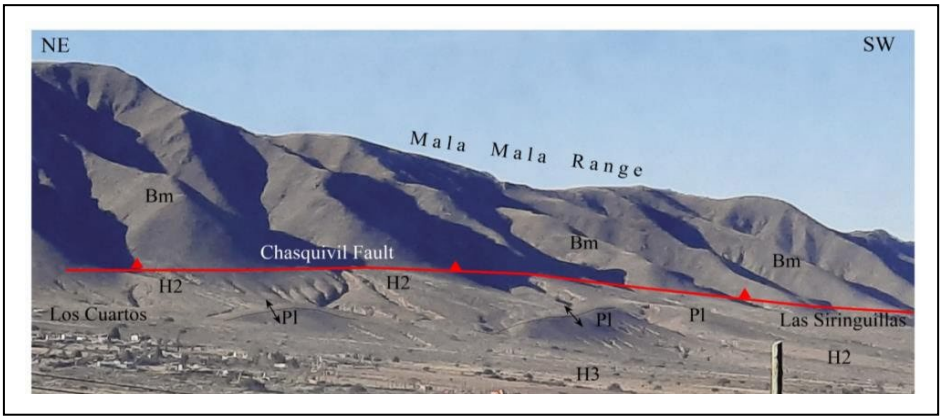

Figure 11: Photo shows the piedmont deformation by neotectonic processes associated with the Chasquivil fault. Hills oriented to the NNW are observed, made up of Pleistocene sediments, modifying the course of surface drainage and disturbing the H2 accumulations. Symbols indicateanticlinal folds.

As part of the geotechnical works in the northern end of the Ambato Block, the company MAA (Minera La Alumbrera S.A.) keeps a continuous record of the displacements of some fractures in the igneous-metamorphic basement (Figure 13a). These fractures have a high degree of dip (145°/70° - 040°/85°). To measure the displacement of some fractures, the company placed gauges that measure movement on three orthogonal axes (A, B, C) (Figure 13b). On axis A, the horizontal separation of the gauge plates is measured in the centre of the overlap zone, parallel to the fracture plane (Figure 13). On the B axis, the horizontal distance between the tips of the gauge plates is measured (Figure 13).

The C axis measures the vertical movement of the fracture. It is the distance between the smaller plate's lower edge and the larger plate's upper edge, measured at the centre of the overlap (Figure 13). A third axis, D, was added to obtain the resulting displacement of B and C (Figure 13a). The measurement uses a digital calliper, achieving an acceptable accuracy of ±1mm.

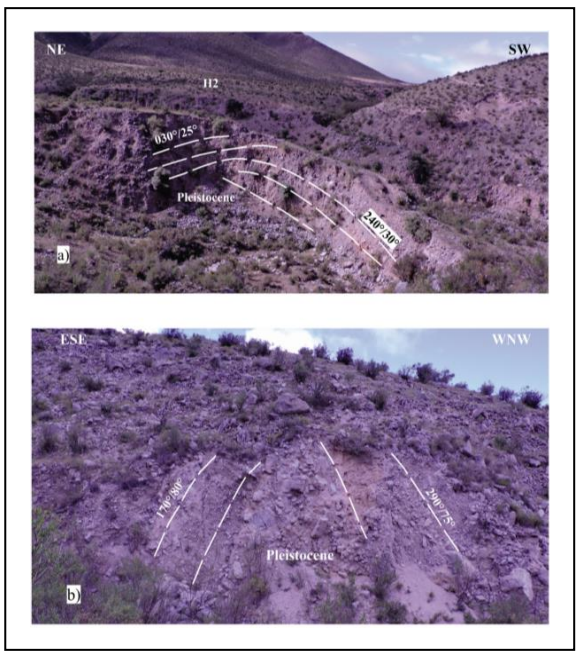

Figure 12: View of folds in the foothills; the folded strata correspond to the Lomitas PegadasFormation. A: Anticline NW strike. B: NE direction fold whose strata show a strong dip.

The company MAA provided the data obtained month by month for 2021 and 2022.

Figure 13a marked the fractures' direction and sense of displacement according to axes A, B, and C. The measurement obtained in B (Figure 13b) also represents a horizontal displacement perpendicular to the fracture plane (Figure 13a). The measurement obtained in C (Figure 13 b) represents the vertical displacement on the fracture plane (Figure 13a). In Figure 13a, arrow D indicates the direction and sense of displacement resulting from the movements in axes B and C.

The Pythagorean theorem (Eq. (2)) was applied to obtain the resultant D:

$$D=(D^2 = B^2 + C^2). \quad (2)$$

From the reading obtained between 2021 and 2022, it is interpreted that the measurements obtained in the different months are variable. The minimum and maximum measurements can determine an average annual displacement. For 2021, the average displacement in the A axis was 0.74 mm/y and for the D axis, 2.55 mm/y. For 2022, the average displacement of the A axis was one mm/y and for the D axis, 2.6 mm/y.

V. Santa Bárbara System

The southernmost end of the Sub-Andean System, south of the Juramento River, is represented by low mountains with few outcrops. The best outcrops occur on the Colorado, Cantero, and Remate hills and the flanks of the La Candelaria, Medina, and del Campo range(Figure 14) (Mon and Gutiérrez, 2007).

Intensely micro-folded low-grade Proterozoic schists form the basement outcrops in the La Candelaria, Medina, del Campo, and La Ramada ranges (Figure 14). Some pink quartzites areattributed to the Cambrian age on the western flank of the La Candelaria range (Ricci and Villanueva, 1969).

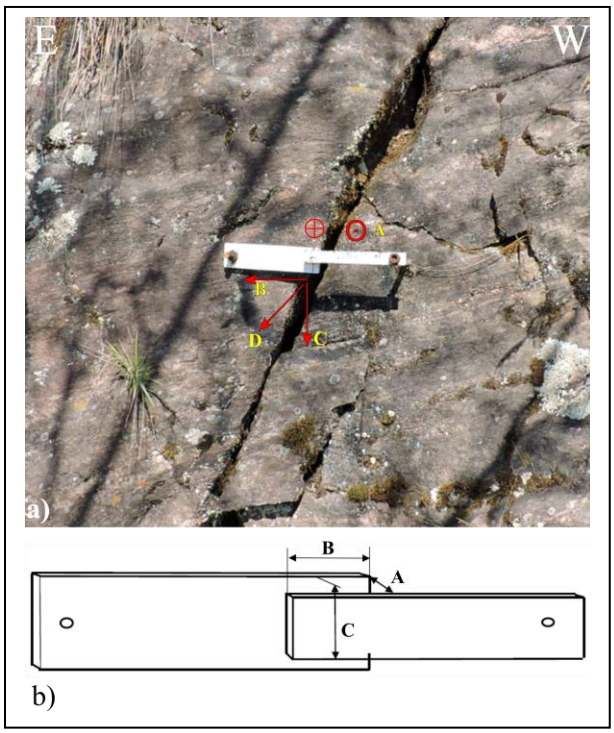

Figure 13: A: Photograph illustrating the gaugeanchored to the fracture to measure displacements in three perpendicular axes. On the fracture, the direction of the displacements is indicated with symbols in red for the measurements of A, B, and C. The circles represent the tip and the tail of an arrow that indicate the direction of displacement. B: Diagram of the meter and the measurements made in three orthogonal axes.

Jakúlica (1948) mentions layers of green and whitish shale from the Ordovician period below white and pink quartzites attributed to the Devonian, at the bottom of an open pit excavation, at Puesto La Aguada, south of Cerro Colorado (Figure 14). These Devonian quartzites also crop out in the anticline cores of the Cantero and Remate hills (Mon and Gutiérrez, 2007). The stratigraphic sequence north of the oblique fault that marks the southern end of the Cerro Colorado range (Figures 14, 15) contains thick Cretaceous sequences of the Salta Group (Mon and Gutiérrez, 2007) (Figure 15). To the south, a few shallow outcrops occur on the western flank of the La Candelaria range and in the Río Nío Valley, proving that the Neogene layers of the Anta Formation sit directly on the Paleozoic (Figure 14). The Quaternary deposits formed by old terraces of the Juramento River are conglomerates with limestone and quartzite boulders of thin thickness; they are tilted to the west with dips greater than 5° (Mon andGutiérrez, 2007).

At the southernmost segment of the Sub-Andean System (Figure 14), which extends for 100 km in the Andean foreland, the basement participates in deformation as in the La Candelaria, Medina, del Campo, and La Ramada ranges (Mon and Gutiérrez, 2007). This set of mountains reaches maximum heights of 2,400 m a.s.l. in the La Candelaria Range. To the east of this mountain range and south of the Juramento River (Figure 14), the most prominent outcrops coincide with Cerro Colorado, which, at its highest point, reaches 1,000 m a.s.l. It continues to the south, a cord of low mountains, with few outcrops, covered by scrub and thorny scrub, in the outermost part of the Andean foreland, where most of the structures are sub-outcrops, only glimpsed in satellite images.

The Andean deformation folded this set of sierras against the faulted edge of the Chaqueña Plain, generating bowing and displacement of the folds (Figure 14, 15). In the Metán basin, the folds and structures are covered by a thick sedimentary sequence of more than 7,000 m thick, only visible in seismic profiles (Mon et al., 2005; Iaffa et al., 2011). In the Choromoro Valley, the folds and structures are also covered, but the sedimentary sequence is not as thick. Therefore, the morphology of the folds is visible in the radar images (Figure 14). The Neogene structures affecting Quaternary deposits are best developed in the La Candelaria range (Gutiérrezet al., 1997) (Figure 14).

The geometry of the Neogene faults was determined on both flanks of the La Candelaria range. This fault geometry was determined by making profiles with 2D electrical resistivity tomography, seismic methods, and digital terrain models prepared with drone images (Aranda-Viana et al., 2017; Arnous et al., 2020).

Repeated offsets during moderate to large earthquakes in the Quaternary are the most likely origin for these scarps, which suggests recurrent, spatially disparate seismogenic quaternary deformation processes in the broken foreland (Aranda-Viana et al., 2017; Arnous et al., 2020).

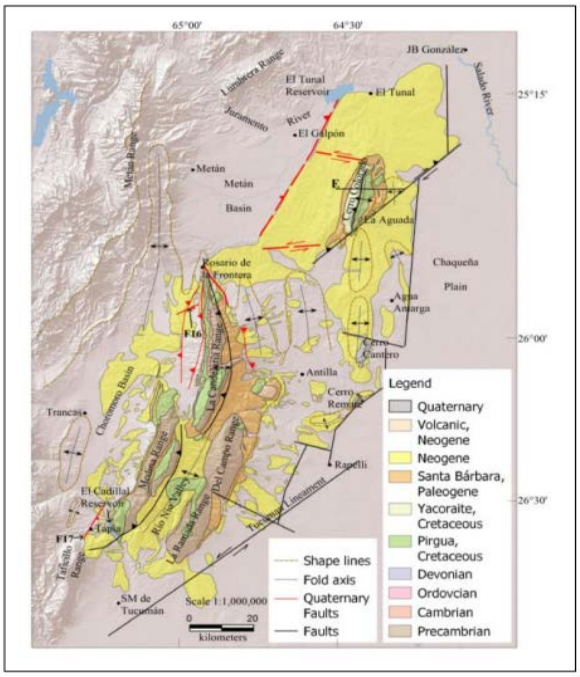

Figure 14: Map of the Santa Barbara System. F16: Figure 16 location. F17: Figure 17 location. Fold contour shape lines were drawnprimarily to indicate the location of buried folds. These lines also allow us to see the curved geometry that the folds acquire due to neotectonic deformation. Dashed red lines indicate blind faults, showing activity without surface expression (Zeckra, 2020).

Some faults are blind, riding quaternary alluvial fans. In Figure 16, the conglomeratic strata and silty deposits are affected by blind faults. The fault dips 30° SE. It is interesting to observe the curved morphology of the terrace surface, which accompanies the displacement of the fault (Figure 16). This curved geometry is also observed in the images of remote sensors in several sectors on the flanks of the La Candelaria range, evidencing that blind faults produce them.

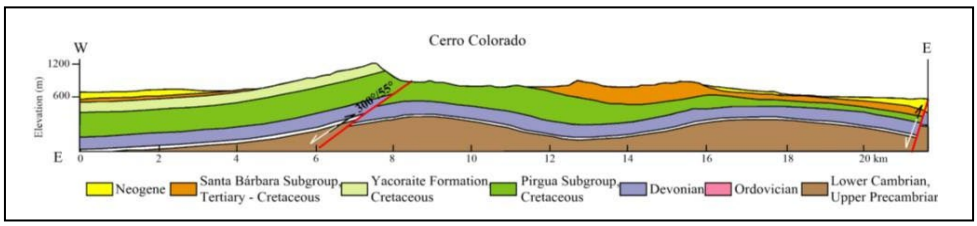

Figure 15: Profile of Cerro Colorado. The complete stratigraphic sequence representing theSanta Bárbara System is shown.

To the north of the Taficillo range, a stratigraphic sequence of the Río Salí Formation of the Miocene age is cut by a thrust fault (Figure 17). The strata are gently folded, dipping to the NE, between 25° and 30°. The fault dips 40° to the SE. A microfold of the strata is observed at itsbase, and in the upper part, the fault affects Quaternary deposits. Other conjugate reverse faults are generated on the left side of the main fault, which also affects the Quaternary deposits. Towards the left side of the outcrop, a normal fault causes a slip of the Quaternary deposits(Figure 17).

VI. Chaqueña Plain

This extensive sedimentary basin extends from the eastern edge of the Santa Bárbara System and Sierras Pampeanas (Figure 1) to join the Paraná basin to the east (Pezzi and Mozetic, 1989). Neotectonic deformation did not bring the stratigraphic sequence that fills it to the surface buried by Quaternary deposits. Its geological history is known and interpreted through information from oil wells, seismic lines and magnetotelluric profiles.

Between the Upper Precambrian and the Silurian, an extensional tectonic event occurred that would be associated with a shear system of significant vertical displacement that affects the crystalline basement and originates basins like Las Breñas fault and its homonymous half- graben, inverting towards the upper Plaeozoic giving rise to the Pampeano-Chaqueño arch (Chebli et al., 1999) (Figures 1, 18). Based on both the geotectonic context and the magnetotelluric results, it conjectured that the sharp lateral discontinuity observed at both sides of the Pampeano-Chaqueño arch in the resistivity model represents the boundary between the Río de la Plata craton and the Pampean terrane or another Precambrian cratonic fragment (Pomposiello et al., 2010).

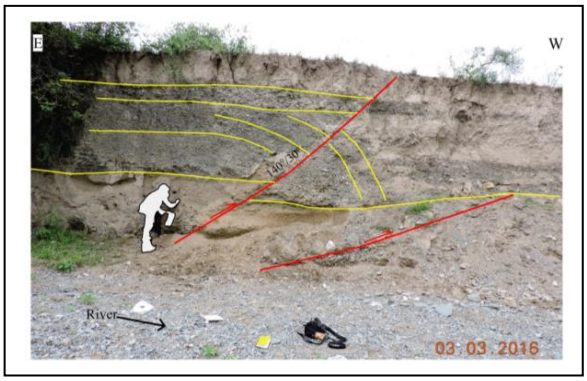

Figure 16: River terrace faulted on the left bank of a river. Location in Figure 14. With yellow lines, the strata are delimited. The red lines mark the faults. Fault data indicates dipdirection/dip.

The Otumpa hills, limited to the east by the Otumpa Lineament (Rossello and Veroslavsky, 2012) (Figure 1), are the surface expression of the Pampeano-Chaqueño arc and constitute a Gondwanan relict morphostructure, with Mesozoic and Cenozoic reactivations (Peri, 2012). The geometry of the subsoil structures in this zone, interpreted through seismic profiles, shows high-angle reverse faults and asymmetric and symmetric folds, revealing tectonic inversion processes (Peri, 2012; Rossello and Veroslavsky, 2012). The Otumpa hills (Figure 1) are mainly linked to an antiform of about 150 kilometres of wavelength originated by double tectonic vergence (Peri, 2012).

According to the isopach map (Chebli et al., 1999) and the magnetotelluric profile (Pomposiello et al., 2010), the Lower Paleozoic basins developed to the west and east of the Pampeano-Chaqueño arc (Figure 19).

The superficial expression of neotectonics is reflected by the paleochannels transversal to the Otumpa hills and by the wedges of the Cenozoic sequences observed in the seismic lines.

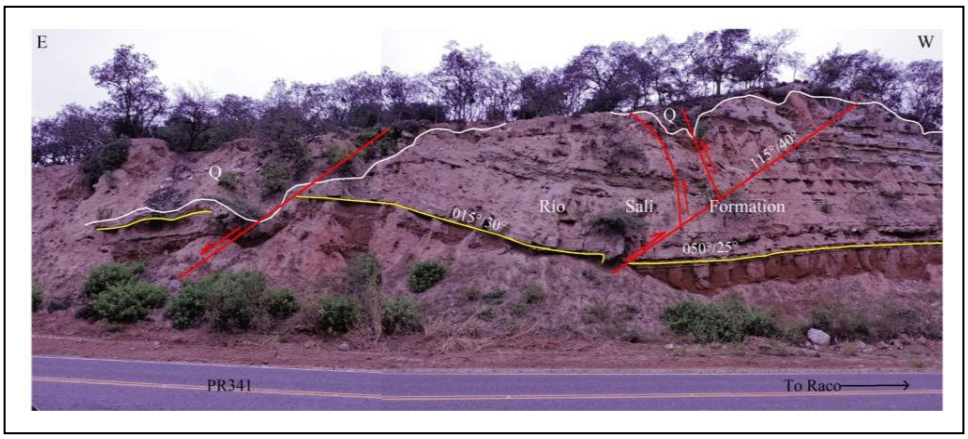

Figure 17: Outcrop of the Río Salí Formation (Miocene) on Provincial Route 341 (PR341). Withyellow lines, the strata are delimited. The red lines mark the faults. White lines mark the contact between the Río Salí Formation and the Quaternary. Fault data indicates dip direction/dip.

These paleochannels, with a W-E strike, represent the primitive direction of the surface runoff of the Salado River. Neotectonic processes diverted runoff from the Salado River to its current course in an N-S direction (Peri and Rossello, 2010) (Figure 1).

The deep seismicity of the Chaco Plain-aligned N-S (Figure 1) was linked to the depth ofthe Pacific slab (Peri, 2012). Our interpretation connects this surface seismic expression with a blind, sub-vertical structure called El Hoyo Lineament (Figures 1, 19). The neotectonic reactivation of the El Hoyo and Otumpa lineaments gave rise to the Otumpa hills and the diversion of surface runoff.

VII. Discussion

The NE compression due to the convergence of the Nazca and South American plates produces deformation through movement in faults of diverse geometries. The deformation is influenced, among other things, by the rheology of the rocks and pre-existing faults (Ikeda, 1983; Iaffa et al., 2011; Gutiérrez et al., 2019; Gutiérrez and Mon, 2008; Riller and Oncken, 2003; Rodgers and Rizer, 1981; Zampieri et al., 2012). Seismic rupture occurs when the elastic stress towhich the rock is subjected exceeds its frictional resistance (Sibson, 1982; Nortje et al., 2011; Kamb et al., 1971; Ikeda, 1983).

Most earthquakes recorded in the study area are of magnitude 3 and 5. These earthquakes occur in the Andean foreland between the first 70 km depth. Earthquakes of magnitude >6 occur less frequently, between 0-33 km and 500-600 km depth (Figure 1; Table 2).

The convergence of NE-directed tectonic plates leads to continuous tectonic deformation of the central Andes in Argentina. Those active tectonics migrated eastward from the Puna since the middle Eocene (Del Papa et al., 2005; Deeken et al., 2006; Carrapa and De Celles, 2015). In the Miocene, it reached the western edge of the Eastern Cordillera (Jordan and Alonso, 1987; Starck and Vergani, 1996; Carrera and Muñoz, 2008; Carrapa et al., 2011; and Pearson et al., 2013). The thick conglomeratic deposits of Pliocene-Pleistocene age on the slopes of Cumbres Calchaquíes, Sierra de Aconquija, Velazco range, Cerro Pampa (Gutiérrez et al., 2003; Gutiérrez et al., 2023; González, 1999) show active tectonics of considerable magnitude. The Lomadas de Otumpa originate in Paleozoic tectonic events, with repeated reactivations of pre-existing structures during Andean tectonics, currently causing the diversion of the surface drainage network (Peri, 2012).

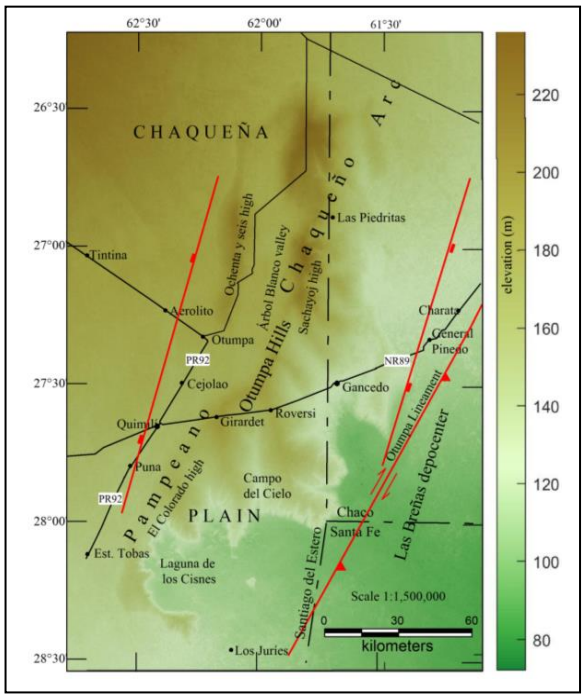

Figure 18: Map image that represents the positive relief of the Otumpa Hills.

Records of neotectonic deformation (Pleistocene-Holocene) in the Andean foreland indicate values between 0.3 to 11 mm/yr (Pearson et al., 2013; McFarland and Bennett, 2017; Echavarria et al., 2003; García et al., 2013; García et al., 2019; Ramos et al., 2006). This work provides data on displacements in basement fractures of 0.74 - 2.6 mm/yr (2021 and 2022). Zeckra (2020) discovered high seismic activity confined along the Andean thrust front with a magnitude of completion MC 1.45 along steep and deep thrust faults generated through the inversion of Cretaceous normal faults.

The thick conglomeratic deposits such as the Yasyamayo (Pliocene) and Lomitas Pegadas (Pleistocene) formations (Figures 5, 12; Table 3) record the last tectonic events of considerable magnitude for the region. Since then, neotectonic deformation appears to have slowed down (Pearson et al., 2013; McFarland and Bennett, 2017; Echavarria et al., 2003, García et al., 2013; García et al., 2019; Ramos et al., 2006).

Considering these deformation values, the neotectonic deformation observed in the outcrops (faults, folds and diversion of the drainage network), and the evidence of the seismic profiles, it is possible to interpret that the seismic activity in the study area from the Pleistocene to the present, remained between the current records (Figure 1; Table 2). This seismic activity, sustained over time, is sufficient to produce deformation in the foothills (Figures 11, 12, 14, 18), reactivate pre-existing faults with small displacements (Figures 5, 8, 17) and generate minor new faults in recent conglomeratic deposits (Figure 16). Many faults are blind. However, the deformation of the landscape and the modification of the drainage network are direct indicators of the activity of these structures.

VIII. Conclusions

The neotectonic deformation occurred in the foothills of the Cumbres Calchaquíes, La Candelaria,

and Taficillo ranges through folds and fractures. Some fractures experienced horizontal movements, and others had reverse displacements, retrovergent to the Andean deformation (Figures 3, 5, 6, 8, 11, 12, 14, 16, 17). Tectonic activity in the piedmont of Cumbres Calchaquíes is affecting deposits dated 630 a BP.

Other manifestations of neotectonic activity are observed in the Santa Bárbara System (Metán, Choromoro basins and east of the La Candelaria range) and Llanura Chaqueña (Figures 1, 14). In the Metán basin, reactivations of Cretaceous fractures are observed in the seismic profiles and on the surface, the deviation of the drainage network. Eventual earthquakes of greater magnitude, such as El Galpón, produce ruptures on the surface. In the Choromoro basin, the landscape appears undulating due to subsoil folds buried by Quaternary deposits that are beginning to be shaped (Figure 14), and new blind faults break the strata of the fluvial terraces (Figure 16). The Colorado, Cantero and Remate hills are folded and folded to the east of the La Candelaria range. Cerro Colorado is the highest expression of the complex. The folds insinuate to the south in the landscape, covered by Quaternary deposits (Figure 14). In the Chaqueña Plain, the subtle uplift of the Lomadas de Otumpa generates control and diversion of the surface drainage network (Figure 1).

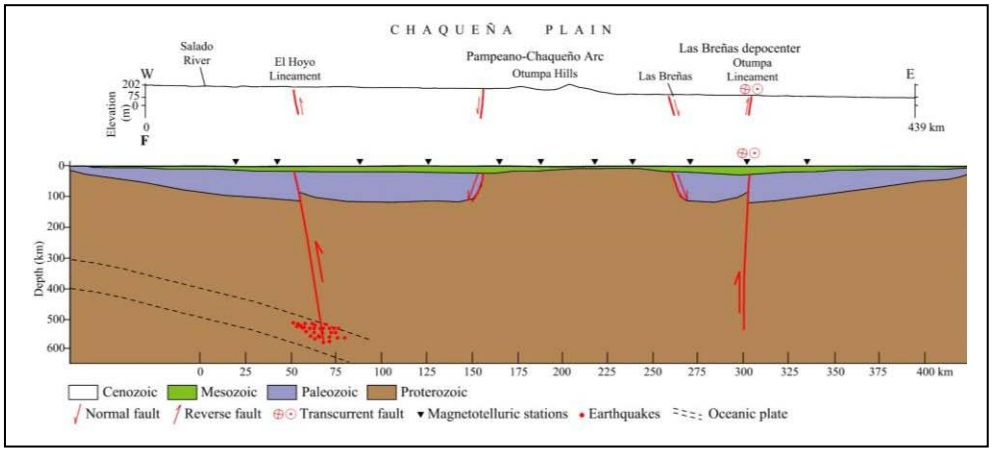

Figure 19: A: Topographic profile of the Chaco Plain. The vertical scale is exaggerated to illustrate the positive relief of the Otumpa Hills. The location of the profile is shown in Figure 1. The profile coincides with the trace of the magnetotelluric stations (Pomposiello et al., 2010) (Figure 1). B: Profile modified from (Pomposiello et al., 2010). To interpret the structures and the stratigraphic sequence in-depth, we have taken the works of (Cristallini et al., 2004; Pezzi and Mozetic, 1989; Chebli et al., 1999; Pomposiello et al., 2010; Peri (2012); Rossello and Veroslavsky, 2012) as a basin.

In the study region, many earthquakes coincide with regional lineaments and faults (Tafí del Valle, Chasquivil, Río Muerto, Los Pinos, Los Hoyos). This coincidence shows these regional faults are active (Figures 1, 2). The seismic activity in the study area from the Pleistocene to the present remained between the current records. It sustained over time is sufficient to produce folds, new faults and reactivation of pre-existed faults in materials of low cohesion.

Acknowledgements

This work was carried out with the support of the National University of Tucumán and the financing of the Argentine-German University Center. My thanks to Minera La Alumbrera S.A. for logistical support and for providing me with geotechnical data. Thanks also to the anonymous reviewers for their suggestions and contributions.

Declarations

Conflict of interest on behalf of all authors, the corresponding author states that there is no conflict of interest.

References Cited

1. Abascal, L.V., 2005, Combined thin-skinned and thick-skinned deformation in the central Andean foreland of northwestern Argentina: Journal of South American Earth Sciences 19: p. 75–81.
2. Aceñolaza, F.G., and Toselli, A.J., 1981, Geología del noroeste argentino: Publicación especial N° 1287 de la Facultad de Ciencias Naturales e IML, Universidad Nacional de Tucumán, Argentina, 212 p.
3. Allen, J.L., and Shaw, C.A., 2011, Seismogenic structure of a crystalline thrust fault: fabric anisotropy and coeval pseudotachylyte-mylonitic pseudotachylyte in the Grizzly Creek Shear Zone, Colorado: In: Fagereng A, Toy VG, Rowland JV (eds) Geology or the earthquake source: a volume in honour of Rick Sibson. Geological Society, v. 359. Special Publications, London, p. 135–151.
4. Ambraseys, N.N., and Tchalenko, J.S., 1969, The Dasht-e-Bayaz (Iran) earthquake of August 31, 1968: a field report: Bull Seismol Soc Am 59: p. 1751–1792.

5. Aranda-Viana, R.G., Bianchi, C., Aramayo, A., Alvarado, L., Arnous, A., Hongn, F., and Strecker, M., 2017, Modelo de imágenes y fotogrametría de la escarpa occidental de la Sierra de la Candelaria con el uso de vehículo aéreo no tripulado: Actas XX Congreso Geológico Argentino, Tucumán 201, Abstracts, 15 p.
6. Arnous, A., Zeckra, M., Venerdini, A., Alvarado, P., Arrowsmith, R., Guillemoteau, J., Landgraf, A., Gutiérrez, A.A., and Strecker, M.R., 2020, Neotectonic Activity in the Low-Strain Broken Foreland (Santa Bárbara System) of the North-Western Argentinean Andes (26°S): Lithosphere, Article ID 8888588, 25 p.
7. Bossi, G.E., Georgieff, S.M., Gavriloff, I.J.C., Ibáñez, L.M., and Muruaga, C.M., 2001, Cenozoic evolution of the intramontane Santa María basin, Pampean Ranges, northwestern Argentina: Journal of Sputh American Earth Sciences 14: p. 725–734.
8. Brace, W., and Byerlee, J.D., 1966, Stick-slip as an earthquake mechanism: Science 153: p. 990– 992.
9. Butler, R.F., Marshall, L.G., Drake, R.E., and Curtis, G.H., 1984, Magnetic polarity stratigraphy and 40K-40Ar dating of late Miocene and early Pliocene continental deposits, Catamarca Province, NW Argentina: Journal of Geology 92(6): p. 623–636.
10. Carrapa, B., and De Celles, P.G., 2015, Regional exhumation and kinematic history of the Central Andes in response to cyclical orogenic processes: Geological Society of America Memoirs 212: p. 201–213. https://doi.org/10.1130/MEM212.
11. Carrapa, B., Trimble, J., and Stockli, D., 2011, Patterns and timing of exhumation and deformation in the Eastern Cordillera of NW Argentina revealed by (U-Th)/He thermochronology: Tectonics 30, TC3003. https://doi.org/10.1029/2010TC002707.
12. Carrapa, B., Adelmann, D., Hilley, G.E., Mortimer, E., Sobel, E.R., and Strecker, M.R., 2005, Oligocene range uplift and development of plateau morphology in the southern Central Andes: Tectonics 24(4), TC4011. https://doi.org/10.1029/2004TC001762.
13. Carrera, N., and Muñoz, J.A., 2008, Thrusting evolution in the southern Cordillera Oriental (northern Argentine Andes): constraints from growth strata: Tectonophysics 459(1-4): p. 107–122. https://doi.org/10.1016/j.tecto.2007.11.068.
14. Chebli, G.A., Mozetic, M.E., Rossello, E.A., and Bühler, M., 1999, Cuencas sedimentarias de la Llanura Chacopampeana: Instituto de Geología y Recursos Minerales, Geología Argentina, Buenos Aires, Anales 29(20): p. 627–644.
15. Collantes, M.M., Powell, J., and Sayago, J.M., 1993, Formación Tafí del Valle (Cuaternario superior), provincia de Tucumán (Argentina): litología, paleontología y pleoambientes: XII Congreso Geológico Argentino y II Congreso de Exploración de Hidrocarburos, Actas II, Abstracts, p. 200–206.
16. Costa, C.H., 2000, Geomorphic signature of Quaternary deformation and strategies for regional mapping in Argentina: In: Proceedings world active faults symposium, 31° International Geological Congress, Brazil, Abstract, CD-Rom.
17. Costa, C.H, Ahumada, E.A., Gardini, C.E., Vázquez, F.R., and Diederix, H., 2014, Quaternary shortening at the orogenic front of the Central Andes of Argentina: the Las Peñas Thrust System: In: Sepúlveda SA, Giambiagi LB, Moreiras SM, Pinto L, Tunik M, Hoke GD, Farías M (eds) Geodynamic processes in the Andes of Central Chile and Argentina. Geological Society, v. 399. Special Publications, London, 21 p.
18. Costa, C.H., 2019, La migración del frente de corrimiento neotectónico de las Sierras Pampeanas y su impronta morfológica: Revista de la Asociación Geológica Argentina 76(4): p. 315– 325.
19. Cristallini, E.O., Comınguez, A.H., Ramos, V.A., and Mercerat, E.D., 2004, Basement double-wedge thrusting in the northern Sierras Pampeanas of Argentina (27°S)- Constraints from deep seismic reflection: In: K.R. McClay (ed) Thrust tectonics and hydrocarbon systems, vol 82. AAPG Memoir, p. 65–90.
20. Cunningham, W.D., and Mann, P., 2007, Tectonics of strike-slip restraining and releasing bends: Geological Society Special Publication N° 290, London, p. 1–12.
21. Deeken, A., Sobel, E.R., Coutand, I., Haschke, M., Riller, U., and Strecker, M.R., 2006, Development of the southern Eastern Cordillera, NW Argentina, constrained by apatite fission track thermochronology: From Early Cretaceous extension to Middle Miocene shortening: Tectonics 25, TC6003. https://doi.org/10.1029/2005TC001894.
22. Del Papa, C., Hongn, F.D., Mon, R., Powell, J., and Petrinovic, I., 2005, Stratigraphy and syndepositional structures of the basal foreland deposits in the northern valley Calchaquí, NW Argentina: 6th International Symposium on Andean Geodynamics, Barcelona, Extended Abstracts, p. 215–217.
23. Echavarria, L., Hernández, R., Allmendinger, R., and Reynolds, J. 2003, Subandean thrust and fold belt of northwestern Argentina: Geometry and timing of the Andean evolution: American Association of Petroleum Geologists Bulletin 87(6): p. 965–985. https://doi.org/10.1306/01200300196.
24. Fagereng, A., and Toy, V.G., 2011, Geology of the earthquake source: an introduction. In: Fagereng A, Toy VG, Rowland JV (eds) Geology or the earthquake source: a volume in honour of Rick Sibson: Geological Society. London, Special Publications, p. 1–16.

25. Figueroa-Villegas, S., Escalante, L., Hongn, F., and Strecker, M., 2017, Deformación tectónica Holocena en la transición entre las Sierras Pampeanas y Cordillera Oriental, valle de Cafayate (26°00' - 25°50' Lat., 66°00' - 65°50' Long.), Salta, Argentina: Actas XX Congreso Geológico Argentino, Sesión Técnica 2, Geología estructural y geotectónica, Abstracts, p. 62–67.
26. García, V.H., Hongn, F.D., Yagupsky, D., Pingel, H., Kinnaird, T., Winocur, D., Cristallini, E., Robinson, R., and Strecker, M.R., 2019, Late Quaternary tectonics controlled by fault reactivation. Insights from a local transpressional system in the intermontane Lerma valley, Cordillera Oriental, NW Argentina: Journal of Structural Geology 128, 103875. https://doi.org/10.1016/j.jsg.2019.103875.
27. García, V.H., Robinson, R.A., Hongn, F.D., Cristallini, E.O., Yagupsky, D.L., Winocur, D., and Vera, D.R., 2013, Late Quaternary uplift rate of Lomas de Carabajal, Lerma valley, Cordillera Oriental, NW Argentina. Insights from structural analysis and OSL dating: Actas CD, Aachen, Alemania: 4th International INQUA Meeting on Paleoseismology, Active Tectonics and Archeoseismology, Actas, Abstracts, CD, Aachen, Alemania.
28. Garralla, S., Muruaga, C., and Herbst, R., 2001, Lago El Rincón, Holoceno del departamento de Tafí del Valle, provincia de Tucumán (Argentina): palinología y facies sedimentarias: Publicación especial-Asociación paleontológica Argentina, Argentina, p. 91–99.
29. Georgieff, S.M., and Díaz, A., 2014, Modelo paleoambiental de la Formación Las Arcas (Mioceno Superior), quebrada del Mal Paso, Valles Calchaquíes del sur de Salta: Reunión Argentina de Sedimentología: 114. Puerto Madryn, Chubut, Abstracts, 2 p.
30. González, O.E., 1999, Geología de La Angostura, valle de Tafí, Tucumán: XIV Congreso Geológico Argentino, Abstracts, Actas I: p. 283–286.
31. González, O.E., 1990, Las vulcanitas del Portezuelo Las Ánimas, sierra de Aconquija, provincias de Catamarca y Tucumán: Revista de la Asociación Geológica Argentina XLV(3-4): p. 386–396.
32. Grier, M.E., Salfity, J.A., and Allmendinger, R.W., 1991, Andean reactivation of the Cretaceous Salta rift, NW Argentine: J S Am Herat Sci 4: p. 351–372.
33. Gutiérrez, A.A., 2000, Morphotectonic Evidences of the Sinestral Rotation of the Pampeanas Mountain Ranges, Argentina: Revista Profil, Band 18, XVII Simposio Latinoamericano de Geología, Stuttgart, Abstracts, 6 p.
34. Gutiérrez, A.A., Alderete, M.C., and Bortolotti, P., 1997, Geomorfología tectónica (neotectónica) en la sierra de La Candelaria, provincia de Salta: IV Simposio Argentino de teledetección, Resúmenes, San Juan, Abstracts, 9 p.
35. Gutiérrez, A.A., and Mon, R., 2008, Macroindicadores cinemáticos en el Bloque Ambato, provincias de Tucumán y Catamarca: Revista de la Asociación Geológica Argentina 63(1): p. 24–28.
36. Gutiérrez, A.A., and Mon, R., 2004, Megageomorfología del valle de Tafí-Aconquija, Tucumán: Revista de la Asociación Geológica Argentina 59(2): p. 303–311.
37. Gutiérrez, A.A., Mon, R., Arnous, A., and Aranda-Viana, R.G., 2021, Piedmont deposits as seismic energy dissipators, Sierras Pampeanas of Argentina: SN Applied Sciences (2021) 3:887, https://doi.org/10.1007/s42452-021-04874-0.
38. Gutiérrez, A.A., Mon, R., Arnous, A., and Cisterna, C.E., 2019, Sinestral rotation and NNW shortening of the ambato block induced by cenozoic NE to E-W transpression, Argentina: Int J Earth Sci Geol 1(2): p. 74–85. https://doi.org/10.18689/ijeg-1000109.
39. Gutiérrez, A.A., Mon, R., Cisterna, C.E., Altenberger, U., and Arnous, A., 2023, Cenozoic Age Counter clockwise Rotation in the Northwest End of the Sierras Pampeanas, Argentina: Open Journal of Geology, 13: p. 345–383. https://doi.org/10.4236/ojg.2023.135018.
40. Gutiérrez, A.A., Mon, R., Sàbat, F., and Iaffa, D.N., 2017, Origin and evolution of the salinas grandes and Salina de Ambargasta, Argentina: In: World multidisciplinary earth sciences symposium, IOP conference series: earth and environmental science, v.(95): p. 022–036. https://doi.org/10.1088/1755-1315/95/2/022036.
41. Gutiérrez, A.A., Mon, R., and Vergara, G., 2003, Neotectónica: captura y decapitación del drenaje, Tucumán-Argentina: Congreso Argentino de Cuaternario y Geomorfología, Abstracts, Tucumán, Actas II, p. 293–300.
42. Hanks, T.C., and Kanamori, H., 1979, A moment magnitude scale: J Geophys Res 84, p. 2348–2350.
43. Iaffa, D.N., Sàbat, F., Bello, D., Ferrer, O., Mon, R., and Gutiérrez, A.A., 2011, Tectonic inversion in a segmented foreland basin from extensional to piggyback settings: the Tucumán basin in NW Argentina: Journal of South American Earth Sciences 31: p. 457– 474.
44. Iaffa, D.N, Sàbat, F., Muñoz, J.A,, Mon, R., and Gutierrez, A.A., 2011, The role of inherited structures in a foreland basin evolution. The Metán Basin in NW Argentina: Journal of Structural Geology, 33: p. 1816–1828.
45. Ikeda, Y., 1983, Thrust front migration and its mechanisms-evolution of intraplate thrust fault

systems: Bulletin of the Geography Department. Univ Tokyo 15: p. 125–159.
46. Incorporated Research Institutions for Seismology (IRIS), 2020, 1200 New York Av. NW Suite 400, Washington, DC 20005, 202- 682-2220. http://ds.iris.edu (accessed June 2023).
47. Instituto Nacional de Prevención Sísmica (INPRES), 2018, Reglamento INPRES-CIRSOC 103, Reglamento Argentino para construcciones sismorresistentes, Parte I: Ministerio dellnterior, Obras Públicas y Vivienda, Secretaría de Planificación Territorial y Coordinación de Obra Pública. 86 p.
48. Jakulica, D., 1948, Estudio geológico en la zona del cerro Colorado: YPF (informe inédito), Buenos Aires, DGE, 341, 18 p.
49. Jordan, T., and Alonso, R., 1987, Cenozoic stratigraphy and basin tectonics of the Andes Mountains, 20-28 South latitude: AAPG Bulletin 71(1): p. 49–64. https://doi.org/10.1306/94886D44-1704-11D7-8645000102C1865D.
50. Kamb, B., Silver, L.T., Abrams, M.J., Carter, B.A., Jordan, T.H., and Minster, J.B., 1971, Pattern of faulting and nature of fault movement in the San Fernando earthquake, in The San Fernando, California, Earthquake of February 9, 1971: U S Geol Surv Prof Pap 733: p.41–54.
51. Lavenu, A., 2006, Neotectónica de los Andes entre 1° N y 47° S (Ecuador, Bolivia y Chile): una revision: Revista de la Asociación Geológica, Argentina 61(4): p. 504–524.
52. Löbens, S., Sobel, E.R., Bense, F.A., Wemmer, K., Dunkl, I., and Siegesmund, S., 2013, Refined exhumation history of the northern Sierras Pampeanas, Argentina: Tectonics 32: p. 453– 472. https://doi.org/10.1002/tect.20038.
53. López, J.P., Altenberger, U., Bellos, L.I., Ferrocchio, B., and Llomparte Frentzel, G., 2017, Petrological and geochemical characteristics of El Pabellón granite, Tafí del Valle, Tucumán, NW of Argentina: XX Congreso Geológico Argentino, Sesión Técnica 4, Petrología y Geoquímica de Rocas Ígneas, Abstracts, San Miguel de Tucumán, Argentina, p. 62–68.
54. Marrett, R.A., Allmendinger, R.W., Alonso, R.N., and Drake, R.E., 1994, Late Cenozoic tectonic evolution of the Puna Plateau and adjacent foreland, Northwestern Argentine Andes: Journal of South American Earth Sciences 7(2): p. 179–207. https://doi.org/10.1016/0895-9811(94)90007-8.
55. Marshall, L.G., and Patterson, B., 1981, Geology and geochronology of the mammal-bearing Tertiary of the Santa María Valley and Corral Quemado River, Catamarca province, Argentina: Field Mus Nat Hist 9: p. 1–78.
56. McFarland, P.K., and Bennett, R.A., 2017, How do regional stress changes following megathrust events affect active retro arc tectonics? A case study of the 27 February 2010 Mw 6.1 Salta earthquake: AGU Fall Meeting Abstracts, G43A-0905, New Orleans, Louisiana, 2 p.
57. Mon, R., 1993, Influencia de la Orogénesis Oclóyica (Ordovícico - Silúrico) en la segmentación andina en el norte argentino: Decimosegundo Congreso Geológico Argentino, Abstracts, 3: p. 65–71.
58. Mon, R., and Drozdzewski, G., 1999, Cinturones doblevergentes en los Andes del norte argentino - Hipótesis sobre su origen: Rev. de la Asociación Geol. Argentina 54: p. 3–8.
59. Mon, R., and Gutiérrez, A.A., 2007, Estructura del extremo sur del Sistema Subandino (provincias de Salta, Santiago del Estero y Tucumán): Revista de la Asociación Geológica Argentina 62(1): 7 p.
60. Mon, R., Gutiérrez, A.A., Sábat, F., and Iaffa, D., 2012, A Miocene Continental Basin associated with the back thrusting of the Eastern Sierras Pampeanas in the Santa Maria Valley, Northwestern Argentina: Italian J Geosci (Boll.Soc.Geol.It.) 131(1): p. 123–135. https://doi.org/10.3301/IJG.2011.27 (Roma).
61. Mon, R., Gutiérrez, A.A., Vergani, G., Pacheco, M.M., and Sábat, F., 2005, Estructura de la depresión tectónica de Metán (Provincia de Salta): Actas del XVI Congreso Geológico Argentino, La Plata, Abstracts, p. 73–80.
62. Nortje, G.S., Olive, N.H.S., Blenkinsop, T.G., Keys, D.L., and Mclellan, J.G., 2011, Oxenburgh S (2011) New faults v fault reactivation: implications for fault cohesion, fluid flow, and copper mineralisation, Mount Gordon Fault Zone, Mount Isa District, Australia: In: Fagereng A, Toy VG, Rowland JV (eds) Geology or the earthquake source: a volume in honour of Rick Sibson. Geological Society, vol 359. Special Publications, London, p. 287–311.
63. Ortíz, P.E., and Jayat, J.P., 2007, Sigmodontinos (Rodentia: Cricetidae) del límite Pleistoceno - Holoceno en el valle de Tafí (Tucumán, Argentina): taxonomía, tafonomía y significación Paleoambiental: Ameghiniana, Revista de la Asociación Paleontológica Argentina, Buenos Aires, 44(4): p. 641–660.
64. Pearson, D.M., Kapp, P., De Celles, P.G., Reiners, P.W., Gehrels, G.E., Ducea, M.N., and Pullen, A., 2013, Influence of pre-Andean crustal structure on Cenozoic thrust belt kinematics and shortening magnitude: northwestern Argentina: Geosphere 9 (6): p. 1766–1782. https://doi.org/10.1130/ges00923.1.
65. Peña-Monné, J.L., and Sampietro-Vattuone, M.M., 2018, Paleoambientes holocenos del valle de Tafí (Noroeste Argentino) a partir de registros morfosedimentarios y geoarqueológicos: In: Polanco JM, Frugone M (eds) Boletín Geológico y Minero. Paleoclimas en Iberoamérica. Un análisis

mediante registros geológicos e indicadores ambientales, vol 129(4): p. 671–691.
66. Peri, V.G., 2012, Caracterización morfotectónica de las Lomadas de Otumpa (gran Chaco, Santiago del Estero y Chaco): Influencias en el control del drenaje: Universidad de Buenos Aires, Facultad de Ciencias Exactas y Naturales, Departamento de Ciencias Geológicas [Tesis doctoral], 321 p.
67. Peri, V.G., and Rossello, E.A., 2010, Anomalías morfoestructurales el drenaje del río Salado sobre las Lomadas de Otumpa (Santiago del Estero y Chaco) detectadas por procesamiento digital: Revista de la Asociación Geológica Argentina 66(4): p. 634–645.
68. Pezzi, E.E., and Mozetic, M.E., 1989, Cuencas sedimentarias de la region Chacoparanaense. Cuencas sedimentarias Argentinas: Serie correlación geológica N° 6, Instituto Superior de Correlación Geológica, Universidad Nacional de Tucumán, p. 65–78.
69. Pilger, R., 1984, Cenozoic plate kinematics, subduction and magmatism South American Andes: J Geol Soc Lond 41: p. 793–802.
70. Pomposiello, C., Peri, V.G., and Favetto, A., 2010, Magnetotelluric model across the Chacopampeana Plain at 27° S, Santiago del Estero and Chaco provinces, Argentina: IAGA WG 1.2 on Electromagnetic Induction in the Earth 20th Workshop Abstract, Giza, Egypt, 4 p.
71. Porto, J.C., Danieli, C., and Ruiz-Huidobro, O.J., 1982, El Grupo Salta en la Provincia de Tucumán: V Congreso Latinoamericano Argentino, Abstracts, Actas IV: p 253–264.
72. Powell, J.E., and González, O.E., 1997, Hallazgo de mamíferos en la Formación Saladillo (Grupo Santa María), próximo al río Amaicha, provincia de Tucumán: Implicancias cronológicas. Ameghiniana 34: p. 124–130.
73. Ramos, V.A., Alonso, R.N., and Strecker, M.R., 2006, Estructura y neotectónica de Las Lomas de Olmedo, zona de transición entre los sistemas Subandino y de Santa Bárbara, Provincia de Salta: Revista de la Asociación Geológica Argentina 61(4): p. 579–588.
74. Ricci, H., and Villanueva, A., 1969, La presencia del Paleozoico inferior en la sierra de La Candelaria (provincia de Salta): Acta Geológica Lilloana, Tucumán, 10(1): p. 1–6.
75. Riller, U., and Oncken, O., 2003, Growth of the Central Andes Plateau by tectonic segmentation is controlled by the gradient in crustal shortening: Journal of Geology 111: p. 367–384.
76. Rodgers, D., and Rizer, W.D., 1981, Deformation and secondary fault- ing near the leading edge of a thrust fault: In Thrust and Nappe: Tectonics, Geol. Soc. London, Spec. Pub., (9): p. 65–77.
77. Rossello, E.A., and Veroslavsky, G., 2012, Definición del límite occidental del Sistema Acuífero Guaraní (Gran Chaco, Argentina): ¿técnico o convencional?: Boletín Geológico y Minero, ISSN: 0366-0176, 123(3): p. 297–310.
78. Ruiz-Huidobro, O.J., 1972, Descripción geológica de la Hoja 11 e, Santa María, provincias de Catamarca y Tucumán: Servicio Nacional Minero Geológico, Boletín, 134, 65 p.
79. Sampietro-Vattuone, M.M., and Peña-Monné, J.L., 2016, Geomorphological dynamic changes during the Holocene through ephemeral stream analyses from Northwest Argentina: CATENA 147: p. 663–677. https://doi.org/10.1016/j.catena.2016.08.029.
80. Sampietro-Vattuone, M.M., Peña-Monné, J.L., Roldán, J., Dip, A.B., Maldonado, M.G., Lefebvre, M.G., and Vattuone, M.A., 2019, Land management and soil degradation evidence during the Late Holocene in Northwest Argentina (La Costa 2 - Tafí Valley): Catena 182, Elsevier, 13 p.
81. Schellenberger, A., Heller, F., and Veit, H., 2002, Magnetostratigraphy and magnetic susceptibility of the Las Carreras loess-paleosol sequence in Valle de Tafí, Tucumán, NW de Argentina: paleoclimatic significance: XV Congreso Geológico, Calafate, Abstracts, Actas CD- ROM, Artículo N° 317, 4 p.
82. Scholz, C.H., 2002, Mechanics of earthquakes and faulting: 2nd ed. Cambridge University Press, New York. https://doi.org/10.1017/CBO9780511818516.
83. Schwanghart, W., and Scherler, D., 2014, TopoToolbox 2 e MATLAB - based software for topographic analysis and modelling in Earth surface sciences: Short Commun Earth Surf Sci Earth Surf Dyn 2(1): p. 1–7.
84. Sibson, R.H., 1982, Fault zone models, heat flow, and the depth distribution of earthquakes in the continental crust of the United States: Bull Seismol Soc Am 72: p. 151–163.
85. Somoza, R., and Ghidella, M.E., 2005, Convergencia en el margen occidental de América del Sur durante el Cenozoico: 16° Congreso Geológico Argentino, La Plata, Abstracts, Actas, p. 43–45.
86. Spagnuolo, C.M., Georgieff, S.M., and Rapalini, A.E., 2015, Magnetostratigraphy of the Miocene las Arcas formation, Santa María valley, northwestern Argentina: Journal of South American Earth Sciences 63: p. 101–113.
87. Starck, D., and Vergani, G., 1996, Desarrollo tecto-sedimentario del Cenozoico en el sur de la Provincia de Salta-Argentina: 13° Congreso Geológico Argentino, Buenos Aires, Abstracts, Actas 8: p. 433–452.
88. Strecker, M.R., Bloom, A., Carrión, M., Villanueva, A., and Naeser, C., 1984, Piedmont terraces in the Valle de Santa María and in front of southwestern

Sierra Aconquija: Actas del 9° Congreso Geológico Argentino San Carlos de Bariloche, Abstracts, 2: p. 448–465.
89. Strecker, M.R., Bloom, A.L., Malizzia, D., Cerveny, P., Bossi, G.E., Bensel, C.H., and Villanueva-García, A., 1987, Nuevos datos Neotectónicos sobre las Sierras Pampeanas Septentrionales (26°-27° S), República Argentina: Décimo Congreso Geológico Argentino, San Miguel de Tucumán, Abstracts, 1: p. 231–234.
90. Strecker, M.R., Cerveny, P., Bloom, A.L., and Malizia, D., 1989, Late Cenozoic tectonism and landscape development in the foreland of the Andes: Northern Sierras Pampeanas (26°-28° S), Argentina: Tectonics 8: p. 517–534.
91. Turner, J.C.M., 1960, Estratigrafía de la sierra de Santa Victoria y adyacencias: Bol. Academia Nacional de Ciencias, Córdoba, 41(2): p. 163–196.
92. Wells, D.L., and Coppersmith, K.J., 1994, New empirical relationships among magnitude, rupture length, rupture width, rupture area, and surface displacement: Bull Seismol Soc Am 84: p. 974–1002.
93. Woodcock, N.H., and Fisher, M., 1986, Strike-slip duplexes: J Struct Geol 8(7): p. 725–735.
94. Zampieri, D., Gutiérrez, A.A., Massironi, M., and Mon, R., 2012, Reconciling opposite strike-slip kinematics in the Sierra Pampeanas (Argentina) transpressional belt: European Geosciences Union General Assembly, Viena, Austria, Abstracts, 2 p.
95. Zeckra, M., 2020, Seismological and Seismotectonic Analysis of the Northwestern Argentine Central Andean Foreland [Ph.D. thesis]: https://doi.org/10.25932/publishup-47324, Potsdam University, 118 p.

Global Journal of human-social science: b
Geography, Geo-Sciences, Environmental Science & Disaster Management
Volume 23 Issue 5 Version 1.0 Year 2023
Type: Double Blind Peer Reviewed International Research Journal
Publisher: Global Journals
Online ISSN: 2249-460x & Print ISSN: 0975-587X

Comparison of Four Protocols for Rapid Assessment of Rivers Applied in the Streams of Maripá, Parana State, Brazil

By Mariza Martins De Jesus Jung & Oscar Vicente Quinonez Fernandez
Universidade Estadual do Oeste do Paraná

Abstract- The application of the rapid river assessment protocol is very important in surveying the environmental conditions of streams. The present work aims to apply the protocols of Callisto et al. (2001), Guimarães et al. (2012), Baião (2014) and Machado (2019) in streams in the municipality of Maripá, western Paraná and compare the results. The proposal by Callisto et al. (2001) was adopted in this work as a reference in the assessment of aquatic habitats, as it is a pioneering protocol in Brazil and includes a greater number of parameters. The finale scores obtained at each monitoring point applying the four protocols were standardized, as each proposal presents classification categories organized on different scales. The normalized values showed that the protocols produced equivalent results. This finding leads us to suggest that both the protocol by Guimarães et al. (2012) such as Baião (2014) and Machado (2019), all of them simpler and less extensive than Callisto et al. (2001) protocol, can be adopted in schools and colleges in Maripá and municipalities in the region, as an instrument of environmental education.

Keywords: *water resources; environmental education; environmental impact.*

GJHSS-B Classification: *LCC: QH541.5*

Comparison of Four Protocols for Rapid Assessment of Rivers Applied in the Streams of Maripá, Parana State, Brazil

Comparação de Quatro Protocolos de Avaliação Rápida de Rios Aplicados Nos Córregos de Maripá (PR)

Mariza Martins De Jesus Jung [α] & Oscar Vicente Quinonez Fernandez [σ]

Resumo- A aplicação do protocolo de avaliação rápida de rios (PAR) tem muita importância no levantamento das condições ambientais dos riachos. O presente trabalho objetiva aplicar os protocolos de Callisto et al. (2001), Guimarães et al. (2012), Baião (2014) e Machado (2019) em córregos do município de Maripá, Oeste do Paraná e comparar os resultados. A proposta de Callisto *et al.* (2001) foi adotada neste trabalho como referência na avaliação de habitats aquáticos, por se tratar de um protocolo pioneiro no Brasil e incluir maior número de parâmetros. As pontuações finais obtidas em cada ponto de monitoramento aplicando os quatro protocolos foram normatizados, já que cada proposta apresenta categorias de classificação organizadas em escalas diferentes. Os valores normatizados mostraram que os protocolos produziram resultados equivalentes. Esta constatação nos leva a sugerir que tanto o protocolo de Guimarães et al. (2012) como o de Baião (2014) e Machado (2019), todos mais simples e menos extensos que o de Callisto et al. (2001), podem ser adotados em escolas e colégios de Maripá e municípios da região, como instrumento de educação ambiental. A compatibilidade dos protocolos verificada nesta pesquisa, deve ser observada com reservas, já que esta condição pode não se repetir em outros ambientes com condições de relevo, clima, vegetação e uso da terra diferentes.

Palavras-Chave: recursos hídricos; educação ambiental; impacto ambiental.

Abstract- The application of the rapid river assessment protocol is very important in surveying the environmental conditions of streams. The present work aims to apply the protocols of Callisto et al. (2001), Guimarães et al. (2012), Baião (2014) and Machado (2019) in streams in the municipality of Maripá, western Paraná and compare the results. The proposal by Callisto et al. (2001) was adopted in this work as a reference in the assessment of aquatic habitats, as it is a pioneering protocol in Brazil and includes a greater number of parameters. The finale scores obtained at each monitoring point applying the four protocols were standardized, as each proposal presents classification categories organized on different scales. The normalized values showed that the protocols produced equivalent results. This finding leads us to suggest that both the protocol by Guimarães et al. (2012) such as Baião (2014) and Machado (2019), all of them simpler and less extensive than Callisto et al. (2001) protocol, can be adopted in schools and colleges in Maripá and municipalities in the region, as an instrument of environmental education. The compatibility of the protocols verified in this research must be observed with reservations, since this condition may not be repeated in other environments with different relief conditions, climate, vegetation and land use.

Keywords: water resources; environmental education; environmental impact.

Resumen- La aplicación del protocolo de evaluación rápida de ríos (PAR) es muy importante en el estudio de las condiciones ambientales de los arroyos. El presente trabajo tiene como objetivo aplicar los protocolos de Callisto et al. (2001), Guimaraes et al. (2012), Baião (2014) y Machado (2019) en arroyos del distrito de Maripá, Oeste de Paraná y comparar los resultados. La propuesta de Callisto et al. (2001) fue adoptada en este trabajo como referencia en la evaluación de hábitats acuáticos, ya que es un protocolo pionero en Brasil e incluye una mayor cantidad de parámetros. Se normalizaron los puntajes finales obtenidos en cada punto de monitoreo, aplicando los cuatro protocolos, ya que cada propuesta presenta categorías de clasificación organizadas en diferentes escalas. Los valores normalizados mostraron que los protocolos produjeron resultados equivalentes. Este hallazgo nos lleva a sugerir que los protocolos de Guimarães et al. (2012), Baião (2014) y Machado (2019) que son más sencillas y menos extensas que el de Callisto et al. (2001) pueden ser utilizados en escuelas y colegios de Maripá y distritos de la región, como instrumento de educación ambiental. La compatibilidad de los protocolos verificados en esta investigación debe ser analizado con cuidado, ya que las condiciones ambientales no se repiten en otras regiones con diferentes condiciones de relieve, clima, vegetación y uso del suelo.

Palabras Clave: recursos hídricos; educación ambiental; impacto ambiental.

I. Introdução

Desde o início da vida no planeta Terra, a água sempre foi um recurso essencial. Qualquer forma de vida depende da água para sua

Author α: Docente da Escola Municipal Professor Leopoldo Kuroli, Maripá. Mestranda em Geografia na Universidade Estadual do Oeste do Paraná (Unioeste), campus de Marechal Cândido Rondon.
e-mail: mariza.jung@escola.pr.gov.br
Author σ: Docente do curso de Graduação e Pós-graduação em Geografia, Universidade Estadual do Oeste do Paraná (Unioeste), campus de Marechal Cândido Rondon.
e-mail: oscar.fernandez@unioeste.br

sobrevivência e desenvolvimento. As grandes civilizações sempre dependeram de água doce para seu desenvolvimento cultural e econômico. Apesar da importância fundamental dos recursos hídricos, a preocupação com a questão ambiental só ganhou destaque a partir da década de 1960, tornando-se objeto de atenção de diversos movimentos sociais e ambientais. A partir daquela década, as discussões ambientais tornaram-se mais frequentes, alcançando dimensões científicas em estudos acadêmicos coordenados por pesquisadores de diferentes países do mundo.

Até a década de 1970 a ênfase no monitoramento ambiental realizado nos Estados Unidos seguiu a tradição das análises quantitativas (RESH e JACKSON, 1993). Em meados da década de 1980, os órgãos ambientais perceberam a necessidade de se estabelecer métodos de avaliação qualitativos devido aos altos custos das pesquisas quantitativas. Em 1986, o órgão federal estadunidense *Environmental Protection Agency* (EPA), iniciou estudos a respeito da qualidade da água juntamente com outras agências de monitoramento de águas superficiais. Desse estudo resultou o relatório da EPA (1987) que enfatiza a reestruturação dos programas de monitoramento praticados e recomendou o desenvolvimento e a aplicação de técnicas de monitoramento biológica e a elaboração de um guia de avaliação do meio físico que além de ser de baixo custo, fosse capaz de identificar os problemas existentes. Com base nestas sugestões, surgiram os protocolos de avaliação rápida que fornecem dados básicos sobre o habitat aquático no tocante a qualidade da água e gerenciamento dos recursos hídricos.

Foram propostos vários protocolos que envolvem diferentes critérios. O primeiro deles foi o de Plafkin et al. (1989). Posteriormente, Hannaford et al. (1997) publicaram um protocolo resultado da junção de vários métodos de avaliação rápida aplicados em regiões temperadas dos Estados Unidos por agências ambientais. No Brasil este protocolo foi adaptado por Callisto et al. (2001) para seu uso no bioma de mata atlântica em ecossistemas lóticos e objetiva uma avaliação geral e qualitativa do nível de preservação das características naturais e antrópica dos cursos de água mediante a observação de 22 parâmetros nos habitats aquáticos.

Tendo como base o trabalho de Callisto et al. (2001), vários pesquisadores propuseram protocolos envolvendo diversos outros parâmetros e critérios de pontuação diferentes para serem aplicados em várias regiões do país (RODRIGUES e CASTRO, 2008; RODRIGUES, 2008; GUIMARÃES et al., 2012, BAIÃO, 2014, MACHADO, 2019).

O presente trabalho tem por objetivo aplicar vários protocolos (CALLISTO et al., 2001; GUIMARÃES et al., 2012; BAIÃO, 2014 e MACHADO, 2019) em córregos no município de Maripá, Oeste do Paraná (Figura 1) e posteriormente comparar os resultados obtidos. Por se tratar de um protocolo pioneiro no Brasil e mais detalhado quanto a abrangência dos parâmetros, a proposta de Callisto *et al*. (2001) foi adotada neste trabalho como referência na avaliação dos habitats aquáticos.

II. Metodologia

a) *Área de estudo*

O município de Maripá está situado na mesorregião geográfica Oeste do estado do Paraná e limita com os municípios de Palotina (Norte), Toledo (Sul), Assis Chateubriand (Leste) e Nova Santa Rosa (Oeste) (Figura 1). A área territorial do município é de 283,79 km^2 e a população estimada para 2021 é de 5.562 habitantes (IBGE, 2022).

O municipio de Maripá está inserido no terceiro planalto paranaense, no qual afloram rochas basálticas de idade cretácea com altitude média de 400 m (MAACK, 2012). O clima no município é subtropical úmido mesotérmico (tipo Cfa - classificação de Köeppen) com altas taxas de precipitação nos meses de verão e geadas nos meses de inverno. A média das temperaturas nos meses mais quentes é superior a 22^o C, e nos meses frios é inferior a 18^{o}C (IAPAR, 2021).

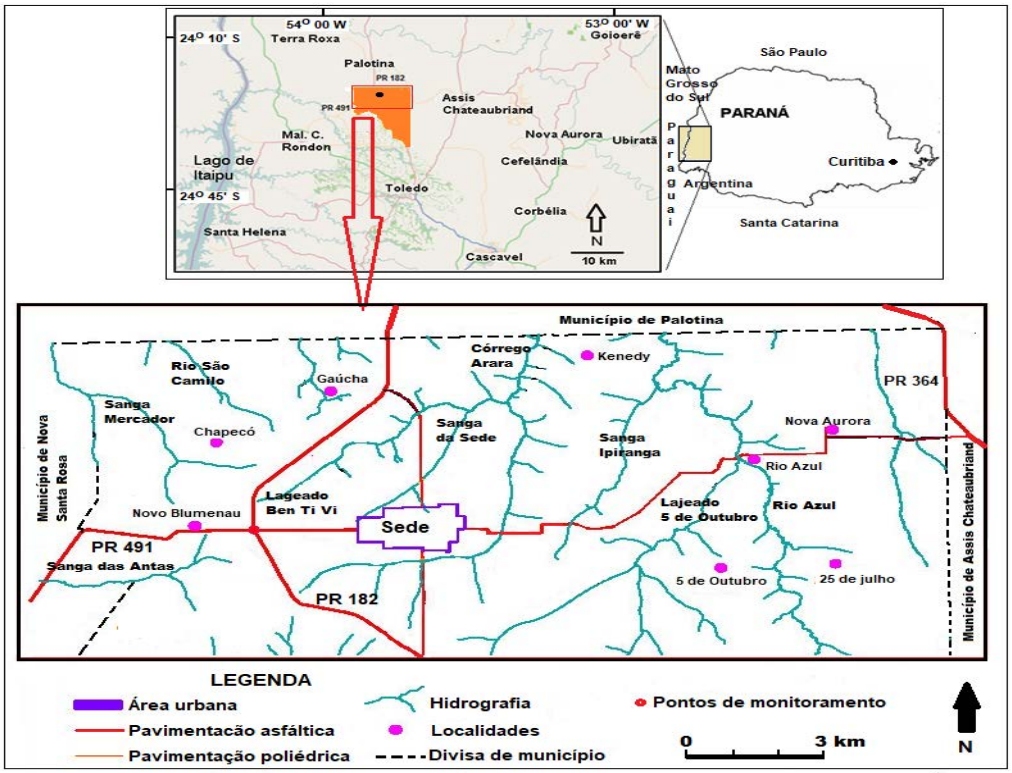

Fonte: os autores.

Figura 1: Localização do município de Maripá, região Oeste do Paraná.

A sede urbana do município está situada no interflúvio do lajeado Arara e da Sanga da Sede (Afluente do lajeado Bem-te-vi). Os principais cursos d`água do município são: o lajeado Arara e seus afluentes lajeado Bem-ti-vi e Sanga da Sede e o rio Azul e seus afluentes Arroio Independente e os lajeados 5 de outubro e Ipiranga (Figura 1). Os termos lajeado e sanga são usados na região, por influência de colonos sul-rio-grandenses e catarinenses, para designar cursos d'água de 1ª a 3ª ordens (classificação de Stralher) com leito rochoso (laje) e leito composto por cascalhos/ areia respectivamente (IBGE, 2010).

A colonização moderna do município de Maripá e região foi iniciada nas décadas de 1940 e 1950 pela Industrial Madeireira Colonizadora Rio Paraná S/A (Companhia Maripá) que incentivou a vinda de colonos oriundos do Rio Grande do Sul e Santa Catarina para extração de madeira e erva mate (GREGORY, 2002). Os colonizadores foram atraídos pelas terras férteis da região e também pela abundância de recursos hídricos. A Vila Maripá foi fundada em 04 de junho de 1953 e foi elevada à categoria de município em 17 de abril de 1990. (PREFEITURA DE MARIPÁ, 2021).

As principais atividades econômicas do município de Maripá estão direcionadas para a agricultura, piscicultura e para o cultivo de orquídeas. A produção de grãos (soja, milho e trigo) constitui a principal atividade econômica do município desde a década de 1970. A pecuária encontra-se presente nas pequenas propriedades rurais e as principais atividades são a criação de bovinos para leite e corte e, criação de peixes e aves.

b) Materiais e métodos

Os protocolos propostos por Callisto et al. (2001), Guimarães et al. (2012), Baião (2014) e Machado (2019) foram aplicados em pontos de monitoramento nos córregos situados em entorno da sede urbana de Maripá (PR).

O protocolo de avaliação rápida de rios (PAR) proposto por Callisto et al. (2001) se baseia na quantificação de 22 parâmetros. Os primeiros 10 parâmetros procuram avaliar as características dos trechos e os impactos ambientais decorrentes de atividades antrópicas e os parâmetros restantes buscam avaliar as condições de hábitat e níveis de conservação das condições naturais (Tabela 1).

A pontuação para cada parâmetro no protocolo é atribuída através da observação das condições do hábitat. As pontuações finais refletem o nível de preservação das condições ecológicas dos trechos de bacias estudados, de 0 a 40 pontos representam trechos Impactados; de 41 a 60 pontos representam trechos Alterados e acima de 61 pontos até 100 pontos, trechos Naturais.

Tabela 1: Parâmetros adotados por Callisto et al. (2001) no protocolo de avaliação rápida dos rios.

	PONTUAÇÃO		
PARÂMETROS	4 pontos	2 pontos	0 pontos
1. Tipo de ocupação das margens do corpo d'água (principal atividade)	Vegetação natural	Campo de pastagem, Agricultura, Monocultura, Reflorestamento	Residencial/Comercial/ Industrial
2. Erosão próxima e/ou nas margens do rio e assoreamento em seu leito	Ausente	Moderada	Acentuada
3. Alterações antrópicas	Ausente	Alterações de origem doméstica (esgoto, lixo)	Alterações de origem industrial/ urbana (fábricas, siderúrgicas, canalização, reutilização do curso do rio)
4. Cobertura vegetal no leito	Parcial	Total	Ausente
5. Odor da água	Nenhum	Esgoto (ovo podre)	óleo/industrial
6. Oleosidade da água	Ausente	Moderada	Abundante
7. Transparência da água	Transparente	Turva/cor de chá-forte	opaca ou colorida
8. Odor do sedimento (fundo)	Nenhum	Esgoto (ovo podre)	óleo/industrial
9. Oleosidade do fundo	Ausente	Moderado	Abundante
10. Tipo de fundo	Pedras ou cascalho	Lama/areia	cimento/canalizado

	PONTUAÇÃO			
PARÂMETROS	5 pontos	3 pontos	2 pontos	0 pontos
11. Tipos de fundo	Mais de 50 % com habitats diversificados: pedaços de troncos submersos; cascalho ou outros habitats estáveis.	30 a 50 % de habitats diversificados: habitats adequados para a manutenção das populações de organismos aquáticos.	10 a 30 % de habitats diversificados: disponibilidade de habitats insuficiente: substratos frequentemente modificados.	Menos que 10 % de habitats iversificados: ausência de habitats óbvia: substrato rochoso instável para fixação dos organismos.
12. Extensão de rápidos	Rápidos e corredeiras bem desenvolvidas: rápidos tão largos quanto o rio e com o comprimento igual ao dobro da largura do rio.	Rápidos com a largura igual a do rio, mas com comprimento menor que o dobro da largura do rio.	Trechos rápidos podem estar ausentes: rápidos não tão largos quanto o rio e seu comprimento menor que o dobro da largura do rio.	Rápidos ou corredeiras inexistentes.
13. Frequência de rápidos	Rápidos relativamente frequentes: distância entre rápidos dividida pela largura do rio entre 5 e 7.	Rápidos não frequentes; distância entre rápidos dividida pela largura do rio entre 7 e 15.	Rápidos ou corredeiras ocasionais; habitats formados pelos contornos do fundo; distância entre rápidos dividida pela largura do rio entre 15 e 25.	Geralmente com lâmina d'água "lisa" ou com rápidos rasos; pobreza de habitats; distância entre rápidos dividida pela largura do rio maior que 25.
14. Tipos de substrato	Seixos abundantes (prevalecendo em nascentes).	Seixos abundantes: cascalho comum.	Fundo formado predominantemente por cascalho: alguns seixos presentes.	Fundo pedregoso: seixos ou lamoso.
15. Deposição de lama	Entre 0 e 25% do fundo coberto por lama.	Entre 25 e 50% do fundo coberto por lama.	Entre 50 e 75% do fundo coberto por lama.	Mais de 75% do fundo coberto por lama.

16. Depósitos sedimentares	Menos de 5% do fundo com deposição de lama: ausência de deposição nos remansos.	Alguma evidência de modificação no fundo, principalmente como aumento de cascalho, areia ou lama; 5 a 30% do fundo afetado; suave deposição nos remansos.	Deposição moderada de cascalho novo, areia ou lama nas margens; entre 30 a 50% do fundo afetado: deposição moderada nos remansos.	Grandes depósitos de lama, maior desenvolvimento das margens; mais de 50% do fundo modificado: remansos ausentes devido a significativa deposição de sedimentos.
17. Alterações no canal do rio	Canalização (retificação) ou dragagem ausente ou mínima: rio com padrão normal.	Alguma canalização presente, normalmente próximo a construção de pontes; evidência de modificações há mais de 20 anos.	Alguma modificação presente nas duas margens: 40 a 80% do rio modificado.	Margens modificadas: acima de 80% do rio modificado.
18. Características do fluxo das águas	Fluxo relativamente igual em toda a largura do rio; mínima quantidade de substrato exposta.	Lâmina d'água acima de 75% do canal do rio; ou menos de 25% do substrato exposto.	Lâmina d'água entre 25 e 75% do canal do rio; e/ou maior parte do substrato nos "rápidos" exposto.	Lâmina d'água escassa e presente apenas nos remansos.
19. Presença de mata ciliar	Acima de 90% com vegetação ripária nativa, incluindo árvores, arbustos ou macrófitas; mínima evidência de deflorestamento; todas as plantas atingindo a altura "normal".	Entre 70 e 90% com vegetação ripária nativa, deflorestamento evidente, mas não afetando o desenvolvimento da vegetação; maioria das plantas atingindo a altura "normal".	Entre 50 e 70% com vegetação ripária nativa, deflorestamento óbvio; trechos com solo exposto ou vegetação eliminada; menos da metade das plantas atingindo a altura "normal".	Menos de 50% de mata ciliar nativa; deflorestamento muito acentuado.
20. Estabilidade das margens	Margens estáveis; evidência de erosão mínima ou ausente; pequeno potencial para problemas futuros. Menos de 5% da margem afetada.	Moderadamente estáveis; pequenas áreas de erosão frequentes. Entre 5 e 30% da margem com erosão.	Moderadamente instável; entre 30 e 60% da margem com erosão. Risco elevado de erosão durante enchentes.	Instável: muitas áreas com erosão; frequentes áreas descobertas nas curvas do rio; erosão óbvia entre 60 e 100% da margem.
21. Extensão de mata ciliar	Largura da vegetação ripária maior que 18 m; sem influência de atividades antrópicas (agropecuária, estradas, etc.).	Largura da vegetação ripária entre 12 e 18 m; mínima influência antrópica.	Largura da vegetação ripária entre 6 e 12 m; influência antrópica intensa.	Largura da vegetação ripária menor que 6 m; vegetação restrita ou ausente devido a atividade antrópica.
22. Presença de plantas aquáticas	Pequenas macrófitas aquáticas e/ou musgos distribuídos pelo leito.	Macrófitas aquáticas ou algas filamentosas ou musgos distribuídos no rio, substrato com periflton.	Algas filamentosas ou macrófitas em poucas pedras ou alguns remansos, periflton abundante e bioflime.	Ausência de vegetação aquática no leito do rio ou grandes bancos macrófitas (p. ex. aguapé).

Fonte: Callisto et al. (2001)

O protocolo de avaliação rápida de rios (PAR) proposto por Guimarães et al. (2012) inclue 11 parâmetros (Tabela 2). Cada parâmetro recebe pontuações que variam de 0, 5 ou 10 pontos conforme o grau de alteração do parâmetro. A pontuação final foi calculada pela soma dos valores dos parâmetros. As pontuações de 0 a 30 indicam trechos Ruins, de 31 a 70 Bons e de 71 a 110 pontos indicam trechos Ótimos.

O protocolo de Baião (2014) é composto por 12 parâmetros (Tabela 3) e a pontuação de cada um deles varia de 0, 3 e 5 pontos. Este protocolo foi baseado nos protocolos de Calllisto et al. (2001) e Guimarães et al.

(2012) e os trechos fluviais são classificados em Impactados quando a pontuação final estiver entre 0 e 25 pontos, Alterados de 26 a 40 pontos e Naturais quando a somatória dos pontos for de 41 a 60 pontos.

O protocolo proposto por Machado (2019) que inclui 13 parâmetros (Tabela 4), foi baseado no protocolo de Guimarães et al. (2012) e foi adicionado dois novos parâmetros (sinuosidade do canal e proteção das margens pela vegetação). Da mesma forma que o protocolo de Guimarães et al. (2012), as pontuações do protocolo ora em apreço variam de 0, 5 e 10 pontos e apresenta três categorias definidas pelas pontuações finais cujas amplitudes de 0 a 52 pontos indicam trecho Impactado, de 53 a 78 trecho Alterado e de 79 a 130 pontos indicam condição Natural. Este protocolo segue as mesmas categorias apresentadas por Callisto et al. (2001).

Para efeito de comparação dos protocolos cujas amplitudes de escala de pontuações são diferentes (0 a 100 pontos no Callisto et al. [2001], de 0 a 110 no Guimarães et al. [2012], de 0 a 60 pontos no Baião [2014] e 0 a 130 pontos no Machado [2019]), optou-se por normatizar os valores finais obtidos nos pontos de monitoramento. A normatização consiste em transformar valores para uma mesma escala que varia de 0 a 1, através da divisão das pontuações finais em cada ponto de monitoramento por 100 no protocolo de Callisto et al. (2001), por 110 no Guimarães et al. (2012), por 60 no Baião (2014) e por 130 no Machado (2019).

Tabela 2: Parâmetros adotados por Guimarães et al. (2012) no protocolo de avaliação rápida dos rios.

Parâmetros		Categorias e pontuações		
		Ótima	Boa	Ruim
01	Características do fundo do rio (substratos).	10	5	0
02	Sedimentos no fundo do rio.	10	5	0
03	Erosão	10	5	0
04	Lixo	10	5	0
05	Alterações no canal do riacho.	10	5	0
06	Esgoto doméstico ou industrial.	10	5	0
07	Oleosidade da água.	10	-	0
08	Plantas aquáticas.	10	5	0
09	Animais	10	5	0
10	Odor da água	10	-	0
11	Ocupação das margens	10	5	0

Fonte: Guimarães et al. (2012)

Tabela 3: Parâmetros adotados por Baião (2014) no protocolo de avaliação rápida dos rios.

Parâmetros		Pontuações		
		5	3	0
01	Tipo de ocupação das margens do corpo d'água	Margens ocupadas por vegetação natural	Margens ocupadas por agricultura, monocultura, reflorestamento ou pastagens	Margens ocupadas por residencias, comércios ou indústrias
02	Erosão ou assoreamento	Sem deslizamentos nas margens	Com deslizamentos em uma margem do rio	Com muito deslizamento nas duas margens do rio
03	Presença de esgoto	Ausente	Moderada	Abundante
04	Presença de plantas aquáticas	Ausencia de macrófitas	Presença moderada de macrófitas	Abundância de macrófitas
05	Odor da água.	Nenhum	Moderado	Forte
06	Oleosidade da água	Ausente	Moderado	Forte
07	Transparência da água.	Transparente	Turva/cor de chá forte	Turva/cor de café
08	Tipo de fundo	Pedras/cascalhos naturais do leito	Lama/areia	Cimento. Canalizado
09	Corredeiras e fluxo d'água	Fluxo igual em toda a largura do rio, sem substrato exposto	Fluxo de água diferenciada com subtrato exposto	Pouco fluxo de água com muito subtrato exposto
10	Presença de lixo	Ausente	Moderada	Abundante
11	Presença de animais	Abundância de peixes, anfíbios e insetos aquáticos	Presença moderada de peixes, anfíbios e insetos aquáticos	Ausentes
12	Presença de mata ciliar	Abundante	Moderada	Ausente

Fonte: Baião (2014)

Tabela 4: Parâmetros adotados por Machado (2019) no protocolo de avaliação rápida dos rios.

Parâmetros		Categorias e pontuações		
		Ótima	Boa	Ruim
01	Características do fundo do rio (substratos).	10	5	0
02	Sedimentos no fundo do rio.	10	5	0
03	Erosão	10	5	0
04	Lixo	10	5	0
05	Alterações no canal do riacho.	10	5	0
06	Esgoto doméstico ou industrial.	10	5	0
07	Oleosidade da água.	10	-	0
08	Plantas aquáticas.	10	5	0
09	Animais	10	5	0
10	Odor da água	10	-	0
11	Sinuosidade do canal	10	5	0
12	Proteção das margens pela vegetação	10	5	0
13	Ocupação das margens	10	5	0

Fonte: Machado (2019)

III. Resultados e Discussão

Os protocolos de Callisto et al. (2001), Guimarães et al. (2012), Baião (2014) e Machado (2019) foram aplicados em oito pontos de monitoramento selecionados em cursos d'água situados em torno da sede urbana de Maripá na segunda quinzena de janeiro de 2021. Seis pontos de monitoramento foram estabelecidos ao longo do lajeado Arara e dois pontos na Sanga da Sede (Figura 2, Tabela 5). A soma das pontuações atribuidas aos parâmetros em cada protocolo é relacionada nas Tabelas 6 ao 9.

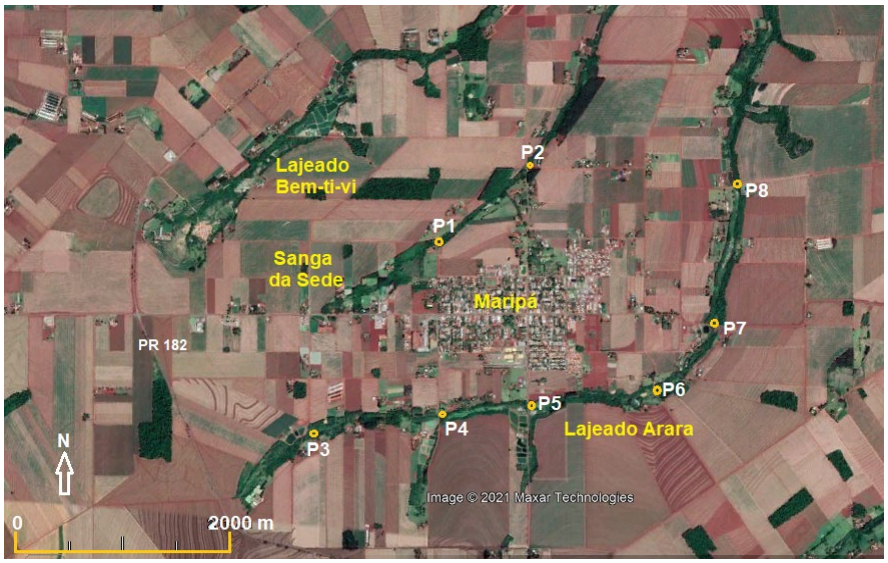

Fonte da imagem: Google Earth ©, Nov. 2019.

Figura 2: Localização dos pontos monitorados na sanga da Sede e no lajeado Arara entorno da sede urbana de Maripá.

Tabela 5: Coordenadas geográficas e área da bacia dos pontos de monitoramento.

Pontos	Curso d'água	Coordenadas geográficas	Área à montante (km²)
P1	Sede	24º 24' 46,87" S e 53º 50' 46,87" W	1,80
P2	Sede	24º 24' 24,25" S e 53º 49' 42,30' W	4,19
P3	Arara	24° 25' 47,71" S e 53° 50' 58,89" W	2,15
P4	Arara	24º 25' 41,68" S e 53º 50' 12,83" W	4,67
P5	Arara	24° 25' 37,71" S e 53° 49' 42,88" W	6,26
P6	Arara	24º 25' 32,65" S e 53º 49' 00,94" W	11,32
P7	Arara	24º 25' 13,10" S e 53º 48' 41,43" W	13,22
P8	Arara	24º 24' 29,90" S e 53º 48' 31,94" W	16,52

Fonte: os autores

Tabela 6: Pontuações atribuídas aos parâmetros no protocolo de Callisto et al. (2001) nos cursos d'água de Maripá (PR).

Parâmetros	Ponto 1	Ponto 2	Ponto 3	Ponto 4	Ponto 5	Ponto 6	Ponto 7	Ponto 8
1	2	2	4	4	2	4	4	4
2	4	2	4	4	2	4	4	4
3	0	2	4	4	2	4	4	4
4	0	0	0	0	0	4	4	4
5	4	4	4	4	4	4	4	4
6	4	4	4	4	4	4	4	4
7	2	2	4	4	2	2	2	2
8	4	4	4	4	4	4	4	4
9	0	4	4	4	4	4	4	4
10	4	2	4	2	2	4	4	4
11	5	3	5	3	2	5	5	5
12	5	5	5	5	2	5	5	5
13	5	5	5	5	2	5	5	5
14	2	2	3	0	0	3	3	3
15	5	5	5	3	0	5	5	5
16	5	2	5	3	0	5	5	5
17	5	2	5	5	2	5	5	5
18	5	3	5	3	2	5	5	5
19	5	0	5	5	0	5	5	5
20	5	2	5	5	2	5	5	5
21	5	2	5	3	0	5	3	5
22	0	0	0	0	0	0	0	0

Fonte: os autores

Tabela 7: Pontuações atribuídas aos parâmetros no protocolo de Guimarães et al. (2012) nos cursos d'água de Maripá (PR).

Parâmetros	Ponto 1	Ponto 2	Ponto 3	Ponto 4	Ponto 5	Ponto 6	Ponto 7	Ponto 8
01	5	5	10	5	0	10	10	10
02	10	5	10	10	0	10	10	10
03	10	5	10	10	0	10	10	10
04	5	5	10	10	0	10	5	5
05	10	5	10	10	5	10	10	10
06	0	5	10	10	10	10	10	10
07	10	10	10	10	10	10	10	10
08	0	0	0	0	0	0	0	0
09	0	5	10	5	0	5	5	5
10	10	10	10	10	10	10	10	10
11	10	10	10	10	5	10	10	10

Fonte: os autores

Tabela 8: Pontuações atribuídas aos parâmetros no protocolo de Baião (2014) nos cursos d'água de Maripá (PR).

Parâmetros	Ponto 1	Ponto 2	Ponto 3	Ponto 4	Ponto 5	Ponto 6	Ponto 7	Ponto 8
01	3	3	5	5	3	5	5	5
02	5	3	5	5	3	5	5	5
03	5	5	5	5	5	5	5	5
04	5	5	5	5	3	5	5	5
05	5	5	5	5	5	5	5	5
06	5	5	5	5	5	5	5	5
07	3	3	5	5	3	3	3	3
08	5	3	5	3	3	5	5	5
09	5	3	5	3	0	5	5	5
10	3	3	5	5	0	5	3	3
11	0	3	5	3	0	3	3	3
12	5	3	5	5	0	5	5	5

Fonte: os autores

Tabela 9: Pontuações atribuídas aos parâmetros no protocolo de Machado (2012) nos cursos d'água de Maripá (PR).

Parâmetros	Ponto 1	Ponto 2	Ponto 3	Ponto 4	Ponto 5	Ponto 6	Ponto 7	Ponto 8
01	5	5	10	5	0	10	10	10
02	10	5	10	10	0	10	10	10
03	10	5	10	10	0	10	10	10
04	5	5	10	10	0	10	5	5
05	10	5	10	10	5	10	10	10
06	0	5	10	10	10	10	10	10
07	10	10	10	10	10	10	10	10
08	0	0	0	0	0	0	0	0
09	0	5	10	5	0	5	5	5
10	10	10	10	10	10	10	10	10
11	5	5	10	5	5	5	10	5
12	10	5	10	10	5	10	10	10
13	10	10	10	10	5	10	10	10

Fonte: os autores

As pontuações totais em cada ponto de monitoramento para cada protocolo são sumariadas na tabela 10. Todos os protocolos utilizam as mesmas nomenclaturas para definir as classificações (Natural, Alterado e Impactado), a exceção da proposta de Guimarães et al. (2012) que usa outros termos como ótimo, bom e ruim.

De acordo com o protocolo de referencia neste trabalho (Callisto et al., 2001), a maioria dos pontos foi classificado na categoria de trecho Natural com exceção dos pontos 2 e 5 que foram classificados nas categorias de Alterado e Impactado respectivamente (Tabela 10, Figuras 3 ao 5). O mesmo resultado foi observado no protocolo de Machado (2019) no qual foram adotadas as mesmas nomenclaturas. Nos pontos 2 e 5 foram verificadas as maiores modificações no canal fluvial, resultado da influencia da área urbana, onde os parâmetros relacionados com o uso do solo e ocupação das margens sofreram as mudanças mais significativas.

Na tabela 10 pode ser observado diferenças quanto a classificação dos pontos de monitoramento entre os protocolos. A maior dificuldade foi verificada nos trechos cujas pontuações estão situadas próximos aos limites das categorias como nos casos dos pontos 1, 2 e 5. Dentre estes pontos, destacamos o ponto 5, classificado como Impactado nos protocolos de Callisto et al. (2001) e Machado (2019), recebeu a classificação de Bom no protocolo de Guimarães et al. (2012) e Alterado no de Baião (2014).

Tabela 10: Resumo das pontuações e da classificação dos trechos monitorados nos cursos d'água de Maripá (PR) pelos protocolos de Callisto et al. (2001), Guimarães et al. (2012), Baião (2014) e Machado (2019).

Pontos	Callisto et al. (2001)		Guimarães et al. (2012)		Baião (2014)		Machado (2019)	
	Pont.	Classif.	Pont.	Classif.	Pont.	Classif.	Pont.	Classif.
1	76	Natural	70	Bom	49	Natural	85	Natural
2	57	Alterado	65	Bom	44	Natural	75	Alterado
3	89	Natural	100	Ótimo	60	Natural	120	Natural
4	74	Natural	90	Ótimo	54	Natural	105	Natural
5	40	Impactado	40	Bom	30	Alterado	50	Impactado
6	93	Natural	95	Ótimo	56	Natural	110	Natural
7	89	Natural	90	Ótimo	54	Natural	110	Natural
8	91	Natural	90	Ótimo	54	Natural	105	Natural

Fonte: os autores

Fonte: os autores.

Figura 3: Registro fotográfico do ponto 3 no Lajeado Arara. Trecho "Natural" no protocolo de Callisto et al. (2001). Vista à montante, data: 16 de fevereiro de 2021.

Fonte: os autores.

Figura 4: Registro fotográfico do ponto 2 da Sanga da Sede. Trecho "Alterado" no protocolo de Callisto et al. (2001). Vista à montante, data: 06 de fevereiro de 2021.

Fonte: os autores.

Figura 5: Registro fotográfico do ponto 5 no Lajeado Arara. Trecho "Impactado" no protocolo de Callisto et al. (2001). Vista à montante, data: 16 de fevereiro de 2021.

Os valores normatizados dos protocolos produziram resultados muito próximos nos trechos 2, 3 e 5 nos protocolos de Callisto et al. (2001), Guimarães et al. (2012) e Machado (2019) e os mais distantes nos trechos 1 e 8 (Figura 6). A exceção foi o protocolo de Baião (2014) que produz valores superiores ao demais, principalmente nos pontos 1 ao 5.

A comparação dos valores normatizados mostrou que na maioria dos pontos (1 ao 5) os protocolos de Guimarães et al. (2012) e Machado (2019) apresentaram resultados similares ao da referência, contrastando com a proposta de Baião (2014) que produz valores superiores ao demais. Entretanto, nos pontos 6 ao 8, os quatro protocolos forneceram resultados semelhantes (Figura 6).

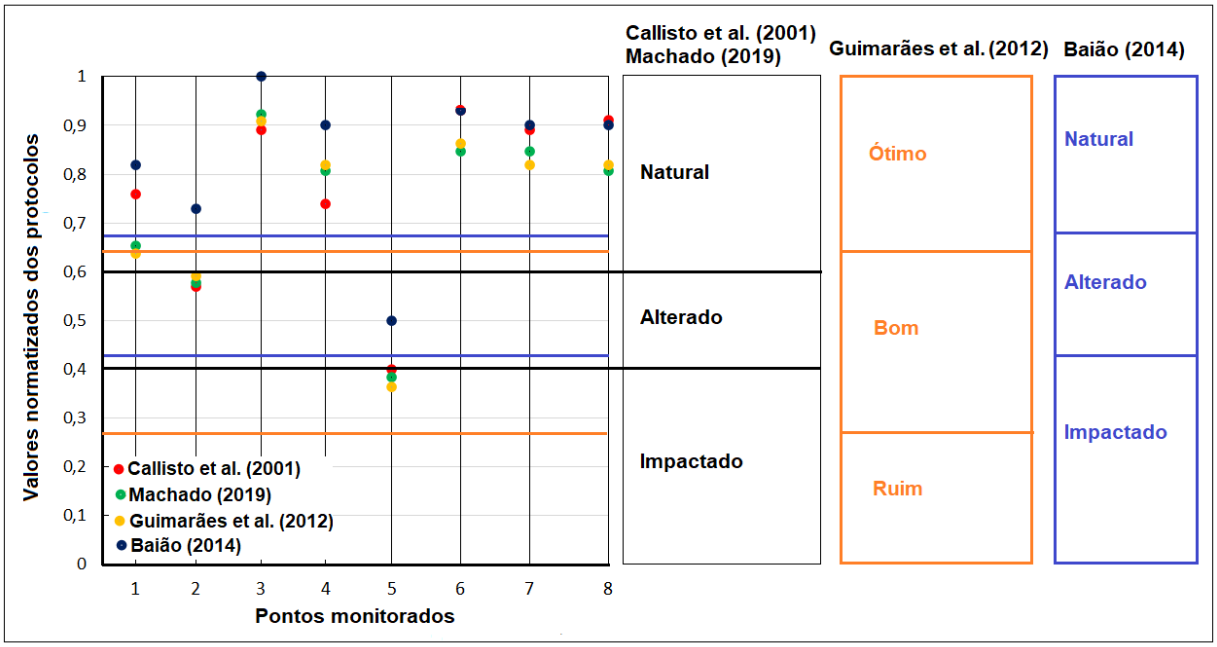

Fonte: os autores.

Figura 6: Valores normatizados das pontuações obtidas nos oito pontos de monitoramento nos córregos de Maripá (PR) empregando os protocolos de Callisto et al. (2001), Guimarães et al. (2012), Baião (2014) e Machado (2019).

Como pode ser observado na Figura 6, as amplitudes das categorias de classificação são diferentes, sendo iguais somente para os protocolos de Callisto et al. (2001) e Machado (2019). Em termos de valores normatizados, ambos os protocolos definiram o limite entre Impactado e Alterado em 0,40 (40÷100) e o limite entre Alterado e Natural em 0,60 (60÷100). Esse mesmo critério não foi adotado nos outros dois protocolos. Para a proposta de Guimarães et al. (2012), esses limites foram de 0,27 (30÷110) e 0,64 (70÷110) e para Baião 0,42 (25÷60) e 0,67 (40÷60) respectivamente. Vale lembrar que o divisor representa a soma da pontuação máxima em cada protocolo. Por essa razão, as categorias são diferentes entre os protocolos tanto em amplitude como nos limites e permite situações como o já citado ponto 5, na qual a classificação pode variar de Impactado para os protocolos de Callisto et al. (2001) e Machado (2019), Bom para Guimarães et al. (2012) e Alterado para Baião (2014) (Ver Tabela 10).

Se os dois últimos protocolos tivessem adotado a mesma proporção de Callisto et al. (2001) para definir os limites das categorias, o ponto 5, por exemplo, teria sido classificado na categoria de trecho Ruim no protocolo de Guimarães et al. (2012) e continuaria como trecho Alterado no de Baião (2014). Assim, o limite Ruim-Bom para o primeiro protocolo teria sido de 44 pontos e o limite Impactado-Alterado para o segundo seria de 24 pontos.

IV. Considerações Finais

Os protocolos de avaliação rápida de diversidade de hábitats disponíveis na literatura nacional são fácil e rápida aplicação e fornece um panorama preliminar da deterioração dos cursos fluviais. Estas qualidades transformam os protocolos num instrumento de educação ambiental e o mapeamento dos valores obtidos ajudam a mostrar a distribuição espacial das condições de preservação ou degradação do ambiente fluvial e pode ser usado na definição de áreas prioritárias para planos de recuperação. Assim, os protocolos podem ser aplicados por ambientalistas, professores e alunos treinados convenientemente.

A comparação entre os quatro protocolos aplicados neste trabalho mostrou que, em geral, os resultados são equivalentes. Assim sendo, os protocolos de Guimarães et al. (2012), Baião (2014) e Machado (2019), todos mais simples e menos extenso que o protocolo de referência (Callisto et al., 2001), podem ser adotados em escolas e colégios de Maripá e municípios vizinhos como um instrumento de educação ambiental. A compatibilidade dos protocolos verificada nesta pesquisa deve ser observada com reservas, já que pode não se repetir em outros ambientes com condições de relevo, clima, vegetação e uso da terra diferentes.

References Références Referencias

1. BAIÃO, Cheila Flávia de Praga. *Contribuição metodológica para ampliação da concepção ambiental no Ensino Fundamental com base no estudo de bacia hidrográfica.* Dissertação (Mestrado em Ciências Ambientais). Departamento de Ciências Agrárias, Universidade de Taubaté. Taubaté, 2014.
2. CALLISTO, Marcos; MORETTI, Marcelo; GOULART, Michael. Macroinvertebrados bentônicos como ferramenta para avaliar a saúde de riachos. *Revista Brasileira de Recursos Hídricos,* 6 (1): 71-82. 2001.
3. EPA (Environmental Protection Agency) *Biological criteria for the protection of aquatic life.* Division of Water Quality Monitoring Assessment. Columbus, Ohio, v. 1-III, 120 p. 1987.
4. GREGORY, Valdir. *Os eurobrasileiros e o espaço colonial: migrações no Oeste do Paraná (1940-1970).* Cascavel. Editora Edunioeste, 2002.
5. GUIMARÃES, Ariane; RODRIGUES, Aline Sueli de Lima; MALAFAIA, Guilherme. Adequação de um protocolo de avaliação rápida de rios para ser usado por estudantes do ensino fundamental. *Revista Ambi-Água,* Taubaté, v. 7, n. 3, p. 241-260, 2012.
6. HANNAFORD, Morgan J.; BARBOUR, Michael T.; RESH, Vincent H. Training reduces observer variability in visual-based assessments of stream habitat. *Journal North American Benthol. Soc.,* v. 16, n. 4, p. 853-860, 1997.
7. IAPAR (Instituto Agronômico do Paraná.) Site oficial. Disponível em: <http://www.iapar.br/>. Acesso em 20 jan. de 2021.
8. IBGE (Instituto Brasileiro de Geografia e Estatística) Glossário dos termos genéricos dos nomes geográficos usados no mapeamento sistemático do Brasil (volume 1). Rio de Janeiro, 36 p., 2010.
9. IBGE (Instituto Brasileiro de Geografia e Estatística) *Cidade de Maripá.* Disponível em: <https://www.ibge.gov.br/cidades-e-estados/pr/maripa.html>. Acesso em setembro de 2022.
10. MAACK, Reinhard. *Geografia Física do Paraná.* Ponta Grossa: Editora UEPG, 2012.
11. MACHADO, Ana Paula Favorito. *Adaptação de um protocolo de avaliação rápida de rios e sua utilização como recurso didático em educação ambiental no ensino médio.* 2019. 68 f. Dissertação (Mestrado em Geografia). Instituto Federal de Educação, Ciência e Tecnologia Goiano, *campus* de Urutaí, 2019.
12. PLAFKIN, James L.; BARBOUR, Michael T.; PORTER, Kimberly D.; GROSS, Sharon K.;

HUGHES, Robert M. *Rapid bioassessment protocols for use in streams and rivers: Benthic macroinvertebrates and fish*. U.S. Environmental Protection Agency, Office of Water Regulations and Standards, Washington, D.C. EPA 440-4-89-001. 1989.

13. PREFEITURA DE MARIPÁ. *História.* Disponível em: <http://www.maripa.pr.gov.br>. Acesso em maio de 2021.
14. RESH, Vincent H.; JACKSON, John K. Rapid assessment approaches to biomonitoring using benthic macroinvertebrates. In: *Freshwater Biomonitoring and Benthic Macroinvertebrates.* D.H. Rosemberg; V.H. Resh (Eds.). New York, Chapman & Hall, 195-233 p. 1993.
15. RODRIGUES, Aline Sueli de Lima. *Adequação de um protocolo de avaliação rápida para o monitoramento e avaliação ambiental de cursos d'água inseridos em campos rupestres.* 2008. 89 f. Dissertação (Mestrado em Ciências Naturais) – Universidade Federal de Ouro Preto. 2008.
16. RODRIGUES, Aline Sueli de Lima; CASTRO, Paulo de Tarso Amorim. Adaptation of a rapid assessment protocol for rivers on rocky meadows. *Acta Limnologica Brasiliense,* Sorocaba, v. 20, n. 4, p. 291- 303, 2008.

This page is intentionally left blank

Global Journal of human-social science: b
Geography, Geo-Sciences, Environmental Science & Disaster Management
Volume 23 Issue 5 Version 1.0 Year 2023
Type: Double Blind Peer Reviewed International Research Journal
Publisher: Global Journals
Online ISSN: 2249-460x & Print ISSN: 0975-587X

Measurement of Vertical Profiles of the Atmospheric Surface Layer with Low-Cost Instrumentation on Board a Drone

By David Christian de Lima Ferreira, Marcio Cataldi, Ivanovich Lache Salcedo, Flávia Rodrigues Pinheiro, Márcio Vinicius Aguiar Soares & Gabriel Ferreira Subtil de Almeida
Federal Fluminense University

Abstract- Atmospheric natural disasters can have their damage mitigated if meteorological alerts are disseminated on time. Among the ways to get data related to weather conditions are the use of atmospheric profilers and numerical models. Such resources can be used for studies related to the surface layer, which covers a range from 20 to 200 meters below the low troposphere. In order to make atmospheric experiments achievable, without great financial expenditure, a low-cost atmospheric profiler was developed together with the Laboratory of Monitoring and Numerical Modeling of Climate Systems (LAMMOC) of the Federal Fluminense University (UFF), to be on board a drone and based on prototyping with Arduino, which had as sensors the DHT22 for measuring temperature and relative humidity and the BMP280 for measuring atmospheric pressure.

Keywords: natural disasters, surface layer, low-cost arduino instrumentation, drone, numerical model weather research and forecasting.

GJHSS-B Classification: LCC: QC879

Strictly as per the compliance and regulations of:

Measurement of Vertical Profiles of the Atmospheric Surface Layer with Low-Cost Instrumentation on Board a Drone

David Christian de Lima Ferreira [α], Marcio Cataldi [σ], Ivanovich Lache Salcedo [ρ], Flávia Rodrigues Pinheiro [ω], Márcio Vinicius Aguiar Soares [¥] & Gabriel Ferreira Subtil de Almeida [§]

Abstract- Atmospheric natural disasters can have their damage mitigated if meteorological alerts are disseminated on time. Among the ways to get data related to weather conditions are the use of atmospheric profilers and numerical models. Such resources can be used for studies related to the surface layer, which covers a range from 20 to 200 meters below the low troposphere. In order to make atmospheric experiments achievable, without great financial expenditure, a low-cost atmospheric profiler was developed together with the Laboratory of Monitoring and Numerical Modeling of Climate Systems (LAMMOC) of the Federal Fluminense University (UFF), to be on board a drone and based on prototyping with Arduino, which had as sensors the DHT22 for measuring temperature and relative humidity and the BMP280 for measuring atmospheric pressure. Thus, this profiler was used in an experiment, from which atmospheric vertical profiles were generated and compared with profiles generated by the numerical model Weather Research and Forecasting (WRF) and post-processed by the WRF-Python routines package. As a result, it was noticed that the observed data profiles described a behavior of the surface layer that indicates the occurrence of thermal inversion and change of regime of this layer, from the stable, passing through the neutral, to the unstable. With this, it is evaluated that the method of using this profiler can be applied in several atmospheric studies, such as atmospheric pollution and nowcasting weather forecast, as well as its potential for use in areas such as operational meteorology and assimilation of data from numerical models shows to be promising.

Keywords: natural disasters, surface layer, low-cost arduino instrumentation, drone, numerical model weather research and forecasting.

I. Introduction

From a perspective related to environmental management and about natural disasters, it is necessary to understand that they are the result of extreme or intense natural phenomena, which cause social impacts and are mainly characterized by their triggering phenomenon (TOBIN & MONTZ, 1997).

According to the National Civil Defense Policy (PNDEC), disasters are the "result of adverse events on a vulnerable ecosystem, causing human, material and/or environmental damage and consequent economic and social damage" (BRASÍLIA, 2007). The PNDEC also classifies disasters into three types: natural, human-made, and mixed. In this regard, Marcelino (2007) and Castro (1998) point out that most natural disasters would be considered mixed if only this criterion were considered.

According to the 2015 Global Assessment Report (GAR15), prepared by the United Nations Office for Disaster Risk Reduction (UNISDR), annual losses between US$ 250 to 300 billion occur worldwide due to natural disasters, and, with a global investment in prevention, a reduction of up to 20% of these values may occur (GAR, 2015).

The investigation of the thermodynamic mechanisms enables a quick identification of the chances of convective activities developing in a short period, causing storms. In this context, obtaining vertical profiles of the atmosphere through soundings is important for the prognosis of meteorological phenomena such as cloud formation, fog, precipitation, or snow, as well as for investigating atmospheric instability indices (GASPARETTO, 2011).

The surface layer has a thickness that varies between 20 and 200 meters closest to the surface, so that, in this layer, frictional drag, heat conduction and surface evaporation cause substantial variations as a function of height in the temperature, humidity and wind. The behavior of the temperature in this layer varies according to the daily cycle, so that it is common to observe a thermal inversion for the night period. As for turbulent flows, they are relatively uniform with height increments (STULL, 2017).

In addition to knowledge of the thermodynamic conditions of the atmosphere, the use of numerical weather forecast models is also important for making the prognosis of atmospheric phenomena, to be a way to enable the issuance of meteorological alerts (LIRA & CATALDI, 2016). Among such models is the Weather Research and Forecasting (WRF), which can

Corresponding Author α: LAMMOC Group, Biosystems Engineering Graduate Program, Department of Agricultural and Environmental Engineering, Federal Fluminense University, Niterói 24210-240, Brazil.
e-mail: davidchristian@id.uff.br
Author ρ ¥ §: LAMMOC Group, Biosystems Engineering Graduate Program, Department of Agricultural and Environmental Engineering, Federal Fluminense University, Niterói 24210-240, Brazil.
Author ω: Navy Hydrography Center – Brazilian Navy – Niterói 24048-900, Brazil.
Author σ: MAR Group, Department of Physics. School of Chemistry. University of Murcia, 30100 Murcia, Spain.

make forecasts of weather conditions for various levels of the atmosphere, among which is the surface layer (BARCELLOS & CATALDI, 2020).

Thus, in this work the developed atmospheric profiler was embedded in a drone, generating vertical atmospheric profiles in the surface layer, enabling a comparative analysis between these profiles and those obtained through numerical modeling. This led to an assessment of how this approach might be relevant to operational meteorology and data assimilation.

II. Low-Cost Instrumentation Initiatives

To analyze the characteristics of this layer, atmospheric soundings can be conducted with low-cost sensors attached to a drone together with vertical profiles generated by numerical modeling, so that the results of one can be qualitatively evaluated as a function of the other.

About the use of drones for work and experiments, their application has proved to be very wide. Darynova et al. (2023) applied several controlled methane releases on an environment test platform. A methane-detecting drone and five ground-sensors recorded the methane concentration simultaneously. The hybrid approach, which evaluated both drone and stationary measurements achieved the highest coefficient of determination and the lowest relative error between the reported and model estimated flow rates.

Lee et al. (2022) measured vertically concentrations of particulate matter 2.5 (PM 2.5), black carbon and ozone using a drone in a high-polluted area in South Korea. They found that the concentration of PM 2.5 and black carbon showed minor concentration changes vertically up to 70 meters from the ground and decreased with height over 70 meters. The ozone concentration increased with height up to 30 meters above the surface and increased slowly thereafter.

Järvi et al. (2023) experimentally evaluated the spatial variability of air pollutant concentrations using observations from a mobile laboratory and a drone. They observed that both mean flow and turbulent fluctuations need to be considered when pollutant dispersion and concentrations are examined, and thermal turbulence has strong impact particularly on the formation of aerosol particle hotspots in winter. They also noticed that prediction equations for vertical pollutant decay in a wide street canyon were developed, and the vertical decay was mostly controlled by seasonal variations in air temperature over mean flow and turbulent processes.

Burgués et al. (2022) performed a drone-based system equipped with a lightweight electronic smell sensor for the prediction of odor concentration in a wastewater treatment plant. The accuracy of the odour predictions by the developed prototype was benchmarked against dynamic olfactometry. They demonstrate that training machine learning algorithms with dynamic sensor signals measured in flight conditions leads to better performance than the traditional approach of using steady-state signals measured in the lab via controlled exposures to odour bags. The comparison of the electronic smell sensor predictions with dynamic olfactometry measurements indicates a negligible bias between the two measurement techniques.

Chang et al. (2018) exploited a novel sampling vehicle, a multi-rotor drone carrying a remote-controlled whole air sampling device, to collect aerial samples with high sample integrity and preservation conditions. An array of 106 volatile organic compounds were analyzed and compared between the aerial samples and the ground-level samples in pairs to inspect for vertical mixing of the trace gases at a coastal location. The study demonstrates that detailed compositions of waste gases can now be easily obtained with superior data quality with the availability of coupling near-surface aerial sampling with laboratory analysis.

Vytovtov et al. (2023) demonstrated how unmanned aerial systems are actively used to provide oil pipelines monitoring, proposed its scientific basis for detecting oil spill accidents formulating the main technical aircraft characteristics applicable for these purposes are formulated and determined the optimal conditions for drone monitoring.

Masic et al. (2021) conducted an experiment in which a robust six-propeller experimental drone was used to launch temperature and suspended particulate matter sensors. In this work, the elements involved in the measurement were placed over the drone hull to avoid the influence of the airflow on the propellers, which was only possible due to the distance of the propellers towards the drone hull.

Karachalios et al. (2021) conducted another experiment with use of a drone with Arduino prototyping to obtain atmospheric data. They proposed that such technology can be especially useful for aviation safety, being able to provide parameters such as temperature, relative humidity, and atmospheric pressure.

Laitinen (2019) attached a Vaisala RD41 probe to the bottom of the DJI Matrice 600 Pro drone. In its case, the propellers were sufficiently far from the sensor. This work aimed to measure temperature and relative humidity. Among its results, it was considered that the airflow coming from the propellers should be a matter to be treated.

Cataldi et al. (2022) developed an equipment based on the Arduino Uno board together with the DHT22 temperature and relative humidity sensor and the BMP280 pressure sensor. This equipment was transported by the DJI Phantom 3 Standard drone with the equipment box fixed to its base. The results pointed

to the suitability of using the DHT22 and BMP280 sensors to measure atmospheric parameters.

It is also useful to list those works that did not necessarily employ drones, but that developed prototypes of sensors of atmospheric parameters.

Oliveira et al. (2016) developed a radiosonde with an Arduino Nano Version 3.0 prototyping board, a BMP180 pressure sensor (previous version of the BMP280 used in this work) and an RF433MHz radiofrequency module, and its radiosonde container it was composed of polystyrene and plastic. This project was conceived to take off with a balloon full of helium gas and for the data to be transmitted by telemetry. The results demonstrated the employability of Arduino technology for this purpose.

Sousa et al. (2022) created a radiosonde with an Arduino Uno board (as used in this work), a DHT11 temperature and relative humidity sensor (previous version of the DHT22 used in this work), an RF433MHz radiofrequency module, a GPS module and a Yagi-Uda type antenna with its adapter. It was conceived for the use of a balloon filled with helium gas, with the differential of having a GPS position transmission to make it easy to be found after its return to the ground.

Ribeiro (2022), with an emphasis on anemometry, used an Arduino Uno board and an MPX5100DP differential pressure sensor associated with a Pitot tube to measure air flows. His device was subjected to several air flows in a low-cost wind tunnel, which allowed him to get a sensor calibration equation.

Aware of this, and with the aim of reducing the costs of atmospheric experimentation campaigns, an atmospheric profiler was developed with the Laboratory for Monitoring and Numerical Modeling of Climate Systems (LAMMOC) at the Fluminense Federal University (UFF), based on Arduino prototyping, which is a programmable computing platform based on the ATmega328P microcontroller with an easy maintenance and capable of interacting with its environment (MCROBERTS, 2011, & ARDUINO, 2023), to be used attached to a drone.

These features enable its association with various devices and sensors, among which are the DHT22, which can be used to measure temperature and relative humidity, and the BMP280, which can be used to measure atmospheric pressure.

III. Materials and Methods

Throughout this work, a low-cost atmospheric profiler based on Arduino prototyping was developed, which was submitted to previous tests, and was used to get the vertical profile of the surface layer. The result of using the profiler was compared to simulated profiles generated by the numerical model Weather Research and Forecasting. Therefore, this section is divided into three parts. The first is dedicated to processes involving the low-cost profiler, the second is dedicated to drone flight tests and atmospheric experiment, and the third is dedicated to the use of WRF as a tool for qualitative verification of the profiler results.

a) Low-Cost Atmospheric Profiler

The first step of the implementation of a low-cost atmospheric profiler consists of seeking in the general market an electronic and programmable technology. To that matter, it is important to consider low values compared with the best-known radiosondes either for scientific use or for large-scale use for economic purposes.

As previously mentioned, the Arduino Uno board is based on the ATmega328P microcontroller. Precisely because its functionalities suit the objectives of the project in question, as well as because of the low cost not only of its acquisition and repair, but also of the other sensors and accessory devices involved, that this prototyping path was chosen.

For the measurement of temperature and relative humidity of the air, the DHT22 was chosen, as it adapts to the prototyping board, its cost is low and the DHT11 (its previous version) had good employability in the study by Sousa et al. (2022). Furthermore, when comparing technical descriptions, it was found that DHT22 is twice as accurate as its predecessor. For the measurement of atmospheric pressure, as well as for the calculation of height as a function of the measured pressure, the BMP280 was chosen because, considering the same criteria, it adapts to the Arduino Uno board, has a low cost, its predecessor, the BMP180, was successfully used in the work of Oliveira, Amorim and Dereczynski (2016) and, when comparing technical descriptions, it was found that the accuracy of both was similar in relation to the central value, but the uncertainty range of the BMP180 could cause the errors reached even more than double those possible in the range of the BMP280.

As accessory devices, an RTC DS3231 programmable clock, a MicroSD card module (with its respective card), a 9V rechargeable battery and a small rectangular cardboard box with holes on the sides, enveloped in white, were used. Finally, to transport the profiler, it was decided to use the DJI Mavic Air 2 drone.

Once all the elements necessary for the manufacture of the low-cost atmospheric profiler are arranged, the next step consists of assembling it, for subsequent configuration through a programming script. The assembly was established with a breadboard contact matrix and jumper cables, so that its structure can be verified in Figure 1. As for the configuration, it was done in Arduino programming language through an own development environment, called Arduino Integrated Development Environment (Arduino IDE). The data sampling rate chosen for this script was 10 seconds, which was adopted as a function of the drone

operator conducting a controlled drone flight with a constant ascent speed of 0.1 m/s (with few occasional variations).

In the test phase, the influence of the descending air from the drone's propellers on the measurements was treated. This treatment was divided into two parts. In the first part, the MPX5100DP differential pressure sensor was installed in the atmospheric profiler to capture the downward airflow from the propellers. The MPX5100DP was able to identify that the propellers were an influencing factor, but a more accurate sensor was needed to measure it. Thus, in the second part, a flight experiment was conducted with the drone and the Akrom KR835 anemometer to decide how far the profiler should be from the propellers to mitigate this influence.

At the end of the processes, the total budget for implementing the low-cost atmospheric profiler was US$ 193.33 without the drone and US$ 2,076.83 with the drone, which can be used indefinitely, against US$ 4,080.48 for launches of conventional radiosondes (considering the set of radiosonde, meteorological balloon, and helium gas for the 4 synoptic times of the day), for which the materials involved are not recovered.

Thus, an atmospheric experiment was conducted in Itaipu, a neighborhood in the city of Niterói, in the State of Rio de Janeiro, up to a maximum height of 400 feet, or approximately 120 meters, in compliance with the provisions of article E94.701, paragraph 2, of Brazilian Special Civil Aviation Regulation No. 94, Amendment No. 2, issued by the National Civil Aviation Agency (BRASÍLIA, 2021).

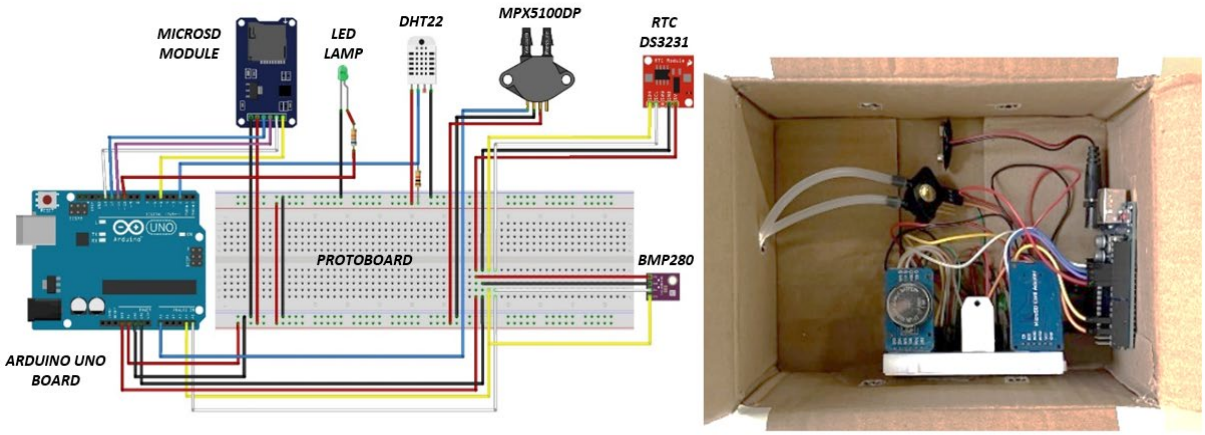

Figure 1: Low-cost atmospheric profiler connections diagram generated in Fritzing software version 0.9.3 (left) and top view of open low-cost atmospheric profiler box (right).

b) Drone Flight Tests And Atmospheric Experiment

The first time the atmospheric profiler was used happened on August 22nd, 2022, as a test, at the Praia Vermelha campus of the Federal Fluminense University (UFF). On that day, the atmospheric profiler box was attached to the base of the DJI Phantom 3 Standard drone by four simple polyamide wires, to distance the atmospheric profiler from the drone.

The second time the atmospheric profiler was used for flight occurred on September 5th, 2022, again on a test basis, also at UFF's Praia Vermelha campus. On that day, the atmospheric profiler box was also attached to the base of the DJI Phantom 3 Standard drone by four simple polyamide wires, but quite short this time, to keep the atmospheric profiler and the drone in permanent contact.

After this second test, in which the box was close to the DJI Phantom 3 Standard drone, the influence of the descending air from the drone's propellers was treated on the measurements on January 18th, 2023, again at the Praia Vermelha campus of UFF. This study included the use of drones (without an onboard profiler) DJI Phantom 3 Standard and DJI Mavic Air 2, and the Akrom KR835 anemometer. The objective was to measure the speed of this air coming from the propellers to decide on the transport distance between the low-cost atmospheric profiler and the drones.

The third time the profiler was used happened on February 14th, 2023, also on a test basis, at UFF's Praia Vermelha campus. On that day, the atmospheric profiler box was attached to a prototype traction cable with 4 thick polyamide wires attached to the rods of the DJI Mavic Air 2 drone's propeller rotors.

The fourth time the profiler was used occurred on March 6th, 2023, on a test basis, at UFF's Praia Vermelha campus. On that day, the atmospheric profiler box was attached to the traction cable adapted from its prototype, this time with 1 thick polyamide thread and a carabiner with lock and eye at each end. This cable, in turn, was attached to a device made up of 4 short polyamide fishing wires and a carabiner mounted close to the bases of each drone. On this occasion, the flight stability of both drones was tested. After this test, it was

decided to only use the DJI Mavic Air 2 drone to transport the low-cost profiler.

Finally, the fifth time the atmospheric profiler was used for 3 consecutive flights on March 14th, 2023, this time to carry out the atmospheric experiment itself, in Itaipu, Rio de Janeiro (as shown in figure 2). On that day, the atmospheric profiler box was attached to the pull cable, and this was attached to the DJI Mavic Air 2 drone.

Figure 2: Low-cost atmospheric profiler in operation in Itaipu, Rio de Janeiro, on March 14th, 2023.

c) Numerical Model Weather Research and Forecasting

When the atmospheric experimentation was scheduled for March 14th, 2023, the Weather Research and Forecasting (WRF) numerical model from the Laboratory for Monitoring and Numerical Modeling of Climate Systems (LAMMOC) was used to generate data for that same day to be count from 00:00 AM GMT until the next subsequent 96 hours. The domain of interest for this round covered the area delimited by points at latitudes 22.50°S and 23.13°S and longitudes 42.72°W and 43.34W (as shown in Figure 3).

Figure 3: Coverage area of the domain of interest of the March 14th, 2023, round of the Weather Research and Forecasting (WRF) numerical model of the Laboratory for Monitoring and Numerical Modeling of Climate Systems (LAMMOC), with emphasis on the location of atmospheric experimentation (in red).

This round generated data for several variables on 34 different vertical levels. For the purposes of this study, data on temperature, relative humidity, atmospheric pressure, and height were used. As the WRF generated more data at higher levels than the atmospheric experimentation campaign with the low-cost profiler, the data of these atmospheric parameters were used for comparative analysis in a range of 995 to 1015 hPa of atmospheric pressure, to cover the entirety of the data observed by the experiment.

More specifically regarding the configuration of the WRF model, the model grid had 64 points from east to west and 70 points from north to south, totaling 4480 points. Data from the Global Forecast System (GFS) model were used as initial and boundary conditions, with a periodicity of 21600 seconds (equivalent to 6 hours) between readings. Relating to the parameterizations used, for Micro Physics (mp_physics) the WRF Single–moment 3–class option was used, for Longwave (ra_lw_physics) the RRTM Longwave Scheme option was used, for Shortwave (ra_sw_physics) the Dudhia Shortwave Scheme option was used, for Surface Layer (sf_sfclay_physics) the Revised MM5 Scheme option was used, for Land Surface (sf_surface_physics) the Unified Noah Land Surface Model option was used, and, finally, for Planetary Boundary Layer (bl_pbl_physics) the Yonsei University Scheme (YSU) option was used). The adopted configuration of the WRF numerical model can be seen in Table 1.

Table 1: Numerical Model Weather Research and Forecasting (WRF) - Configuration and parameters.

time_control	
start (year/month/day/hour/minute/second)	2023/03/14 00:00:00
end (year/month/day/hour/minute/second)	2023/03/18 00:00:00
interval_seconds	21600
domains	
e_we	64
e_sn	70
e_vert	35
dx	1000
dy	1000
physics	
mp_physics	WRF Single–moment 3–class
ra_lw_physics	RRTM Longwave Scheme
ra_sw_physics	Dudhia Shortwave Scheme
sf_sfclay_physics	Revised MM5 Scheme
sf_surface_physics	Unified Noah Land Surface Model
bl_pbl_physics	Yonsei University Scheme (YSU)

Environmental data modeled by WRF for March 14, 2023, were post-processed with the WRF-Python, which is a package of diagnostic and interpolation routines. For this, an integrated development environment was established in the Windows operating system, which was Anaconda. This environment features the Anaconda Navigator, which is a graphical user interface that allows the user to launch applications and manage "conda" programming packages. Among the applications made available by Anaconda Navigator, JupyterLab was chosen, which is a user interface that offers all the familiar building blocks of the classic Jupyter Notebook application in a flexible World Wide Web (WWW) based format, which makes its employment quite common among data scientists.

IV. Results and Discussion

Regarding the results of this work, they are subdivided between the treatment of the influence of the drone's propellers, the surface layer profiles generated by the low-cost atmospheric profiler and the comparison of these profiles with those simulated by the WRF.

a) Treatment of the Influence of the Drone's Propellers

With the measurement of downward airflow from the propellers by the MPX5100DP, it became evident that this influence should be treated.

Thus, the DJI Mavic Air 2 drone had its downward airflow speed measured for different distances by the Akrom KR835 anemometer (as shown in the Figure 4). With this, it was possible to obtain subsidies for the decision regarding which operating distance should be maintained between the low-cost atmospheric profiler and the drone.

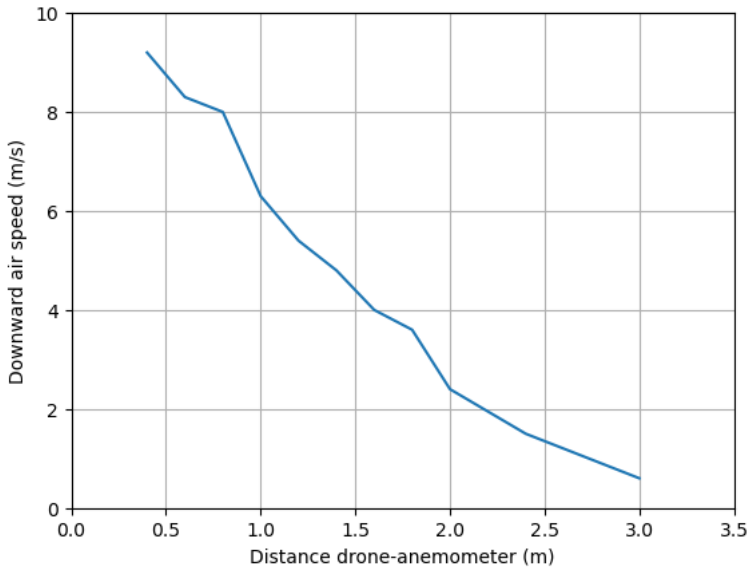

Figure 4: Measurement of the downward air speed from the propellers of the drone DJI Mavic Air 2 as a function of the distance to the Akrom KR835 anemometer (January 18th, 2023).

As a result, it was noticed that the behavior of the airflow speed was inversely proportional to the distance to the anemometer, so that speed became near to zero when this distance reached 3 meters.

In view of this, an attempt was made to use a traction cable that maintained the distance between the profiler and the drone at 3 meters. It was noticed, however, that the profiler had a pendular movement that could endanger the flight safety. This adverse movement was fully mitigated when 2.5 meters was maintained between them. With this solution, it was possible to get low influence of the propellers and satisfactory flight safety at the same time.

When the atmospheric experiment was conducted at Itaipu on March 14th, 2023, it was observed that the profiler remained stable throughout the operation, without any oscillation to disturb the aircraft's steering or decrease the safety of the experiment.

b) Surface Layer Profiles Generated by the Low-Cost Atmospheric Profiler

In the atmospheric experimentation carried out on March 14, 2023, it was possible to obtain data on temperature, relative humidity, and atmospheric pressure. From the measured pressure it was possible to calculate the height for the measurements. Altogether, 3 vertical flights were performed from 08:03 to 08:14 AM, from 08:19 to 08:26 AM and from 08:46 to 08:54 AM.

About temperature data (as shown in the Figure 5), the first flight registered maximum values just above 28°C in the range between 40 and 60 meters high, which corresponds to the range between 1010 and 1008 hPa of atmospheric pressure. The profile data for this flight indicates that there was a thermal inversion from the ground to just over 40 meters in height, which appears to be a residual result of the end of the stable regime of the nocturnal surface layer. From that level upwards, the surface layer behaved like a partially neutral layer.

On the second flight, the temperature values were higher, reaching 28.5°C in the range from 80 meters (1006 hPa of atmospheric pressure) to the maximum height. The data from this flight indicates the reduction of the inversion gradient observed in the first flight, presenting a mainly neutral surface layer, with very little vertical temperature variation.

On the third flight, the temperature variation was even greater, registering 30.1°C in the first 20 meters of the profile, with values of 1014 to 1012 hPa of atmospheric pressure. Regarding the profile generated for this flight, its data indicate the occurrence of a small inversion in the first 20 meters of height, from where the surface layer becomes neutral up to 60 meters, and, from that level to the top, the profile develops the behavior of an unstable surface layer, with vertical temperature variation approximately logarithmic.

Thus, the data from the three temperature profiles suggested a change in the surface layer regime, which varies from a nocturnal stable layer with slight inversion, passing through a neutral stability layer, until manifesting the beginning of the instability condition.

Regarding relative humidity data (as shown in the Figure 6), on the first flight, values between 65% and 68% were recorded throughout the entire profile. On the second flight, the recorded values were between 66.2% and 70.2%. And on the third flight, the relative humidity values began to cover a range from 70.8% close to ground level, around 1014 hPa of atmospheric pressure, to a minimum of 61.6% in the range close to 80 meters in height, comprehending values between 1006 and 1004 hPa of atmospheric pressure.

The range comprising the relative humidity maximums and minimums in each profile became increasingly wider with the passage of time and consequent increase in temperature, so that the third profile presented the most pronounced variation in the observed values, with a significant increase of humidity close to the soil level, which is consistent with the expected increase in the evaporation rate for the morning period, since the experiment occurred in a grassy field. In addition, the decrease in humidity with height, more markedly at the last measurement time, is another factor associated with the beginning of the instability regime of the surface layer.

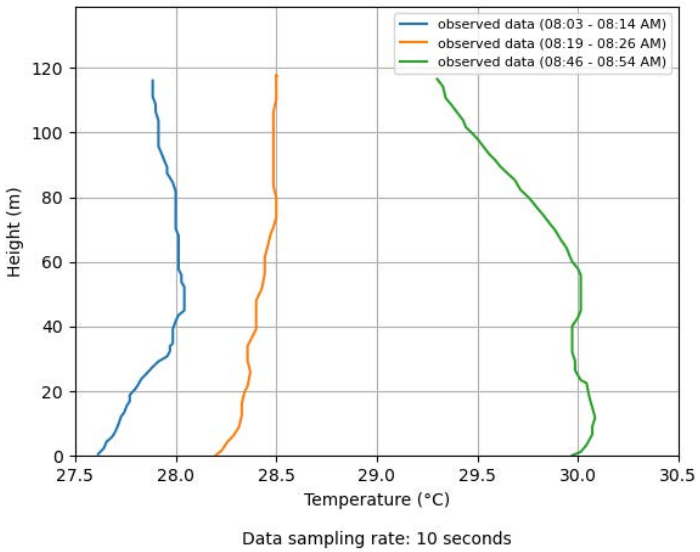

Figure 5: Vertical temperature profiles generated by observed data for Itaipu on March 14th, 2023.

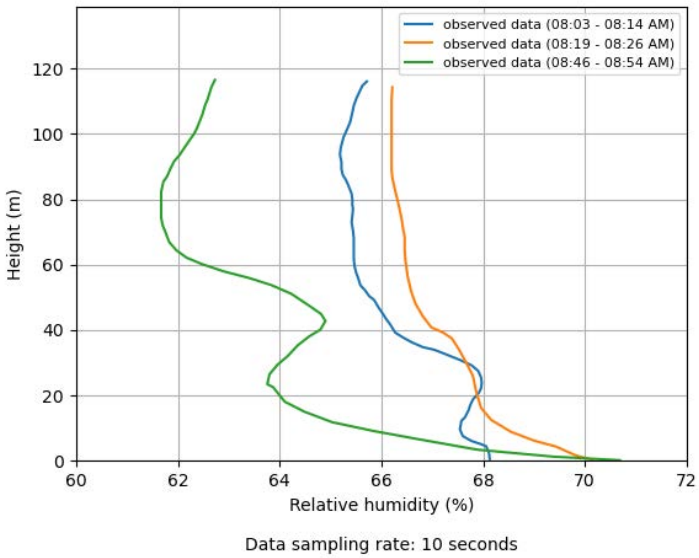

Figure 6: Vertical relative humidity profiles generated by observed data for Itaipu on March 14th, 2023.

Concerning atmospheric pressure data, as the three flights reached a maximum height of 120 meters (with the profiler box reaching 2.5 meters less to avoid propellers influence), all profiles generated by this experiment recorded pressures in the range between 1014.4 and 1001 hPa (as shown in the Figure 7).

About height, it is possible to notice a mainly linear behavior in relation to pressure for the three profiles, with slight oscillations that are probably related to the profiler's ascent speed variations. As previously mentioned, the speed adopted by the profiler remained about 0.1 m/s, which is low enough to avoid oscillations in flight, but difficult to maintain invariable, as the remote control is very sensitive, being able to vary the speed until 4.0 m/s in ascent.

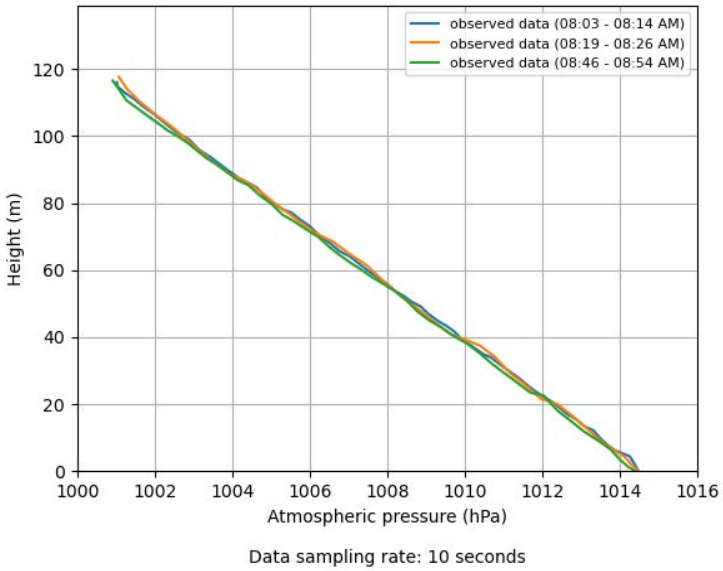

Figure 7: Height profiles as a function of atmospheric pressure generated\nby observed data for Itaipu on March 14th, 2023.

This atmospheric experimentation was significant to demonstrate the applicability of the low-cost profiler with its sensors and its configuration. Moreover, the profiler demonstrated to have thermal inertia small enough to obtain measurements of change in the stability regime of the surface layer. This ability to detect thermal inversion and change in the regime of this layer, from stable, through neutral, to unstable behavior, make it possible for this profiler to be used in studies on atmospheric pollution and nowcasting weather forecast, for example.

c) *Comparison between Observed and Simulated Surface Layer Profiles*

Regarding the comparison between the vertical temperature profiles generated by observed data and by numerical modeling (shown in Figure 8), it is possible to notice that in both cases there was an increase in values as a function of time advance. The observed data are in the range of 27.6°C to 30.1°C, while the modeled data are in the range of 24.8°C to 26.4°C at the lowest level of the surface layer. This represents a maximum difference of 3.7°C between them.

About the detection of thermal inversion and a subtle change in the regime of the surface layer, from stable, through neutral, to unstable, it is only possible to be seen in the observed data, because the modeled data do not have sufficient sensitivity for this purpose.

This fact highlights the importance of this type of experiment, since it could be performed every day (at a very low cost – related only to the electrical energy associated with charging the batteries) and these data could be assimilated by operational models, such as the WRF, increasing its capacity to represent the surface fluxes and, consequently, all the thermal energy transferred to the middle atmosphere.

In the case of the comparison between the vertical profiles of relative humidity generated by observed data and by modeling (shown in Figure 9), the values of the observed data first experience an increase and then suffer a greater reduction, while the modeled values show only the decrease in the considered interval.

It is observed that in the region where it is possible to compare the data, the relative humidity simulated by the WRF was predominantly higher than that observed in the experiment, which may be associated with the underestimation of the air temperature verified in the model simulations at these same levels, which would increase the water vapor retention capacity in the air parcel and, consequently, the relative humidity.

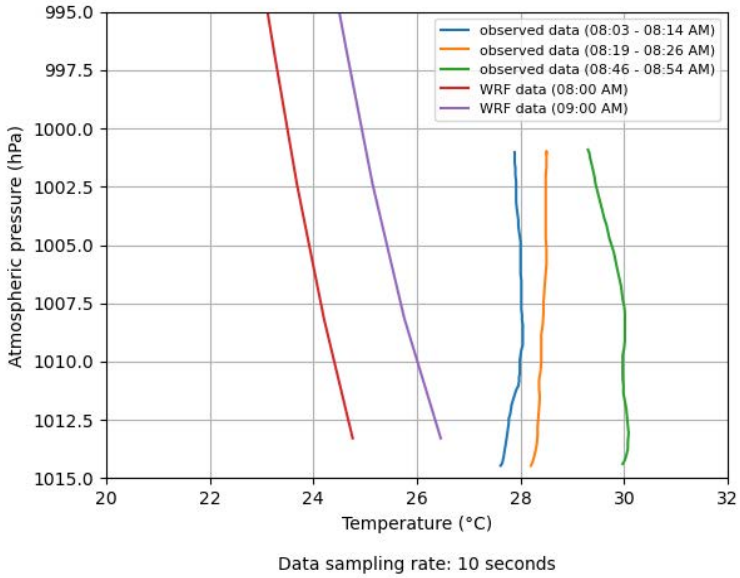

Figure 8: Comparison between vertical temperature profiles generated by observed data and numerical modeling by WRF for Itaipu on March 14th, 2023.

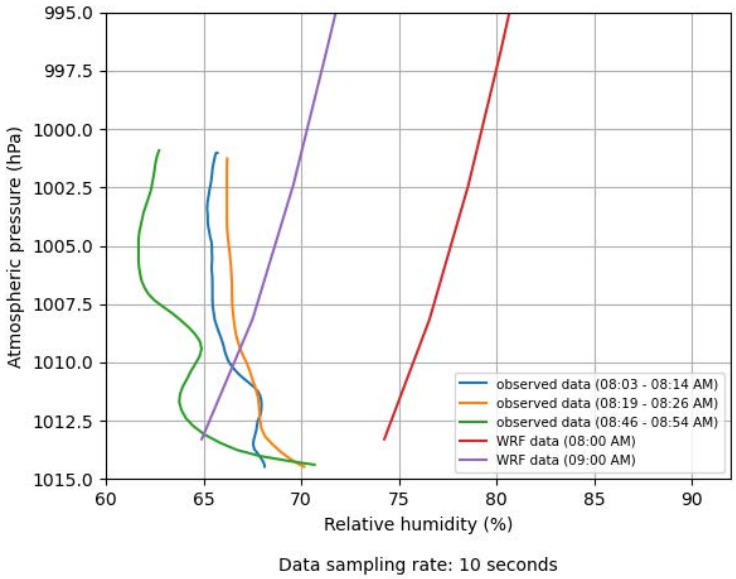

Figure 9: Comparison between vertical relative humidity profiles generated by observed data and numerical modeling by WRF for Itaipu on March 14th, 2023.

As for the comparison between the height profiles as a function of atmospheric pressure generated by observed data and by modeling (shown in the Figure 10), there is a correlation between the profiles of their modalities, but a mismatch that varies from 1.6 to 1.8 hPa between the profiles generated by observed and modeled data (which are shown superimposed in Figure 9). This may be associated with the difference in atmospheric density between both, since the temperature near the surface simulated by the WRF was about 4°C lower than the observed temperature to the same level.

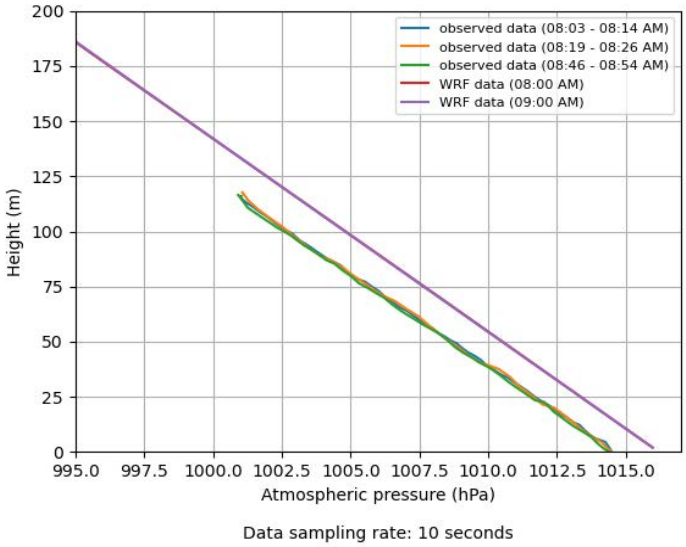

Figure 10: Comparison between height profiles as a function of atmospheric pressure generated by observed data and numerical modeling by WRF for Itaipu on March 14th, 2023.

During the course of this study, it was possible to expand the results in relation to the work of Ribeiro (2022), because in addition to anemometry, it was also possible to obtain temperature, humidity and pressure data in a way that was as efficient and economical as his work. Furthermore, the association of the Pitot tube with the MPX5100DP differential pressure sensor made by Ribeiro (2022) could be adapted in this work to reach the perception that drone propellers are an influencing factor for capturing atmospheric data.

The results of the work by Cataldi et al. (2022) pointed to the feasibility of using the DHT22 and BMP280 sensors to measure atmospheric parameters together with the Arduino Uno prototyping board. In light of this, this work not only confirmed the feasibility reported by Cataldi et al. (2022) but also led to the generation of atmospheric vertical profiles, which were analytically compared to numerical modeling profiles, leading to the conclusion that observing data in the atmospheric surface layer with the low-cost profiler contributes positively to a better understanding of the behavior and phenomena of the lower troposphere.

V. Conclusion

As a result of the development of the atmospheric profiler with low-cost technology and sensors, the collected data indicate that it was possible to verify small changes of regime of the surface layer, from its stable, passing through neutral, to unstable behavior. This unfolds the suitability of this profiler to be used in various atmospheric studies, such as atmospheric pollution, calibration of numerical models and nowcasting weather forecast.

It should be noted that this modality of loading sensors, even though they are low cost, on a drone enables successive measurements indefinitely, which is a significant difference in relation to the launch of conventional radiosondes carried by weather balloon due to the high operating costs involved with such launches.

Thus, it is believed that the work fulfilled its purpose, which was to build a methodological approach that allows its replication and improvement for measuring the vertical profile of the atmosphere, initially limited to the surface layer, in addition to having contributed to illustrate the deficiency of atmospheric models in representing surface fluxes, which impacts the predictability of several variables.

Finally, concerning future works, it is recommended that more experiments be performed intensively, at different times of the day, and that other sensors be considered in the prototyping of atmospheric profilers, preferably those that attend guidelines issued by the World Meteorological Organization (WMO). It is also desirable to achieve measurement heights at higher levels, not because of impacts on results, which are satisfactory for the surface layer, but to extend studies beyond this layer. About the profiler's ability to get atmospheric data, it is opportune to study a way to perform measurements of wind speed and direction, considering the type of sensor to be used and the load capacity of the vehicles used to transport it, whether remotely-piloted aircraft or any other.

Acknowledgments

We are grateful to Fluminense Federal University (UFF) for academic and financial support, to the Brazilian Navy for providing technical staff, and to the Laboratory for Monitoring and Numerical Modeling of Climate Systems of this university (LAMMOC-UFF) for support related to resource management. We also thank Mr. Daniel Peçanha Simões for his support in designing the low-cost atmospheric profiler prototype.

References Références Referencias

1. AOSONG ELETRONICS. Digital-output relative humidity & temperature sensor/module DHT22 (DHT22 also named as AM2302). Aosong Eletronics Limited Company, 2017. https://pdf1.alldatasheet.com/datasheet-pdf/view/1132459/ETC2/DHT22.html.
2. ARDUINO. Arduino Uno Rev3, 2023. https://store.arduino.cc/products/arduino-uno-rev3.
3. BARCELLOS, P. C. L.; CATALDI, M. Flash Flood and Extreme Rainfall Forecast through One-Way Coupling of WRF-SMAP Models: Natural Hazards in Rio de Janeiro State. Atmosphere, v. 11, p. 834, 2020. https://doi.org/10.3390/atmos11080834.
4. BOSCH. BMP280 Digital Pressure Sensor. Bosch Sensortec, 2018. https://pdf1.alldatasheet.com/datasheet-pdf/view/1132069/BOSCH/BMP280.html.
5. BRASÍLIA, Ministério da Infraestrutura. Agência Nacional de Aviação Civil. Regulamento Brasileiro da Aviação Civil Especial, N° 94, emenda N° 2. 2021. https://www.anac.gov.br/assuntos/legislacao/legislacao-1/boletim-de-pessoal/2021/47s1/anexo-ii-rbac-e-no-94-emenda-02.
6. BRASÍLIA, Ministério da Integração Nacional. Política Nacional de Defesa Civil. 2007. https://antigo.mdr.gov.br/images/stories/ArquivosDefesaCivil/ArquivosPDF/publicacoes/pndc.pdf.
7. BURGUÉS J. et al. Characterization of odour emissions in a wastewater treatment plant using a drone-based chemical sensor system. Science of the Total Environment, v. 846, 2022. https://doi.org/10.1016/j.scitotenv.2022.157290
8. CASTRO, A. L. C. Glossário de Defesa Civil: estudos de riscos e medicina de desastres. 283 p. Brasília, 1998. https://www.defesacivil.mg.gov.br/images/documentos/Defesa%20Civil/manuais/GLOSSARIO-Dicionario-Defesa-Civil.pdf.
9. CATALDI, M.; et al. Atmospheric experimentation with low-cost radiosonde attached to a drone. In: VIII Workshop on Biosystems Engineering, Niterói, 2022. https://app.uff.br/riuff/bitstream/handle/1/27951/Anais%20WEB_VIII_2023-02-20_B.pdf?sequence=1&isAllowed=y.
10. CHANG C. C. et al. A study of atmospheric mixing of trace gases by aerial sampling with a multi-rotor drone. Atmospheric Environment, v. 184, 2018. https://doi.org/10.1016/j.atmosenv.2018.04.032.
11. DARYNOVA Z. et al. Data assimilation method for quantifying controlled methane releases using a drone and ground-sensors. Atmospheric Environment: X, v. 17, 2023. https://doi.org/10.1016/j.aeaoa.2023.100210.
12. FLEMONS K. et al. The use of drones for the delivery of diagnostic test kits and medical supplies to remote First Nations communities during Covid-19. American Journal of Infection Control, v. 50, 2022. https://doi.org/10.1016/j.ajic.2022.03.004.
13. GAR. Global Assessment Report on Disaster Risk Reduction, 2015. https://www.undrr.org/publication/global-assessment-report-disaster-risk-reduction-2015.
14. GASPARETTO, P. Relações entre a altura média da camada limite planetária e as condições de instabilidade atmosférica na região metropolitana de Fortaleza – Ceará. 2011. 68 p. Course conclusion monograph (Bachelor's Degree in Physics) – Ceara State University, Fortaleza, 2011. https://www.uece.br/posla/wp-content/uploads/sites/28/2021/08/monografia_-_priscila_gasparetto_27.07.2011.pdf.
15. GRAHAM C. T. et al. Drones can reliably, accurately and with high levels of precision, collect large volume water samples and physio-chemical data from lakes. Science of the Total Environment, v. 824, 2022. https://doi.org/10.1016/j.scitotenv.2022.153875.
16. JÄRVI, L. et al. Determinants of spatial variability of air pollutant concentrations in a street canyon network measured using a mobile laboratory and a drone. Science of the Total Environment, v. 856, 2023. https://doi.org/10.1016/j.scitotenv.2022.158974.
17. KARACHALIOS, T.; KANELLOPOULOS, D.; LAZARINIS, F. Arduino sensor integrated drone for weather indices: a prototype for pre-flight preparation. arXiv preprint ar-Xiv:2106.16083, 2021. https://doi.org/10.7251/JIT2101005K.
18. LAITINEN, A. Utilization of drones in vertical profile measurements of the atmosphere. 2019. 74 p. Dissertation (Master's Degree in Engineering and Natural Sciences) – Tampere University, 2019. https://core.ac.uk/download/pdf/250168303.pdf.
19. LEE S.; HWANG H.; LEE J. Y. Vertical measurements of roadside air pollutants using a drone. Atmospheric Pollution Research, v. 13, 2022. https://doi.org/10.1016/j.apr.2022.101609.
20. LIRA, C. B. M.; CATALDI, M. Avaliação do ensemble de parametrizações físicas do mode-lo MM5 no evento de precipitação intensa ocorrido entre os dias 05 e 06 de abril de 2010 no município do Rio de Janeiro. Ciência e Natura, v.38, 2016. https://doi.org/10.5902/2179460X17116.
21. MARCELINO, E. V. Desastres naturais e geotecnologias: Conceitos básicos. 2007, Santa Maria, Rio Grande do Sul. http://mtc-m16c.sid.inpe.br/col/sid.inpe.br/mtc-m18@80/2008/07.02.16.22/doc/publicacao.pdf.
22. MASIC, A. et al. Drone measurements of temperature inversion characteristics and particulate matter vertical profiles in urban enviroments. In: DAAAM Symposium, Vienna, 2021. doi: 10.2507/32nd.daaam.proceedings.018.

23. MCROBERTS, M. Arduíno Básico. São Paulo: Novatec, 2011. https://edisciplinas.usp.br/pluginfile.php/4287597/mod_resource/content/2/Ardu%C3%ADno%20B%C3%A1sico%20-%20Michael%20McRoberts.pdf.
24. OLIVEIRA, F.P.; AMORIM, H. S.; DERECZYNSKI, C. P. Montagem de uma radiossonda de baixo custo. 2016. 30 f. Instructional material (Professional Master's Degree in Physics Teaching) – Rio de Janeiro Federal University, Rio de Janeiro, 2016. http://pef.if.ufrj.br/producao_academica/dissertacoes/2016_Fabiano_Oliveira/material_instrucional_Fabiano_Oliveira.pdf.
25. RIBEIRO, F. F. Desenvolvimento de sensor embarcado para medição de velocidade do vento. 2022. 111 p. Course conclusion monograph (Bachelor's Degree in Water Resources and Environmental Engineering) – Fluminense Federal University, Niterói, 2022.
26. SCHOLZ S. S. et al. AED delivery at night – Can drones do the Job? A feasibility study of unmanned aerial systems to transport automated external defibrillators during night-time. Resuscitation, v. 185, 2023. https://doi.org/10.1016/j.resuscitation.2023.109734.
27. SOUSA, P. A. et al. Lançamento de uma sonda atmosférica de baixo custo. Revista Brasileira de Ensino de Física. v. 44, 2022. https://doi.org/10.1590/1806-9126-RBEF-2022-0238.
28. STULL, R. B. Practical Meteorology: An Algebra-based Survey of Atmospheric Science, Version 1.02b. University of British Columbia, Vancouver, 2017. https://www.eoas.ubc.ca/books/Practical_ Meteorology/.
29. TOBIN G. A, MONTZ B. E. Natural hazards: explanation and integration. New York: The Guilford Press, 1997. https://digitalcommons.usf.edu/geo_facpub/40/.
30. VYTOVTOV A. et al. Scientific Bases Development for Oil Spill Accidents Automated Detection Using Drones. In: XIII International Conference on Transport Infrastructure: Territory Development and Sustainability. Transportation Research Procedia, v. 68, 2023. https://doi.org/10.1016/j.trpro.2023.02.080.

Global Journals Guidelines Handbook 2023

www.GlobalJournals.org

Memberships

Fellows/Associates of Social Science Research Council

FSSRC/ASSRC Memberships

Introduction

FSSRC/ASSRC is the most prestigious membership of Global Journals accredited by Open Association of Research Society, U.S.A (OARS). The credentials of Fellow and Associate designations signify that the researcher has gained the knowledge of the fundamental and high-level concepts, and is a subject matter expert, proficient in an expertise course covering the professional code of conduct, and follows recognized standards of practice. The credentials are designated only to the researchers, scientists, and professionals that have been selected by a rigorous process by our Editorial Board and Management Board.

Associates of FSSRC/ASSRC are scientists and researchers from around the world are working on projects/researches that have huge potentials. Members support Global Journals' mission to advance technology for humanity and the profession.

FSSRC

Fellow of Social Science Research Council

FELLOW OF SOCIAL SCIENCE RESEARCH COUNCIL is the most prestigious membership of Global Journals. It is an award and membership granted to individuals that the Open Association of Research Society judges to have made a 'substantial contribution to the improvement of computer science, technology, and electronics engineering.

The primary objective is to recognize the leaders in research and scientific fields of the current era with a global perspective and to create a channel between them and other researchers for better exposure and knowledge sharing. Members are most eminent scientists, engineers, and technologists from all across the world. Fellows are elected for life through a peer review process on the basis of excellence in the respective domain. There is no limit on the number of new nominations made in any year. Each year, the Open Association of Research Society elect up to 12 new Fellow Members.

Benefit

To the institution

Get letter of appreciation

Global Journals sends a letter of appreciation of author to the Dean or CEO of the University or Company of which author is a part, signed by editor in chief or chief author.

Exclusive Network

Get access to a closed network

A FSSRC member gets access to a closed network of Tier 1 researchers and scientists with direct communication channel through our website. Fellows can reach out to other members or researchers directly. They should also be open to reaching out by other.

Career | Credibility | Exclusive | Reputation

Certificate

Certificate, LOR and Laser-Momento

Fellows receive a printed copy of a certificate signed by our Chief Author that may be used for academic purposes and a personal recommendation letter to the dean of member's university.

Career | Credibility | Exclusive | Reputation

Designation

Get honored title of membership

Fellows can use the honored title of membership. The “FSSRC” is an honored title which is accorded to a person’s name viz. Dr. John E. Hall, Ph.D., FSSRC or William Walldroff, M.S., FSSRC.

Career | Credibility | Exclusive | Reputation

Recognition on the Platform

Better visibility and citation

All the Fellow members of FSSRC get a badge of "Leading Member of Global Journals" on the Research Community that distinguishes them from others. Additionally, the profile is also partially maintained by our team for better visibility and citation. All fellows get a dedicated page on the website with their biography.

Career | Credibility | Reputation

Future Work

Get discounts on the future publications

Fellows receive discounts on future publications with Global Journals up to 60%. Through our recommendation programs, members also receive discounts on publications made with OARS affiliated organizations.

Career | Financial

GJ Account

Unlimited forward of Emails

Fellows get secure and fast GJ work emails with unlimited forward of emails that they may use them as their primary email. For example,
john [AT] globaljournals [DOT] org.

Career | Credibility | Reputation

Premium Tools

Access to all the premium tools

To take future researches to the zenith, fellows receive access to all the premium tools that Global Journals have to offer along with the partnership with some of the best marketing leading tools out there.

Financial

Conferences & Events

Organize seminar/conference

Fellows are authorized to organize symposium/seminar/conference on behalf of Global Journal Incorporation (USA). They can also participate in the same organized by another institution as representative of Global Journal. In both the cases, it is mandatory for him to discuss with us and obtain our consent. Additionally, they get free research conferences (and others) alerts.

Career | Credibility | Financial

Early Invitations

Early invitations to all the symposiums, seminars, conferences

All fellows receive the early invitations to all the symposiums, seminars, conferences and webinars hosted by Global Journals in their subject.

Exclusive

Publishing Articles & Books

Earn 60% of sales proceeds

To take future researches to the zenith, fellows receive access to all the premium tools that Global Journals have to offer along with the partnership with some of the best marketing leading tools out there.

Exclusive | Financial

Reviewers

Get a remuneration of 15% of author fees

Fellow members are eligible to join as a paid peer reviewer at Global Journals Incorporation (USA) and can get a remuneration of 15% of author fees, taken from the author of a respective paper.

Financial

Access to Editorial Board

Become a member of the Editorial Board

Fellows may join as a member of the Editorial Board of Global Journals Incorporation (USA) after successful completion of three years as Fellow and as Peer Reviewer. Additionally, Fellows get a chance to nominate other members for Editorial Board.

Career | Credibility | Exclusive | Reputation

And Much More

Get access to scientific museums and observatories across the globe

All members get access to 5 selected scientific museums and observatories across the globe. All researches published with Global Journals will be kept under deep archival facilities across regions for future protections and disaster recovery. They get 10 GB free secure cloud access for storing research files.

ASSRC

ASSOCIATE OF SOCIAL SCIENCE RESEARCH COUNCIL

ASSOCIATE OF SOCIAL SCIENCE RESEARCH COUNCIL is the membership of Global Journals awarded to individuals that the Open Association of Research Society judges to have made a 'substantial contribution to the improvement of computer science, technology, and electronics engineering.

The primary objective is to recognize the leaders in research and scientific fields of the current era with a global perspective and to create a channel between them and other researchers for better exposure and knowledge sharing. Members are most eminent scientists, engineers, and technologists from all across the world. Associate membership can later be promoted to Fellow Membership. Associates are elected for life through a peer review process on the basis of excellence in the respective domain. There is no limit on the number of new nominations made in any year. Each year, the Open Association of Research Society elect up to 12 new Associate Members.

Benefit

To the institution

Get letter of appreciation

Global Journals sends a letter of appreciation of author to the Dean or CEO of the University or Company of which author is a part, signed by editor in chief or chief author.

Exclusive Network

Get access to a closed network

A ASSRC member gets access to a closed network of Tier 2 researchers and scientists with direct communication channel through our website. Associates can reach out to other members or researchers directly. They should also be open to reaching out by other.

Career | Credibility | Exclusive | Reputation

Certificate

Certificate, LoR and Laser-Momento

Associates receive a printed copy of a certificate signed by our Chief Author that may be used for academic purposes and a personal recommendation letter to the dean of member's university.

Career | Credibility | Exclusive | Reputation

Designation

Get honored title of membership

Associates can use the honored title of membership. The “ASSRC” is an honored title which is accorded to a person’s name viz. Dr. John E. Hall, Ph.D., ASSRC or William Walldroff, M.S., ASSRC.

Career | Credibility | Exclusive | Reputation

Recognition on the Platform

Better visibility and citation

All the Associate members of ASSRC get a badge of "Leading Member of Global Journals" on the Research Community that distinguishes them from others. Additionally, the profile is also partially maintained by our team for better visibility and citation.

Career | Credibility | Reputation

Future Work

Get discounts on the future publications

Associates receive discounts on future publications with Global Journals up to 30%. Through our recommendation programs, members also receive discounts on publications made with OARS affiliated organizations.

Career | Financial

GJ Account

Unlimited forward of Emails

Associates get secure and fast GJ work emails with 5GB forward of emails that they may use them as their primary email. For example, john [AT] globaljournals [DOT] org.

Career | Credibility | Reputation

Premium Tools

Access to all the premium tools

To take future researches to the zenith, fellows receive access to almost all the premium tools that Global Journals have to offer along with the partnership with some of the best marketing leading tools out there.

Financial

Conferences & Events

Organize seminar/conference

Associates are authorized to organize symposium/seminar/conference on behalf of Global Journal Incorporation (USA). They can also participate in the same organized by another institution as representative of Global Journal. In both the cases, it is mandatory for him to discuss with us and obtain our consent. Additionally, they get free research conferences (and others) alerts.

Career | Credibility | Financial

Early Invitations

Early invitations to all the symposiums, seminars, conferences

All associates receive the early invitations to all the symposiums, seminars, conferences and webinars hosted by Global Journals in their subject.

Exclusive

Publishing Articles & Books

Earn 60% of sales proceeds

Associates can publish articles (limited) without any fees. Also, they can earn up to 30-40% of sales proceeds from the sale of reference/review books/literature/publishing of research paper.

Exclusive | Financial

Reviewers

Get a remuneration of 15% of author fees

Associate members are eligible to join as a paid peer reviewer at Global Journals Incorporation (USA) and can get a remuneration of 15% of author fees, taken from the author of a respective paper.

Financial

And Much More

Get access to scientific museums and observatories across the globe

All members get access to 2 selected scientific museums and observatories across the globe. All researches published with Global Journals will be kept under deep archival facilities across regions for future protections and disaster recovery. They get 5 GB free secure cloud access for storing research files.

Associate	Fellow	Research Group	Basic
$4800 **lifetime designation**	$6800 **lifetime designation**	$12500.00 **organizational**	APC **per article**
Certificate, LoR and Momento **2** discounted publishing/year **Gradation** of Research **10** research contacts/day **1 GB** Cloud Storage **GJ** Community Access	**Certificate,** LoR and Momento **Unlimited** discounted publishing/year **Gradation** of Research **Unlimited** research contacts/day **5 GB** Cloud Storage **Online Presense** Assistance **GJ** Community Access	**Certificates,** LoRs and Momentos **Unlimited** free publishing/year **Gradation** of Research **Unlimited** research contacts/day **Unlimited** Cloud Storage **Online Presense** Assistance **GJ** Community Access	**GJ** Community Access

Preferred Author Guidelines

We accept the manuscript submissions in any standard (generic) format.

We typeset manuscripts using advanced typesetting tools like Adobe In Design, CorelDraw, TeXnicCenter, and TeXStudio. We usually recommend authors submit their research using any standard format they are comfortable with, and let Global Journals do the rest.

Alternatively, you can download our basic template from https://globaljournals.org/Template.zip

Authors should submit their complete paper/article, including text illustrations, graphics, conclusions, artwork, and tables. Authors who are not able to submit manuscript using the form above can email the manuscript department at submit@globaljournals.org or get in touch with chiefeditor@globaljournals.org if they wish to send the abstract before submission.

Before and during Submission

Authors must ensure the information provided during the submission of a paper is authentic. Please go through the following checklist before submitting:

1. Authors must go through the complete author guideline and understand and *agree to Global Journals' ethics and code of conduct,* along with author responsibilities.
2. Authors must accept the privacy policy, terms, and conditions of Global Journals.
3. Ensure corresponding author's email address and postal address are accurate and reachable.
4. Manuscript to be submitted must include keywords, an abstract, a paper title, co-author(s') names and details (email address, name, phone number, and institution), figures and illustrations in vector format including appropriate captions, tables, including titles and footnotes, a conclusion, results, acknowledgments and references.
5. Authors should submit paper in a ZIP archive if any supplementary files are required along with the paper.
6. Proper permissions must be acquired for the use of any copyrighted material.
7. Manuscript submitted *must not have been submitted or published elsewhere* and all authors must be aware of the submission.

Declaration of Conflicts of Interest

It is required for authors to declare all financial, institutional, and personal relationships with other individuals and organizations that could influence (bias) their research.

Policy on Plagiarism

Plagiarism is not acceptable in Global Journals submissions at all.

Plagiarized content will not be considered for publication. We reserve the right to inform authors' institutions about plagiarism detected either before or after publication. If plagiarism is identified, we will follow COPE guidelines:

Authors are solely responsible for all the plagiarism that is found. The author must not fabricate, falsify or plagiarize existing research data. The following, if copied, will be considered plagiarism:

- Words (language)
- Ideas
- Findings
- Writings
- Diagrams
- Graphs
- Illustrations
- Lectures

- Printed material
- Graphic representations
- Computer programs
- Electronic material
- Any other original work

Authorship Policies

Global Journals follows the definition of authorship set up by the Open Association of Research Society, USA. According to its guidelines, authorship criteria must be based on:

1. Substantial contributions to the conception and acquisition of data, analysis, and interpretation of findings.
2. Drafting the paper and revising it critically regarding important academic content.
3. Final approval of the version of the paper to be published.

Changes in Authorship

The corresponding author should mention the name and complete details of all co-authors during submission and in manuscript. We support addition, rearrangement, manipulation, and deletions in authors list till the early view publication of the journal. We expect that corresponding author will notify all co-authors of submission. We follow COPE guidelines for changes in authorship.

Copyright

During submission of the manuscript, the author is confirming an exclusive license agreement with Global Journals which gives Global Journals the authority to reproduce, reuse, and republish authors' research. We also believe in flexible copyright terms where copyright may remain with authors/employers/institutions as well. Contact your editor after acceptance to choose your copyright policy. You may follow this form for copyright transfers.

Appealing Decisions

Unless specified in the notification, the Editorial Board's decision on publication of the paper is final and cannot be appealed before making the major change in the manuscript.

Acknowledgments

Contributors to the research other than authors credited should be mentioned in Acknowledgments. The source of funding for the research can be included. Suppliers of resources may be mentioned along with their addresses.

Declaration of funding sources

Global Journals is in partnership with various universities, laboratories, and other institutions worldwide in the research domain. Authors are requested to disclose their source of funding during every stage of their research, such as making analysis, performing laboratory operations, computing data, and using institutional resources, from writing an article to its submission. This will also help authors to get reimbursements by requesting an open access publication letter from Global Journals and submitting to the respective funding source.

Preparing your Manuscript

Authors can submit papers and articles in an acceptable file format: MS Word (doc, docx), LaTeX (.tex, .zip or .rar including all of your files), Adobe PDF (.pdf), rich text format (.rtf), simple text document (.txt), Open Document Text (.odt), and Apple Pages (.pages). Our professional layout editors will format the entire paper according to our official guidelines. This is one of the highlights of publishing with Global Journals—authors should not be concerned about the formatting of their paper. Global Journals accepts articles and manuscripts in every major language, be it Spanish, Chinese, Japanese, Portuguese, Russian, French, German, Dutch, Italian, Greek, or any other national language, but the title, subtitle, and abstract should be in English. This will facilitate indexing and the pre-peer review process.

The following is the official style and template developed for publication of a research paper. Authors are not required to follow this style during the submission of the paper. It is just for reference purposes.

Manuscript Style Instruction (Optional)

- Microsoft Word Document Setting Instructions.
- Font type of all text should be Swis721 Lt BT.
- Page size: 8.27" x 11'", left margin: 0.65, right margin: 0.65, bottom margin: 0.75.
- Paper title should be in one column of font size 24.
- Author name in font size of 11 in one column.
- Abstract: font size 9 with the word "Abstract" in bold italics.
- Main text: font size 10 with two justified columns.
- Two columns with equal column width of 3.38 and spacing of 0.2.
- First character must be three lines drop-capped.
- The paragraph before spacing of 1 pt and after of 0 pt.
- Line spacing of 1 pt.
- Large images must be in one column.
- The names of first main headings (Heading 1) must be in Roman font, capital letters, and font size of 10.
- The names of second main headings (Heading 2) must not include numbers and must be in italics with a font size of 10.

Structure and Format of Manuscript

The recommended size of an original research paper is under 15,000 words and review papers under 7,000 words. Research articles should be less than 10,000 words. Research papers are usually longer than review papers. Review papers are reports of significant research (typically less than 7,000 words, including tables, figures, and references)

A research paper must include:

a) A title which should be relevant to the theme of the paper.
b) A summary, known as an abstract (less than 150 words), containing the major results and conclusions.
c) Up to 10 keywords that precisely identify the paper's subject, purpose, and focus.
d) An introduction, giving fundamental background objectives.
e) Resources and techniques with sufficient complete experimental details (wherever possible by reference) to permit repetition, sources of information must be given, and numerical methods must be specified by reference.
f) Results which should be presented concisely by well-designed tables and figures.
g) Suitable statistical data should also be given.
h) All data must have been gathered with attention to numerical detail in the planning stage.

Design has been recognized to be essential to experiments for a considerable time, and the editor has decided that any paper that appears not to have adequate numerical treatments of the data will be returned unrefereed.

i) Discussion should cover implications and consequences and not just recapitulate the results; conclusions should also be summarized.
j) There should be brief acknowledgments.
k) There ought to be references in the conventional format. Global Journals recommends APA format.

Authors should carefully consider the preparation of papers to ensure that they communicate effectively. Papers are much more likely to be accepted if they are carefully designed and laid out, contain few or no errors, are summarizing, and follow instructions. They will also be published with much fewer delays than those that require much technical and editorial correction.

The Editorial Board reserves the right to make literary corrections and suggestions to improve brevity.

Format Structure

It is necessary that authors take care in submitting a manuscript that is written in simple language and adheres to published guidelines.

All manuscripts submitted to Global Journals should include:

Title

The title page must carry an informative title that reflects the content, a running title (less than 45 characters together with spaces), names of the authors and co-authors, and the place(s) where the work was carried out.

Author details

The full postal address of any related author(s) must be specified.

Abstract

The abstract is the foundation of the research paper. It should be clear and concise and must contain the objective of the paper and inferences drawn. It is advised to not include big mathematical equations or complicated jargon.

Many researchers searching for information online will use search engines such as Google, Yahoo or others. By optimizing your paper for search engines, you will amplify the chance of someone finding it. In turn, this will make it more likely to be viewed and cited in further works. Global Journals has compiled these guidelines to facilitate you to maximize the web-friendliness of the most public part of your paper.

Keywords

A major lynchpin of research work for the writing of research papers is the keyword search, which one will employ to find both library and internet resources. Up to eleven keywords or very brief phrases have to be given to help data retrieval, mining, and indexing.

One must be persistent and creative in using keywords. An effective keyword search requires a strategy: planning of a list of possible keywords and phrases to try.

Choice of the main keywords is the first tool of writing a research paper. Research paper writing is an art. Keyword search should be as strategic as possible.

One should start brainstorming lists of potential keywords before even beginning searching. Think about the most important concepts related to research work. Ask, “What words would a source have to include to be truly valuable in a research paper?” Then consider synonyms for the important words.

It may take the discovery of only one important paper to steer in the right keyword direction because, in most databases, the keywords under which a research paper is abstracted are listed with the paper.

Numerical Methods

Numerical methods used should be transparent and, where appropriate, supported by references.

Abbreviations

Authors must list all the abbreviations used in the paper at the end of the paper or in a separate table before using them.

Formulas and equations

Authors are advised to submit any mathematical equation using either MathJax, KaTeX, or LaTeX, or in a very high-quality image.

Tables, Figures, and Figure Legends

Tables: Tables should be cautiously designed, uncrowned, and include only essential data. Each must have an Arabic number, e.g., Table 4, a self-explanatory caption, and be on a separate sheet. Authors must submit tables in an editable format and not as images. References to these tables (if any) must be mentioned accurately.

Figures

Figures are supposed to be submitted as separate files. Always include a citation in the text for each figure using Arabic numbers, e.g., Fig. 4. Artwork must be submitted online in vector electronic form or by emailing it.

Preparation of Eletronic Figures for Publication

Although low-quality images are sufficient for review purposes, print publication requires high-quality images to prevent the final product being blurred or fuzzy. Submit (possibly by e-mail) EPS (line art) or TIFF (halftone/ photographs) files only. MS PowerPoint and Word Graphics are unsuitable for printed pictures. Avoid using pixel-oriented software. Scans (TIFF only) should have a resolution of at least 350 dpi (halftone) or 700 to 1100 dpi (line drawings). Please give the data for figures in black and white or submit a Color Work Agreement form. EPS files must be saved with fonts embedded (and with a TIFF preview, if possible).

For scanned images, the scanning resolution at final image size ought to be as follows to ensure good reproduction: line art: >650 dpi; halftones (including gel photographs): >350 dpi; figures containing both halftone and line images: >650 dpi.

Color charges: Authors are advised to pay the full cost for the reproduction of their color artwork. Hence, please note that if there is color artwork in your manuscript when it is accepted for publication, we would require you to complete and return a Color Work Agreement form before your paper can be published. Also, you can email your editor to remove the color fee after acceptance of the paper.

Tips for writing a good quality Social Science Research Paper

Techniques for writing a good quality homan social science research paper:

1. Choosing the topic: In most cases, the topic is selected by the interests of the author, but it can also be suggested by the guides. You can have several topics, and then judge which you are most comfortable with. This may be done by asking several questions of yourself, like "Will I be able to carry out a search in this area? Will I find all necessary resources to accomplish the search? Will I be able to find all information in this field area?" If the answer to this type of question is "yes," then you ought to choose that topic. In most cases, you may have to conduct surveys and visit several places. Also, you might have to do a lot of work to find all the rises and falls of the various data on that subject. Sometimes, detailed information plays a vital role, instead of short information. Evaluators are human: The first thing to remember is that evaluators are also human beings. They are not only meant for rejecting a paper. They are here to evaluate your paper. So present your best aspect.

2. Think like evaluators: If you are in confusion or getting demotivated because your paper may not be accepted by the evaluators, then think, and try to evaluate your paper like an evaluator. Try to understand what an evaluator wants in your research paper, and you will automatically have your answer. Make blueprints of paper: The outline is the plan or framework that will help you to arrange your thoughts. It will make your paper logical. But remember that all points of your outline must be related to the topic you have chosen.

3. Ask your guides: If you are having any difficulty with your research, then do not hesitate to share your difficulty with your guide (if you have one). They will surely help you out and resolve your doubts. If you can't clarify what exactly you require for your work, then ask your supervisor to help you with an alternative. He or she might also provide you with a list of essential readings.

4. Use of computer is recommended: As you are doing research in the field of homan social science then this point is quite obvious. Use right software: Always use good quality software packages. If you are not capable of judging good software, then you can lose the quality of your paper unknowingly. There are various programs available to help you which you can get through the internet.

5. Use the internet for help: An excellent start for your paper is using Google. It is a wondrous search engine, where you can have your doubts resolved. You may also read some answers for the frequent question of how to write your research paper or find a model research paper. You can download books from the internet. If you have all the required books, place importance on reading, selecting, and analyzing the specified information. Then sketch out your research paper. Use big pictures: You may use encyclopedias like Wikipedia to get pictures with the best resolution. At Global Journals, you should strictly follow here.

6. Bookmarks are useful: When you read any book or magazine, you generally use bookmarks, right? It is a good habit which helps to not lose your continuity. You should always use bookmarks while searching on the internet also, which will make your search easier.

7. Revise what you wrote: When you write anything, always read it, summarize it, and then finalize it.

8. Make every effort: Make every effort to mention what you are going to write in your paper. That means always have a good start. Try to mention everything in the introduction—what is the need for a particular research paper. Polish your work with good writing skills and always give an evaluator what he wants. Make backups: When you are going to do any important thing like making a research paper, you should always have backup copies of it either on your computer or on paper. This protects you from losing any portion of your important data.

9. Produce good diagrams of your own: Always try to include good charts or diagrams in your paper to improve quality. Using several unnecessary diagrams will degrade the quality of your paper by creating a hodgepodge. So always try to include diagrams which were made by you to improve the readability of your paper. Use of direct quotes: When you do research relevant to literature, history, or current affairs, then use of quotes becomes essential, but if the study is relevant to science, use of quotes is not preferable.

10. Use proper verb tense: Use proper verb tenses in your paper. Use past tense to present those events that have happened. Use present tense to indicate events that are going on. Use future tense to indicate events that will happen in the future. Use of wrong tenses will confuse the evaluator. Avoid sentences that are incomplete.

11. Pick a good study spot: Always try to pick a spot for your research which is quiet. Not every spot is good for studying.

12. Know what you know: Always try to know what you know by making objectives, otherwise you will be confused and unable to achieve your target.

13. Use good grammar: Always use good grammar and words that will have a positive impact on the evaluator; use of good vocabulary does not mean using tough words which the evaluator has to find in a dictionary. Do not fragment sentences. Eliminate one-word sentences. Do not ever use a big word when a smaller one would suffice.

Verbs have to be in agreement with their subjects. In a research paper, do not start sentences with conjunctions or finish them with prepositions. When writing formally, it is advisable to never split an infinitive because someone will (wrongly) complain. Avoid clichés like a disease. Always shun irritating alliteration. Use language which is simple and straightforward. Put together a neat summary.

14. Arrangement of information: Each section of the main body should start with an opening sentence, and there should be a changeover at the end of the section. Give only valid and powerful arguments for your topic. You may also maintain your arguments with records.

15. Never start at the last minute: Always allow enough time for research work. Leaving everything to the last minute will degrade your paper and spoil your work.

16. Multitasking in research is not good: Doing several things at the same time is a bad habit in the case of research activity. Research is an area where everything has a particular time slot. Divide your research work into parts, and do a particular part in a particular time slot.

17. Never copy others' work: Never copy others' work and give it your name because if the evaluator has seen it anywhere, you will be in trouble. Take proper rest and food: No matter how many hours you spend on your research activity, if you are not taking care of your health, then all your efforts will have been in vain. For quality research, take proper rest and food.

18. Go to seminars: Attend seminars if the topic is relevant to your research area. Utilize all your resources.
Refresh your mind after intervals: Try to give your mind a rest by listening to soft music or sleeping in intervals. This will also improve your memory. Acquire colleagues: Always try to acquire colleagues. No matter how sharp you are, if you acquire colleagues, they can give you ideas which will be helpful to your research.

19. Think technically: Always think technically. If anything happens, search for its reasons, benefits, and demerits. Think and then print: When you go to print your paper, check that tables are not split, headings are not detached from their descriptions, and page sequence is maintained.

20. Adding unnecessary information: Do not add unnecessary information like "I have used MS Excel to draw graphs." Irrelevant and inappropriate material is superfluous. Foreign terminology and phrases are not apropos. One should never take a broad view. Analogy is like feathers on a snake. Use words properly, regardless of how others use them. Remove quotations. Puns are for kids, not grunt readers. Never oversimplify: When adding material to your research paper, never go for oversimplification; this will definitely irritate the evaluator. Be specific. Never use rhythmic redundancies. Contractions shouldn't be used in a research paper. Comparisons are as terrible as clichés. Give up ampersands, abbreviations, and so on. Remove commas that are not necessary. Parenthetical words should be between brackets or commas. Understatement is always the best way to put forward earth-shaking thoughts. Give a detailed literary review.

21. Report concluded results: Use concluded results. From raw data, filter the results, and then conclude your studies based on measurements and observations taken. An appropriate number of decimal places should be used. Parenthetical remarks are prohibited here. Proofread carefully at the final stage. At the end, give an outline to your arguments. Spot perspectives of further study of the subject. Justify your conclusion at the bottom sufficiently, which will probably include examples.

22. Upon conclusion: Once you have concluded your research, the next most important step is to present your findings. Presentation is extremely important as it is the definite medium though which your research is going to be in print for the rest of the crowd. Care should be taken to categorize your thoughts well and present them in a logical and neat manner. A good quality research paper format is essential because it serves to highlight your research paper and bring to light all necessary aspects of your research.

.

Informal Guidelines of Research Paper Writing

Key points to remember:

- Submit all work in its final form.
- Write your paper in the form which is presented in the guidelines using the template.
- Please note the criteria peer reviewers will use for grading the final paper.

Final points:

One purpose of organizing a research paper is to let people interpret your efforts selectively. The journal requires the following sections, submitted in the order listed, with each section starting on a new page:

The introduction: This will be compiled from reference matter and reflect the design processes or outline of basis that directed you to make a study. As you carry out the process of study, the method and process section will be constructed like that. The results segment will show related statistics in nearly sequential order and direct reviewers to similar intellectual paths throughout the data that you gathered to carry out your study.

The discussion section:

This will provide understanding of the data and projections as to the implications of the results. The use of good quality references throughout the paper will give the effort trustworthiness by representing an alertness to prior workings.

Writing a research paper is not an easy job, no matter how trouble-free the actual research or concept. Practice, excellent preparation, and controlled record-keeping are the only means to make straightforward progression.

General style:

Specific editorial column necessities for compliance of a manuscript will always take over from directions in these general guidelines.

To make a paper clear: Adhere to recommended page limits.

Mistakes to avoid:

- Insertion of a title at the foot of a page with subsequent text on the next page.
- Separating a table, chart, or figure—confine each to a single page.
- Submitting a manuscript with pages out of sequence.
- In every section of your document, use standard writing style, including articles ("a" and "the").
- Keep paying attention to the topic of the paper.
- Use paragraphs to split each significant point (excluding the abstract).
- Align the primary line of each section.
- Present your points in sound order.
- Use present tense to report well-accepted matters.
- Use past tense to describe specific results.
- Do not use familiar wording; don't address the reviewer directly. Don't use slang or superlatives.
- Avoid use of extra pictures—include only those figures essential to presenting results.

Title page:

Choose a revealing title. It should be short and include the name(s) and address(es) of all authors. It should not have acronyms or abbreviations or exceed two printed lines.

Abstract: This summary should be two hundred words or less. It should clearly and briefly explain the key findings reported in the manuscript and must have precise statistics. It should not have acronyms or abbreviations. It should be logical in itself. Do not cite references at this point.

An abstract is a brief, distinct paragraph summary of finished work or work in development. In a minute or less, a reviewer can be taught the foundation behind the study, common approaches to the problem, relevant results, and significant conclusions or new questions.

Write your summary when your paper is completed because how can you write the summary of anything which is not yet written? Wealth of terminology is very essential in abstract. Use comprehensive sentences, and do not sacrifice readability for brevity; you can maintain it succinctly by phrasing sentences so that they provide more than a lone rationale. The author can at this moment go straight to shortening the outcome. Sum up the study with the subsequent elements in any summary. Try to limit the initial two items to no more than one line each.

Reason for writing the article—theory, overall issue, purpose.

- Fundamental goal.
- To-the-point depiction of the research.
- Consequences, including definite statistics—if the consequences are quantitative in nature, account for this; results of any numerical analysis should be reported. Significant conclusions or questions that emerge from the research.

Approach:

- Single section and succinct.
- An outline of the job done is always written in past tense.
- Concentrate on shortening results—limit background information to a verdict or two.
- Exact spelling, clarity of sentences and phrases, and appropriate reporting of quantities (proper units, important statistics) are just as significant in an abstract as they are anywhere else.

Introduction:

The introduction should "introduce" the manuscript. The reviewer should be presented with sufficient background information to be capable of comprehending and calculating the purpose of your study without having to refer to other works. The basis for the study should be offered. Give the most important references, but avoid making a comprehensive appraisal of the topic. Describe the problem visibly. If the problem is not acknowledged in a logical, reasonable way, the reviewer will give no attention to your results. Speak in common terms about techniques used to explain the problem, if needed, but do not present any particulars about the protocols here.

The following approach can create a valuable beginning:

- Explain the value (significance) of the study.
- Defend the model—why did you employ this particular system or method? What is its compensation? Remark upon its appropriateness from an abstract point of view as well as pointing out sensible reasons for using it.
- Present a justification. State your particular theory(-ies) or aim(s), and describe the logic that led you to choose them.
- Briefly explain the study's tentative purpose and how it meets the declared objectives.

Approach:

Use past tense except for when referring to recognized facts. After all, the manuscript will be submitted after the entire job is done. Sort out your thoughts; manufacture one key point for every section. If you make the four points listed above, you will need at least four paragraphs. Present surrounding information only when it is necessary to support a situation. The reviewer does not desire to read everything you know about a topic. Shape the theory specifically—do not take a broad view.

As always, give awareness to spelling, simplicity, and correctness of sentences and phrases.

Procedures (methods and materials):

This part is supposed to be the easiest to carve if you have good skills. A soundly written procedures segment allows a capable scientist to replicate your results. Present precise information about your supplies. The suppliers and clarity of reagents can be helpful bits of information. Present methods in sequential order, but linked methodologies can be grouped as a segment. Be concise when relating the protocols. Attempt to give the least amount of information that would permit another capable scientist to replicate your outcome, but be cautious that vital information is integrated. The use of subheadings is suggested and ought to be synchronized with the results section.

When a technique is used that has been well-described in another section, mention the specific item describing the way, but draw the basic principle while stating the situation. The purpose is to show all particular resources and broad procedures so that another person may use some or all of the methods in one more study or referee the scientific value of your work. It is not to be a step-by-step report of the whole thing you did, nor is a methods section a set of orders.

Materials:

Materials may be reported in part of a section or else they may be recognized along with your measures.

Methods:

- Report the method and not the particulars of each process that engaged the same methodology.
- Describe the method entirely.
- To be succinct, present methods under headings dedicated to specific dealings or groups of measures.
- Simplify—detail how procedures were completed, not how they were performed on a particular day.
- If well-known procedures were used, account for the procedure by name, possibly with a reference, and that's all.

Approach:

It is embarrassing to use vigorous voice when documenting methods without using first person, which would focus the reviewer's interest on the researcher rather than the job. As a result, when writing up the methods, most authors use third person passive voice.

Use standard style in this and every other part of the paper—avoid familiar lists, and use full sentences.

What to keep away from:

- Resources and methods are not a set of information.
- Skip all descriptive information and surroundings—save it for the argument.
- Leave out information that is immaterial to a third party.

Results:

The principle of a results segment is to present and demonstrate your conclusion. Create this part as entirely objective details of the outcome, and save all understanding for the discussion.

The page length of this segment is set by the sum and types of data to be reported. Use statistics and tables, if suitable, to present consequences most efficiently.

You must clearly differentiate material which would usually be incorporated in a study editorial from any unprocessed data or additional appendix matter that would not be available. In fact, such matters should not be submitted at all except if requested by the instructor.

Content:

- Sum up your conclusions in text and demonstrate them, if suitable, with figures and tables.
- In the manuscript, explain each of your consequences, and point the reader to remarks that are most appropriate.
- Present a background, such as by describing the question that was addressed by creation of an exacting study.
- Explain results of control experiments and give remarks that are not accessible in a prescribed figure or table, if appropriate.
- Examine your data, then prepare the analyzed (transformed) data in the form of a figure (graph), table, or manuscript.

What to stay away from:

- Do not discuss or infer your outcome, report surrounding information, or try to explain anything.
- Do not include raw data or intermediate calculations in a research manuscript.
- Do not present similar data more than once.
- A manuscript should complement any figures or tables, not duplicate information.
- Never confuse figures with tables—there is a difference.

Approach:

As always, use past tense when you submit your results, and put the whole thing in a reasonable order.

Put figures and tables, appropriately numbered, in order at the end of the report.

If you desire, you may place your figures and tables properly within the text of your results section.

Figures and tables:

If you put figures and tables at the end of some details, make certain that they are visibly distinguished from any attached appendix materials, such as raw facts. Whatever the position, each table must be titled, numbered one after the other, and include a heading. All figures and tables must be divided from the text.

Discussion:

The discussion is expected to be the trickiest segment to write. A lot of papers submitted to the journal are discarded based on problems with the discussion. There is no rule for how long an argument should be.

Position your understanding of the outcome visibly to lead the reviewer through your conclusions, and then finish the paper with a summing up of the implications of the study. The purpose here is to offer an understanding of your results and support all of your conclusions, using facts from your research and generally accepted information, if suitable. The implication of results should be fully described.

Infer your data in the conversation in suitable depth. This means that when you clarify an observable fact, you must explain mechanisms that may account for the observation. If your results vary from your prospect, make clear why that may have happened. If your results agree, then explain the theory that the proof supported. It is never suitable to just state that the data approved the prospect, and let it drop at that. Make a decision as to whether each premise is supported or discarded or if you cannot make a conclusion with assurance. Do not just dismiss a study or part of a study as "uncertain."

Research papers are not acknowledged if the work is imperfect. Draw what conclusions you can based upon the results that you have, and take care of the study as a finished work.

- You may propose future guidelines, such as how an experiment might be personalized to accomplish a new idea.
- Give details of all of your remarks as much as possible, focusing on mechanisms.
- Make a decision as to whether the tentative design sufficiently addressed the theory and whether or not it was correctly restricted. Try to present substitute explanations if they are sensible alternatives.
- One piece of research will not counter an overall question, so maintain the large picture in mind. Where do you go next? The best studies unlock new avenues of study. What questions remain?
- Recommendations for detailed papers will offer supplementary suggestions.

Approach:

When you refer to information, differentiate data generated by your own studies from other available information. Present work done by specific persons (including you) in past tense.

Describe generally acknowledged facts and main beliefs in present tense.

The Administration Rules

Administration Rules to Be Strictly Followed before Submitting Your Research Paper to Global Journals Inc.

Please read the following rules and regulations carefully before submitting your research paper to Global Journals Inc. to avoid rejection.

Segment draft and final research paper: You have to strictly follow the template of a research paper, failing which your paper may get rejected. You are expected to write each part of the paper wholly on your own. The peer reviewers need to identify your own perspective of the concepts in your own terms. Please do not extract straight from any other source, and do not rephrase someone else's analysis. Do not allow anyone else to proofread your manuscript.

Written material: You may discuss this with your guides and key sources. Do not copy anyone else's paper, even if this is only imitation, otherwise it will be rejected on the grounds of plagiarism, which is illegal. Various methods to avoid plagiarism are strictly applied by us to every paper, and, if found guilty, you may be blacklisted, which could affect your career adversely. To guard yourself and others from possible illegal use, please do not permit anyone to use or even read your paper and file.

Criterion for Grading a Research Paper (Compilation) by Global Journals

Please note that following table is only a Grading of "Paper Compilation" and not on "Performed/Stated Research" whose grading solely depends on Individual Assigned Peer Reviewer and Editorial Board Member. These can be available only on request and after decision of Paper. This report will be the property of Global Journals

Topics	Grades		
	A-B	**C-D**	**E-F**
Abstract	Clear and concise with appropriate content, Correct format. 200 words or below	Unclear summary and no specific data, Incorrect form Above 200 words	No specific data with ambiguous information Above 250 words
Introduction	Containing all background details with clear goal and appropriate details, flow specification, no grammar and spelling mistake, well organized sentence and paragraph, reference cited	Unclear and confusing data, appropriate format, grammar and spelling errors with unorganized matter	Out of place depth and content, hazy format
Methods and Procedures	Clear and to the point with well arranged paragraph, precision and accuracy of facts and figures, well organized subheads	Difficult to comprehend with embarrassed text, too much explanation but completed	Incorrect and unorganized structure with hazy meaning
Result	Well organized, Clear and specific, Correct units with precision, correct data, well structuring of paragraph, no grammar and spelling mistake	Complete and embarrassed text, difficult to comprehend	Irregular format with wrong facts and figures
Discussion	Well organized, meaningful specification, sound conclusion, logical and concise explanation, highly structured paragraph reference cited	Wordy, unclear conclusion, spurious	Conclusion is not cited, unorganized, difficult to comprehend
References	Complete and correct format, well organized	Beside the point, Incomplete	Wrong format and structuring

INDEX

save our planet

Global Journal of Human Social Science

Visit us on the Web at www.GlobalJournals.org | www.SocialScienceResearch.org
or email us at helpdesk@globaljournals.org

ISSN 975587